8-2003

Burnable Poison Design for the International Reactor, Innovative and Secure (IRIS)

Allan Benton Wollaber
University of Tennessee - Knoxville

To the Graduate Council:

I am submitting herewith a thesis written by Allan Benton Wollaber entitled "Burnable Poison Design for the International Reactor, Innovative and Secure (IRIS)." I have examined the final electronic copy of this thesis for form and content and recommend that it be accepted in partial fulfillment of the requirements for the degree of Master of Science, with a major in Nuclear Engineering.

Ronald E. Pevey, Major Professor

We have read this thesis and recommend its acceptance:

Lawrence W. Townsend, Laurence F. Miller

Accepted for the Council:
Carolyn R. Hodges

Vice Provost and Dean of the Graduate School

(Original signatures are on file with official student records.)

To the Graduate Council:

I am submitting herewith a thesis written by Allan Benton Wollaber entitled "Burnable Poison Design for the International Reactor, Innovative and Secure (IRIS)." I have examined the final electronic copy of this thesis for form and content and recommend that it be accepted in partial fulfillment of the requirements for the degree of Master of Science, with a major in Nuclear Engineering.

Ronald E. Pevey
Major Professor

We have read this thesis
and recommend its acceptance:

Lawrence W. Townsend

Laurence F. Miller

Acceptance for the Council:

Anne Mayhew
Vice Provost and Dean of Graduate Studies

(Original signatures are on file with official student records.)

Burnable Poison Design for the International Reactor, Innovative and Secure (IRIS)

A Thesis
Presented for the
Master of Science
Degree
The University of Tennessee, Knoxville

Allan Benton Wollaber
August 2003

Dedication

To my darling wife, Carrie.

Acknowledgments

Special thanks is due to Jess Gehin, whose knowledge, patience, and guidance gave this research life. I would also like to thank my adviser, Ronald Pevey, for allowing me the freedom to pursue any avenue I found interesting. Mario Carelli, Bojan Petrovic, and other members of the Westinghouse design team deserve ample credit for the creation and direction of the IRIS project.

This work was funded in part by the Oak Ridge National Laboratory Laboratory Directed Research and Development program and the Nuclear Engineering Student Laboratory Synthesis program. I would also like to thank Tau Beta Pi and the American Nuclear Society for their financial support by way of fellowships.

I would like to thank my family and friends, whose support provides me the daily encouragement to continue my work.

Abstract

The purpose of this research was to create computer models to expedite the core design of the International Reactor, Innovative and Secure (IRIS), specifically, so that it may employ burnable absorbers to achieve a longer cycle length and enhanced safety while minimizing the use of soluble boron. The IRIS is a next-generation, integral pressurized water reactor (PWR) being designed by an international consortium led by Westinghouse Electric.

Two series of comparison benchmarks, defined by Westinghouse, were completed to validate computer models of representative pin cell, assembly, and whole core geometries. The models were created using the collision probability code HELIOS and a conversion utility to pass cross sections to NESTLE, a nodal diffusion code. Gadolinium and erbium were chosen as the two best qualified elements to be employed as burnable absorbers. Research was performed to create burnable absorber configurations for assemblies that minimize reactivity swing over their expected lifetimes. These optimal assembly designs were then loaded into a simple full reactor geometry to emulate a two-batch core, and the critical soluble boron letdown curves were calculated. While both gadolinium and erbium cores met the requirements for maximum soluble boron levels, neither configuration satisfies all thermal hydraulic safety margins. Future work will address the optimization of core loadings so that these safety margins are met. This work will contribute to establishing an attractive, safe, and economic core design for the IRIS long cycle.

Contents

List of Tables

List of Figures

Chapter 1

Introduction

The International Reactor, Innovative and Secure (IRIS) is an advanced, integral pressurized water reactor (PWR) being designed by an international consortium led by Westinghouse Electric Company [1] [2]. This research has been organized through a collaboration between Oak Ridge National Laboratory (ORNL) and the designers at Westinghouse, as well as an agreement between the University of Tennessee (UT) and ORNL. It addresses a neutronics aspect of the IRIS core, specifically, a technique that allows the core to have a longer cycle length.

1.1 IRIS

Two of the IRIS's feature design goals for near-term deployment are a long core life for improved economics and proliferation resistance - the current reference design has a cycle length of over three years - and increased safety by design [3]. The integral layout is shown in Figure A.1[1]. All major components, including helical steam generators, pressurizer, and reactor coolant pumps, are located inside the reactor vessel. This configuration is beneficial in terms of economy and radiation safety, as there is only a single pressure vessel, which enables the reduction of the containment size and, thus, the plant footprint. The coolant is driven downward through the helical steam generators with the aid of internal spool pumps, yet, in an accident scenario, calculations have shown that natural circulation removes sufficient heat from the fuel to prevent dryout. The IRIS reference design is for a 1000 MW-thermal core. IRIS is modular, providing flexibility in the total generating power for a multi-unit site. In addition to the reference multi-batch core reload, IRIS offers an alternative option that utilizes a single batch, straight-burn core. This improves proliferation resistance, but also further increases the BOL excess reactivity required. The IRIS project is truly international – currently, design for this reactor is being performed in the States, the United Kingdom, Italy, Croatia, Brazil, Mexico, Spain, Russia, and Japan [2]. ORNL is but one member of a

[1] All figures and tables are located in the Appendix.

large consortium. The research presented in this thesis has been mostly coordinated with Westinghouse and The University of Zagreb.

Since the IRIS is a rising competitor in an international market, specific details concerning its design must be omitted from this document. It should also be stated that the models used in this document are not the principal design tools employed by Westinghouse, but are rather used to make recommendations to the current design team. Therefore, in this document, design specifications are only given in cases where they are needed for clarity in presentation, and only then when the data have already been made public.

1.2 The Role of Burnable Poisons in Reactor Core Design

For the most part, the state of a nuclear reactor may be summed up with a single, integral parameter, the effective multiplication factor, or k_{eff}. This parameter may be loosely thought of as a ratio of produced to lost neutrons in one generation. Naturally, real reactors never enter a state in which the neutron population begins to grow or fall without bound, so much of the designer's job is to consider various methods of keeping this ratio near unity, i.e., critical. A reactor's main source of neutrons initially comes as a result of a fission with a ^{235}U nucleus, hence, this isotope accounts for the primary "fuel" of a reactor. Since, this isotope is consumed upon fissioning, it is necessary to have substantial excess amounts of this fuel present in the beginning of the life (BOL) of a reactor than that required for criticality. Large amounts of fuel in a volume the size of a pressure vessel, however, would cause k_{eff} to rise beyond the limits of control. Thus the tradeoff of having a nuclear reactor last a long time is the need to suppress what is known as the "excess" reactivity at BOL.

The natural solution to this problem is to introduce an element in the presence of the fuel that absorbs neutrons (a loss mechanism) which might otherwise cause a fission. The control rods of a reactor are just that – strongly absorbing materials that may be inserted into the core of a reactor to provide a fine level of control. However, it is not common to use control rods to suppress large amounts of reactivity, as this leads to power peaking – fuel rods not near the control rods must contribute most of the power in this state, and that can potentially lead to unsafe situations such as in-core boiling and fuel rod failure. Rather, control rods are generally used in the start-up and shut-down of a reactor. Current generation PWRs use boron dissolved in the coolant to control excess reactivity, as it has the advantages of offering a fine level of control to the operators, and its homogeneity eliminates the power peaking that occurs with control rod usage. Boron is naturally composed of 19.9% ^{10}B, a very strong neutron absorber. Using soluble boron in the amounts required to reduce the IRIS BOL reactivity would compromise safety, though, as it would prohibitively increase the moderator density coefficient, meaning that a decrease in moderator density (increased voiding) would lead to an increase in k_{eff}. Additionally, large amounts of boron solute in the water increase the likelihood of crystallization. For these reasons, the concentration

is commonly "limited to a value of the order of 1500 ppm" in light water reactors [4]. An alternative method of controlling reactivity is to place a neutron-absorbing element in the presence of the fuel that would transmute to a non-absorbing element over the course of fuel depletion. There are several different kinds of such burnable absorbers (or burnable poisons) in existence; boron, gadolinium, and erbium are among the most popular.

1.3 Objectives

The goal of this work is to investigate the use of different burnable absorbers to provide reactivity control over the core life. More specifically, the goal of this research is to put a methodology of core design in place that enables the designers of the IRIS to choose among various core configurations that employ burnable absorbers. For the most part, the research is performed from the perspective of minimizing the swing in k_{eff}, particularly, arriving at some sample core configurations that maintain soluble boron levels under 1500 ppm.

Chapter 2

Computer Methodology

In the approach used in this research, the first step is to create a fuel assembly model detailed enough to allow the investigation of small amounts of burnable poisons in various configurations. The next is to narrow down potential burnable poisons to a few options for deeper investigation. Finally, feasible assembly and core models must be created to provide a design recommendation. To accomplish this, several computer modeling tools must be employed and, in some cases, linked together to share information.

2.1 Computer Modeling

The process of creating a model for a nuclear reactor generally begins by representing a pin cell, assembly, and full core in that order, all of which may be performed with different computer modeling codes. There are two major reasons for this modeling approach. The first reason is that much of the reactor is regular enough that to repeat, say, the magnitude of flux depression in a fuel pin for each of the thousands of fuel pins would be wasteful. The second, less obvious, reason is that global calculations may often be accurately performed with less complicated neutronics models, provided that the parameters underlying them are properly created. As Weston Stacey puts it, "The general procedure that is followed in nuclear reactor analysis is to perform very detailed energy and spatial calculations on a local basis to obtain cross sections averaged over energy and spatial detail which can be used in few group global core calculations" [5]. This is what is known as "homogenization theory," and its central, driving feature is the conservation of reaction rates. In this manner, one may convert a detailed fuel assembly model into several "smeared" cross section parameters, provided the original solution has enough spatial and energy discretizations to account for any effects that can lead to flux variations throughout the assembly. The total absorption rate for the detailed calculation is then defined to be the absorption rate for the entire assembly. Of course, it is impossible to model the exact conditions that a particular assembly may experience in a particular region of a reactor core, so these cross sections are generated

by employing totally reflected boundary conditions along the edges of each assembly.

Once all of the potential assemblies have been modeled in detail, it is the job of a global code to model the interaction of the smeared assemblies with each other to simulate a full core. Typically, this is done with diffusion theory using spatial approximations that allow for meshes larger than the shortest neutron diffusion length [5]. Nodal methods, in particular, solve a neutron balance equation by using high-order spatial approximations to relate node leakages to average fluxes of neighboring nodes. The homogenization procedure for large nodes can introduce substantial errors for heterogeneous assemblies. Therefore, the fluxes are allowed to be discontinuous at the borders via the use of assembly discontinuity factors (ADFs), defined as the ratio of the heterogeneous flux to the node-average flux at a given interface. These ADFs are also calculated during the detailed homogenization process.

2.2 HELIOS

For these studies, the pin cell and assembly are modeled using HELIOS, a two-dimensional, general collision probability code that is highly configurable [6]. HELIOS was developed by Rudi J.J. Stamm'ler for Studsvik Scandpower, and it is widely used for lattice physics calculations at national laboratories and universities. It provides a suite of cross section libraries, based upon ENDF/B-VI, that contain 190 or 45 neutron groups that have been adjusted for the ^{238}U resonance or left unadjusted. A 112 group fast reactor cross section library is also available. "Reentrant polygons" are allowed as flat flux regions, that is, it is not necessary that the boundary of a flat flux region be convex. The user is also required to specify the angular current coupling order at interfaces, allowing for non-uniform cosine currents along a given boundary. The HELIOS program is composed of an input preprocessor, AURORA, the transport code HELIOS, and the output processor ZENITH. AURORA allows the user to designate flat flux regions (thereby controlling modeling accuracy), to create various reactor states to calculate perturbations in modeling conditions, and to specify burnup parameters such as depletion step length and a choice of depletion spectra, among many other things. ZENITH is used to process the raw output data sets in a way that allows the user to examine number densities, power peaking, and cross sections of various kinds.

2.3 NESTLE and FORMOSA-P

The reactor core is modeled using NESTLE, a diffusion code developed by North Carolina State University (NCSU) [7]. NESTLE uses a nodal expansion method to efficiently solve the diffusion equation, and consequently requires homogenized cross section sets. NESTLE allows a choice of two or four energy groups for cross section treatment. Cross sections may be handled using a macroscopic or microscopic model; the microscopic model uses a macroscopic background cross section and explicit microscopic cross sections for eight heavy metals, xenon and samarium, and a simple burnable

poison. Core input geometries may be hexagonal or Cartesian. NESTLE also allows for thermal hydraulic feedback effects, if desired, through the use of a homogeneous equilibrium mixture model. For this modeling capability, coefficients must be created that fit the cross sections to a Taylor expansion about the reference thermal hydraulic state, which is perturbed in coolant density, temperature, soluble boron level, and fuel temperature. Transient scenarios may also be simulated.

FORMOSA-P was also developed by NCSU [8]. It is an optimization code that uses "simulated annealing" [9] to effectively examine a large number of combinations of different assembly types throughout the core to minimize a parameter of interest (like maximum discharge burnup). FORMOSA-P also uses a nodal expansion method to solve the few-group diffusion equation. The user designates a choice of assembly types to shuffle and design constraints such as maximum power peaking or BOL fuel enrichments. The optimization then proceeds by performing a global geometry search, allowing for many dissimilar core geometries, and then constricting the search to simpler geometry perturbations in an effort to explore the promising solutions obtained in the global search. FORMOSA-P models thermal hydraulic feedback much the same way as NESTLE, through the generation of cross section coefficients. Solutions are stored by dissimilarity and by their maximum radial power peaking.

Both diffusion codes use assembly cross sections from HELIOS using an intermediate conversion utility. NESTLE accepts only one core geometry as input but performs more detailed calculations for transient analyses and thermal parameters. FORMOSA-P will eventually be used to output several design suggestions to Westinghouse.

Chapter 3

Computer Benchmarks

Since the creation of a full core model takes several steps and tends to be susceptible to errors, it is common for several models to be created and compared among different groups. Westinghouse has led a series of two such reactor physics benchmarks, differentiated by assembly geometries and absorber materials. The first series employs a 15×15 assembly design and ZrB_2 as an Integral Fuel Burnable Absorber (IFBA). The second series uses a 17×17 assembly design and Er_2O_3 distributed homogeneously in the fuel. This chapter is an account of these two benchmarking efforts. Each series of benchmarks incorporates models of a representative pin cell, assembly, and full core.

3.1 The Original 15×15 Benchmarks

The original IRIS benchmarks (15×15 assembly design) consist of several pin cell cases, an assembly case, and a core depletion case [10]. They are designated as the Pin Cell, Assembly, IFBA Pin Cell, and Core benchmarks, or simply benchmarks one through four. In the first three, only the AURORA-HELIOS-ZENITH code sequence is used. The last requires the use of a core diffusion code for the various assemblies, for which NESTLE is used. In all cases a 45-neutron-group library based on ENDF/B-VI is employed. Both HELIOS and NESTLE use a predictor-corrector method for fuel depletion, so the reactivity profile is not highly dependent on burnup step size. For these benchmarks, Westinghouse has employed the codes PHOENIX-P and ANC, the University of California at Berkeley (UCB) uses MOCUP, and the Instituto Nacional Investigaciones Nucleares (ININ) also uses HELIOS. The original purpose of these benchmarks was to ensure that the various IRIS groups involved all had similar starting points before they moved on to other studies. Thus, these benchmarks are focused on removing divergent assumptions among the groups, rather than obtaining precise results. Comparisons in this document are mostly made on a percent difference to average basis, although it can not be assured that the average solution is the nearest to the actual solution.

3.1.1 Pin Cell Benchmark

Specifications

The purpose of the pin cell benchmark is to compare results among the IRIS group with a simple case constrained with exact assumptions. Figure B.1 illustrates the simple geometry and was generated using the ORION viewer. The geometry is essentially a fuel pin surrounded by cladding and moderator, for spacing in a square array.

The fuel is smeared across the gap; therefore, the cladding's inner diameter equals the pellet's outer diameter. The fuel is uranium oxide enriched to 4.95 wt% Uranium-235. The number density is adjusted to empirical data and for pellet dishing. The cladding is zircaloy. The boundary condition at the edge of the pin cell is specular reflection. Burnup is performed to 48 MWD/kgU. There are no adjustments for thermal expansion, as differences in the computer codes used between the IRIS groups could potentially contribute to differences in results.

Infinite Multiplication Factor

The swing in k_∞ over the life of this pin cell is quite large, ranging from a k_∞ of about 1.4 to 1.0 from the BOL to the end of life (EOL) of the cell (see Table B.1). This is due to the relatively high enrichment without the presence of poisons. A graphical depiction of this is also presented in Figure B.2. All of the results are within a 0.5% spread, which, for these purposes, is acceptable agreement; this is shown in Figure B.3. The Westinghouse percent difference to the average reported is not shown in this or any of the following benchmark results due to proprietary issues, although the results are included in the calculation of the average. This explains why the results of Figure B.3 do not combine to zero.

EOL Isotopics

The number densities of some heavy elements at the last burnup point are presented in Table B.2 in units of atoms/cm^3. A visual comparison is found in Figure B.4; there the isotopic number densities are presented as a ratio to the reported average. There is excellent agreement among all the isotopes with the exception of ^{242}Am. This is probably due to differing treatments of the metastable version of this isotope. The half-life of ^{242m}Am is 160 years, while ^{242}Am has a half-life of 16 hours. Thus, ^{242}Am does not exist in appreciable quantities in LWRs, and is not followed in the HELIOS code schema. Some hand calculations[1] confirm this fact. The number density reported by UT/ORNL is only due to ^{242m}Am; others may have reported the sum of the two states. Also, since the scope of this work does not include fuel reprocessing or related activities, close agreement in this section is not critical.

[1]The decay rate of this isotope is three orders of magnitude more than its absorption rate in a typical LWR flux.

Fluxes

Several flux parameters were requested for benchmark 1. The first of these are the total cell-average fluxes, which are reported in Table B.3. UT/ORNL results are within two percent of the average.

The second set of flux parameters are the fast and thermal fluxes, along with their ratios, reported both at BOL and EOL for the pin cell. These data are found in Table B.4. UCB did not report these numbers. Averages for these figures were not computed, but, UT/ORNL results were found to be in agreement among the groups that did report these values.

Finally there are the region-wise flux ratios, found in Table B.5. Nowhere do the UT/ORNL results vary from the mean by more than 0.11%; in fact, no group member's data deviates by more than 0.37%. From these and the above data, one may draw the preliminary conclusion that benchmark 1 is successful and we may proceed to the assembly benchmark.

3.1.2 Assembly Benchmark

Specifications

The results for benchmark 2, the fuel assembly benchmark are presented below. All parameters for the fuel cells are identical to those in the pin cell benchmark, but with the zirconium grids smeared into the moderator – one percent by volume. The entire assembly is composed of 15×15 unit cells, which is subdivided into 204 fuel cells, 20 guide tubes, and 1 instrumentation tube. The non-fuel cells are modeled as moderator with zirconium tubes. A quarter-assembly geometry is shown in Figure C.1. This Figure was generated using the ORION viewer and also illustrates the nodalization created in HELIOS. The guide tube material is zirconium for this benchmark and is an independent material from the fuel cell cladding. The guide tubes are filled with moderator.

Infinite Multiplication Factor

The results for k_∞ show good agreement among the IRIS consortium (see Figure C.2). At all burnup points the UT/ORNL results are within 0.11% from the average of the team results. The percent difference is shown in Figure C.3, and a chart is provided as Table C.1.

Pin Burnup Distributions

Results for the individual pin burnups are only available from Westinghouse. The UT/ORNL results are presented in Table C.2 according to their burnup point. The tables are laid out such that they represent the upper left quarter of an assembly. Empty spaces are non-fuel locations, and the table is lower triangular since the assembly is symmetric about the diagonal. In all cases the pin-wise burnups are within one percent

of the reported Westinghouse burnups. The units are in MWD/kgU. The highest burnups occur at the pins nearest the control rod guide tubes. This is because the thermal neutron population is greater in those regions due to the additional moderation that the water-filled control rods provide. The distribution, however, is relatively uniform, and this contributes to the good agreement between UT/ORNL and Westinghouse – the maximum percentage difference is 1.0%.

Relative Pin Powers

As a further check of pin-specific parameters, the relative pin powers are presented in Tables C.3 and C.4 for BOL and EOL respectively. These values represent one eighth of an assembly, the upper left corner corresponding to the upper left corner of the assembly, according to their burnups. Benchmark reporting required data at several depletion steps but only BOL and EOL data are shown here. These data also agree relatively well, as the greatest percentage difference at BOL and EOL between UT/ORNL and Westinghouse is 0.9% and 1.1%, respectively .

The results reported are volume-averaged over the assembly according to Equation 3.1.

$$\frac{\sum_{allregions} \kappa\Sigma_f \phi V}{\sum_{allregions} V} = 1 \tag{3.1}$$

HELIOS produces $\kappa\Sigma_f$ as the fission energy production cross section (in joules/cm) generated per user-designated region, group, and burnup. ZENITH then performs sums over these regions and normalizes the powers to unity. To double-check the power distribution, these normalizations were also performed using the fission rate distribution given by Equation 3.2. The results were found to be comparable, the greatest difference being less than 0.1% for any given pin at EOL. Using the fission energy production is more accurate since the Σ_f approach does not account for differences in the average energy per fission for different fissioning isotopes. The values agree, however, since this quantity does not vary much. See Table C.5 for an example comparison.

$$\frac{\sum_{allregions} \Sigma_f \phi V}{\sum_{allregions} V} = 1 \tag{3.2}$$

Once again, for this section the only reported results are from Westinghouse, and all UT/ORNL results are within 1.14% of these.

EOL Isotopics

As in benchmark 1, there is good agreement among the IRIS groups for the residual heavy elements, but the Americium discrepancy remains. Curium isotopes are also reported in this benchmark, and a major discrepancy exists with ^{244}Cm. The reasons for this are unknown; they are perhaps due to different treatments of the burnup chains between different codes. The discrepancy may be tolerated, however, since this isotope

is found in LWRs in only small amounts, and its effect on the design parameters is negligible. See Figure C.4 for a chart of the isotopic ratios to their averages minus one, and Table C.6 for detailed data.

Fluxes

There are no data with which to compare these results, but the benchmark specifications require their reporting. Both thermal and fast fluxes are presented, with the thermal group cut-off at 0.625 eV. The "spectral index," or the ratio of the fast to thermal flux, is shown in Table C.7.

3.1.3 IFBA Pin Cell Benchmark

Specifications

The purpose of this benchmark is to create models for the Integral Fuel Burnable Absorber (IFBA) fuel pellets. The absorber is ^{10}B, and it is designated in units of milligrams per centimeter. All parameters excepting those that involve this absorber layer are identical to benchmark 1.

IFBA fuel pellets contain a very thin outer layer of ZrB_2. This coating is so thin (less than a micrometer) that it was difficult to model explicitly with HELIOS. Parametric studies were performed to compare the BOL k_∞ versus increasing annular thicknesses while holding the ^{10}B content constant by adjusting its number density. At the smallest thickness HELIOS allows (0.001 cm), HELIOS exhibited a differing trend when compared to an identical MCNP study. Refining the collision parameters[2] remedied this effect, which was not too large to begin with, and we continued with the benchmark. Thus, in all cases a 0.00101-cm annular thickness on the outside of the pellet was used, with number densities adjusted to the varying ^{10}B concentrations. For a more thorough discussion on this matter, please see Appendix D.

Infinite Multiplication Factor

The only parameter requested for reporting in this benchmark is k_∞. The data are reported in graphically as Figure E.1. There are also four corresponding figures depicting the percent differences from the reported average (Figures E.2 through E.5). These data do not agree as well as in previous benchmarks. At BOL there is a spread of about 1% among the results of the deterministic codes, and another 1.5% to Monte Carlo results. Reasons for the larger differences are likely due to varying approaches in the handling of the burnable absorber layer between different codes or different nuclear data. In fact, even within the same code, differences larger than half a percent may be obtained as a result of different modeling assumptions (again, see Appendix D for more information).

[2]In the CP section of the HELIOS RUN statement the default values of options one through three were halved and option four was doubled.

The EOL isotopics and fluxes were also investigated; they are much the same as in benchmark 1. The BOL fluxes differ significantly, though, in that for higher IFBA concentrations the flux must also be higher. This is because to achieve the same burnup, more neutrons must be present. Breaking the data down into the fast and thermal groups found the thermal populations to be nearly uniform, which is expected since the thermal flux is the dominant contributor to the power level, but there are significantly more fast neutrons for higher IFBA concentrations. The spectrum is hardened because additional fast neutrons must be generated to compensate for the thermal neutrons being lost to the absorber.

3.1.4 Core Benchmark

The purpose of this benchmark is to provide a simple case that demonstrates the accuracies and abilities of the core depletion tool each IRIS team member decides to use [10]. For UT/ORNL, this tool is NESTLE, and later, for optimization, FORMOSA. These analyses required the modification of a utility created for processing cross section output from HELIOS for input into NESTLE. Thus a single assembly was created to compare results to the above assembly benchmark to assure the accuracy of the utility. It should be noted that the configuration used in this benchmark is not intended to represent a realistic core, in fact, thermal hydraulic feedback is intentionally not modeled in an attempt to reduce differences due to feedback modeling. Power peaking factors are therefore expected to be much higher than usual.

Specifications

Since thermal hydraulic feedback is not modeled, those parameters are not specified. Also, as in the above benchmarks, thermal expansion is neglected. The use of control rods is also not investigated in this benchmark. The fuel enrichments are axially uniform, while radially a 2.6% blanket surrounds the assemblies (i.e. most of the peripheral fuel assemblies have their enrichment reduced to 2.6%). There are ten different types of fuel bundles that are dependent on IFBA concentrations and fuel enrichments; these are shown in Figures F.1 and F.2, obtained from the specification document. The poisoned fuel section has two axial zones with the lower half containing twenty percent more ^{10}B than the upper half. The ^{10}B is modeled as in the IFBA benchmark, in a thin layer surrounding the fuel pellet. The core is fourteen feet tall, with only the middle twelve feet being coated with ZrB_2. The entire core is surrounded by a reflector made up of fifty percent stainless steel and fifty percent water by volume. The reflector is specified as 40-cm thick, which is essentially (neutronically) infinite. Reflector cross sections are generated by placing the volumetrically homogenized reflector material to the right of an assembly with the blanket enrichment, and specifying total reflective boundary conditions to the left with vacuum boundary conditions to the right. A HELIOS calculation is then performed at zero burnup to form collapsed macroscopic cross sections. The assembly discontinuity factors are fixed to unity since the reflector

is homogeneous.

The number densities for the fuel are identical to those used in the assembly benchmark. The moderator density has been changed since from that used in the assembly benchmark to 0.702 g/cm^3. The clad and the grids are made up of zircaloy-4, and the grids are homogenized in the moderator at one volume percent. Since NESTLE accepts geometry inputs in maps, the reflector material was placed around the core in "bundles" such that the smallest dimension to the edge of the core is at least 40 cm. Table F.1 shows the actual inputs, with each number representing a different assembly type. Numbers one through ten correspond to fuel numbers with various fuel enrichment and IFBA concentrations, and number eleven is the reflector. For each bundle there are two nodes; these nodes are one half the assembly pitch for the fuel bundles and twenty cm for the reflector. The axial mesh has 32 six-inch nodes, with the middle 28 making up the active core. Equilibrium xenon and samarium conditions are employed. The fission products, with the exception of xenon and samarium, are handled through the conversion utility by lumping their cross-sections together by group and burnup, and passing this information to NESTLE. NESTLE then treats all the fission products as one isotope and calculates accordingly. Note that boron is explicitly handled as a lumped burnable poison. The outer iterations (k_{eff}) are set to converge to a tolerance of 1×10^{-6}, and the inner iterations (fluxes) to 0.5×10^{-5}. The predictor/corrector mode for depletion calculations is also available in NESTLE.

Conversion Utility Verification

For this section a simple "core" was made that consisted of an assembly identical in all ways to that specified in benchmark 2. The cross sections from HELIOS were processed with the utility and formatted for input into NESTLE version 5.0.2. A table of the results for k_∞ is given in Table F.2 . This accuracy is enough to conclude that the conversion utility is not introducing significant error into the core modeling program. The discrepancy at the beginning is due to differences in the treatment of xenon and samarium.

Results

Even with the addition of IFBA, the BOL k_{eff} begins at values higher than 1.2. Results are shown in Figure F.3. From these results, the POLIMI core ends its life at 34 MWD/kgU while the UT/ORNL core ends at 32 MWD/kgU.

The axial offset is the difference in the power produced in the top half of a reactor core and the bottom half divided by the total power. Figure F.4 depicts the axial offset of the core power over burnup. The value swings from high to low during the lifetime of the core due to the differences in IFBA loading in the top and bottom sections of the core. The UT/ORNL values swing to slightly more extreme values than POLIMI's, reaching maximum values at around ± 45 percent. This high value of axial offset, as well as that of the axial and total peaking factors, is due to intentionally neglecting the thermal

hydraulic feedback in this benchmarking analysis. Figure F.5 depicts the maximum relative nodal power peaking over the core lifetime for POLIMI and UT/ORNL. The maximum occurs at 3.8 or so for UT/ORNL, and at 4.5 for POLIMI. The trends look similar. The last two figures for reporting are the radial and axial power profiles, Figures F.6 and F.7. While the BOL profiles, in general, look a little different, the remaining data follow similar trends. The BOL variations in all of the above cases are probably due to differences between POLIMI's and UT/ORNL's treatment of xenon and samarium. Finally, the bundle-wise burnup is provided at the EOL in Table F.3.

3.2 Erbium Benchmarks

This series of benchmarks [11] consists of several pin cell and assembly cases and a core depletion case that includes thermal hydraulic feedback. Each of these benchmarks are calculated with four absorber states. a no-poison case, a 1.0 wt% and 2.2 wt% case, and a soluble-boron letdown case, simulating actual operation, that contains 1.0 wt% erbium. The main objective of this series is again to allow each IRIS team member to create computer models that do not contain divergent assumptions, or, at least, to understand modeling differences obtained from using different codes. Participants include Westinghouse and the University of Zagreb. Another objective is to approach a more realistic core design through the simulation of a two-batch loading that incorporates thermal-hydraulic feedback.

3.2.1 Erbium Pin Cell

Each pin cell is modeled using the collision probability code HELIOS and a 190-neutron group ENDF/B-VI cross section library.[3] The fuel pins are subdivided into five flat flux regions, and a parametric study was performed to evaluate the effect of refining the mesh of the fuel regions. The critical buckling spectrum is used for depletion, but the infinite spectrum multiplication factor is reported at each burnup step. Thermal expansion is not modeled, but the materials are set to nominal operating temperatures as dictated in the benchmark specifications. The soluble boron pin cell case is modeled in discrete steps. The boron is modeled as 19.9% ^{10}B and 80.1% ^{11}B.

Specifications

While it is somewhat easy to calculate the number densities for the no erbium fuel, in the other three benchmarks the UO_2 number density must reduced by the necessary amount to account for the presence of Er_2O_3. This is done according to the method given in the specification document [11]; this document cites the method published in *The CRC Handbook of Chemistry*. Using Equation 3.3 one can develop a correction

[3] Actually, the HELIOS manual states that "Erbium and Thulium data have not been taken from the ENDF/B-VI files. Instead, they have been obtained as described by Sing and Johnson (1993)," with Mughabghab *et al* providing resonance parameters.

factor to modify the original density. That is, if α is defined as in Equation 3.4, then the fuel density is given by Equation 3.5.

$$\frac{1}{\rho_{mix}} = \frac{W_{UO_2}}{\rho_{UO_2}} + \frac{W_{Er_2O_3}}{\rho_{Er_2O_3}} \tag{3.3}$$

$$\alpha = \frac{\rho_{UO_2}}{\rho_{Er_2O_3}} - 1 \tag{3.4}$$

$$\rho_{mix} = \rho_{UO_2} \frac{1}{1 + \alpha W_{Er_2O_3}} \tag{3.5}$$

Erbium is isotopically modeled according to Table G.1, whose data are obtained online from the Brookhaven Chart of the Nuclides [12]. The simplified version ignores the neutronically unimportant isotopes ^{162}Er and ^{164}Er. UT/ORNL employs the simplified version, as these two isotopes are not in the HELIOS working library.

Infinite Multiplication Factor

Table G.2 reports the k_∞ values for the four pin cell cases, and they are presented graphically in Figure G.1. "SB" should be understood to represent the soluble boron case with 1.0 wt% erbium. The other three vary only by erbium content.

Isotopics

The number densities for some important heavy isotopes, fission products, and burnable absorbers at 60 MWD/kgU are presented in Table G.3. As expected, there is a significant amount of erbium left even this late in the burnup (2.92% of ^{167}Er). The isotopes are designated in the traditional "ZZAAA" format.

Fluxes

The cell averaged fluxes for the beginning and end burnup points are presented in Table G.4. The cutoff for the thermal group is 0.625 eV. As expected, increasing the amounts of erbium or soluble boron contribute to harder spectra, as illustrated in the ratios of the fast to thermal fluxes.

Fuel Region Sensitivity

A sensitivity study was performed to examine the sensitivity of k_∞ to the refinement of the number of fuel regions. This is necessary since in HELIOS the collision probabilities for a given region are dependent on the flux in that region, and flux values are uniform within each region. The base case for this comparison study contains 2.2 wt% erbium with geometry given by a pin cell containing the greatest refinement – nine equal area regions. Four other cases were investigated, all identical excepting the refinement level of the fuel material. The first case contains a single region, the second contains

two regions such that the outermost region is defined by 0.9 times the pellet radius, the third contains three regions such that the outermost region is 0.9 times the pellet radius while the inner two regions are equal area, and the fourth contains five equal area regions. Results are presented on a percent difference to the base case in Figure G.2.

3.2.2 Erbium Assembly

As in the 15×15 IRIS benchmarking effort [13], the fuel cells in the assembly case are identical to the pin cell cases with the exception that additional zirconium is now smeared into the moderator at one percent by volume. The assembly is an array of 17×17 unit cells, which are made up of 264 fuel rods, 24 control rod guide tubes, and one central instrument tube. There are four cases examined in this benchmark as well, corresponding to the no-erbium case, 1.0 wt% Er, 2.2 wt% Er, and 1.0 wt% Er with a soluble boron letdown curve. The first three cases are also examined with control rods fully inserted at BOL. A quarter-assembly geometry is shown in Figure H.1. Thermal expansion is modeled with the materials set to nominal operating temperatures as dictated in the benchmark specifications. The expansion coefficients and temperatures employed are given in Table H.1.

The control rods are silver, indium, and cadmium at 80, 15, and 5 weight percent respectively. The control rod cladding is stainless steel (SS304). The temperature of the control rod material is set to that of the moderator.

Infinite Multiplication Factor

The results for k_∞ for all four assembly models are given in Figure H.2 and Table H.2. "SB" should be understood to mean the soluble boron case at 1.0% erbium.

Power Distribution

The pin-wise power distribution may be found in Tables H.3 through H.6. the addition of erbium tends to make the pin power peaking slightly worse, as may be seen by comparing Table H.3 to Table H.5. The ranges of relative power in these two cases are [0.930, 1.063] and [0.919, 1.076]. The fuel pins nearest the moderator cells generate more power on the average; this is probably due to erbium's strong epithermal absorption resonance. That is, with the addition of erbium, it becomes even more important for the neutrons to slow down in the moderator. This is expected since erbium is known to have a relatively large resonance integral.

Pin Burnup Distributions

Data for pin-wise burnups may be found in Tables H.7 through H.10. An increase in pin power peaking also leads to an increase in the variance of pin-wise burnup values. Table H.9 had the largest variance, with the range being in [57.0, 62.4] for an average burnup of 60 MWD/kgU. As expected, the highest burnup occurs in a fuel cell

surrounded by guide tubes, and it is this same cell that exhibited the highest power peaking.

Isotopics

The number densities for some important heavy isotopes, fission products, and burnable absorbers at 60 MWD/kgU are presented in Table H.11. As expected, there is a significant amount of erbium left even this late in the burnup (about 2.85% of ^{167}Er). The isotopes are designated in the traditional "ZZAAA" format.

Fluxes

The assembly-averaged fluxes for the beginning and end burnup points are presented in Table H.12. The spectra for the assembly are notably softer than those for the pin cell case due to the presence of extra moderator regions.

Rodded Fuel Assembly Benchmark

The multiplication factor at zero burnup was also requested for rodded assemblies, incorporating 1000 ppm of soluble boron for all three erbium loadings. Table H.13 reports the k_∞ values for the rodded assemblies at BOL. Although the magnitude of reduction of k_∞ reduces with greater amounts of erbium poison, the reactivity change (as computed by Equation 3.6) increases.

$$\frac{\delta k}{k} = \frac{k_1 - k_2}{k_1 k_2} * 100\% \tag{3.6}$$

In the rodded assembly studies, the presence of erbium assists the control rods; reactivity changes increase from 29.3 to 33.7% in the cases without soluble boron, and from 29.1 to 32.9 in the cases with 1000 ppm of soluble boron. Pin power peaking is, of course, much greater than the uncontrolled assemblies – the largest range is [0.826, 1.293], found in the no erbium case. The range for 2.2 wt% erbium loading is [0.849, 1.243]. Adding soluble boron dampens the power peaking by a slight amount in all cases.

Thermal Expansion Sensitivity

A sensitivity study was performed to analyze the effects of modeling or not modeling thermal expansion. Calculations were performed on the three assembly cases without soluble boron, the reference cases being those outlined in the specifications above. The comparison cases were identical in all regards except that they employed cold dimensions (expansion coefficients set to zero). The comparison case that amounted to the most difference was the 1.0 wt% erbium fuel case. The greatest percent difference amounted to -76 pcm at the initial burnup point. After an initial dip, the errors tended to grow

slowly (in value) over the assembly lifetime. Results are presented on a percent mille difference to the base case in Figure H.3.

3.2.3 Erbium Core

The purpose of this benchmark is much the same as the original IRIS core benchmark, but this core is more realistic in that it contains thermal hydraulic feedback, employs a geometry more characteristic of a two-batch core loading scheme, and uses erbium burnable absorber. Detailed core specifications are listed in an internal Westinghouse document [11]. As in the above core model, the cross section conversion utility was verified for accuracy.

Specifications

Each assembly is modeled using the collision-probability code HELIOS and a 190-neutron group ENDF/B-VI cross section library. The fuel pins are subdivided into five flat flux regions. Thermal expansion is modeled implicitly through the generation of cross sections in HELIOS, and explicitly by putting expanded assembly dimensions into NESTLE.

Thermal hydraulic feedback is modeled, so "branch cases" to produce cross section coefficients were performed. The coefficients are created using second-order Taylor expansions for soluble boron and moderator density, and first order for the moderator temperature and square root of the fuel temperature – a total of six branch cases. Coolant properties are modeled based on polynomial fits to table data, and fuel temperature and thermal properties are also fitted to data from a simple heat transfer model. Since the benchmark specified a core inlet and outlet temperature, and NESTLE accepts an inlet temperature and flow rate as input, a coolant mass flow rate was calculated and adjusted to obtain the proper core exit temperature. The use of control rods is not investigated in this benchmark. The axial and radial reflector cross section data are provided by Westinghouse, and are modeled to be constant with respect to depletion and thermal hydraulic feedback. There are four different types of fuel bundles that are dependent on erbium loadings and fuel enrichments. The number densities for the fuel are created using the same method employed in the assembly benchmark. The clad and the grids are made up of zircaloy-4, and the grids are homogenized in the moderator at one volume percent. A core average fuel density and heavy metal ratio were calculated for input into NESTLE.

Since NESTLE accepts geometry inputs in maps, the reflector material was placed around the core in "bundles" such that the smallest dimension to the edge of the core is at the specified length. Table I.1 shows the actual inputs, with each number representing a different assembly type. Numbers one through four correspond to appropriate fuel assemblies with various fuel enrichments and erbium loadings, and number five is the reflector. For each bundle there are two nodes The axial mesh has 32 nodes, with the middle 28 making up the active core. The core is depleted at a power density that

corresponds to 1000 MW-thermal. Equilibrium xenon and samarium conditions are employed throughout the core life with the exception of the zero burnup "clean" condition. The fission products, with the exception of xenon and samarium, are handled through the conversion utility by lumping their cross sections together by group and burnup and passing this information to NESTLE. NESTLE then treats all the fission products as one isotope and calculates accordingly. Erbium isotopics are handled implicitly in the background macroscopic cross sections. The outer iterations (k_{eff}) are set to converge to a tolerance of 1×10^{-6}, and the inner iterations (fluxes) to 0.5×10^{-4}. The predictor/corrector mode for depletion calculations is also available in NESTLE.

Conversion Utility Verification

Since the burnable absorber type for this core changed due to new specifications, and several cross section coefficients resulting from branch cases had to be provided to NESTLE, it is necessary to again verify the fidelity of the conversion utility. A simple "core" was made that consisted of an assembly with a 1.5% erbium loading, depleted with 600 ppm soluble boron in the moderator. The cross sections from HELIOS were processed with the utility and formatted for input into NESTLE version 5.0.2. A comparison of the resulting k_∞ values is given in Table I.2. The accuracy is enough to conclude that the conversion utility is not introducing significant error into the core-modeling program. The discrepancy at the beginning is due to differences in the treatment of xenon and samarium, an effect that is remedied in the version the core model employs (5.0.3).

Results

After equilibrium Xe and Sm conditions are reached, the soluble boron level stabilizes at approximately 1100 ppm before dropping to 10 ppm at a (projected) burnup of 24.98 MWD/kgU. Results are shown in Figure I.1 and Table I.3. Table I.3 also contains the results for the maximum nodal power by peaking by node (Fq), averaged axial node (FZ), and average radial bundle (FdH), as well as the percentage axial offset. Pin-wise maximum power peaking is not available in NESTLE for cores employing a square pitch. A figure depicting the axial offset of the core power over burnup is provided as Figure I.2. The value swings from high to low during the lifetime of the core due to the differences in erbium loading in the top fourth and bottom three fourths of the core, and ranges from 17% to -6%. Figure I.3 depicts the maximum relative nodal power peaking (full core, axial, and radial) over the core lifetime. The maximum is about 2.3. The last two figures for reporting are the radial and axial power profiles, Figure I.4 and Figure I.5. It should be noted that, in the case of the radial profile, NESTLE only produces the average relative power per bundle. Node-wise power peaking maps by vertical slice and burnup point are available, though. Additionally, Tables I.4 and I.5 report the radial power peaking maps for two core average burnups. Finally, the bundle-wise burnup is provided at 24 MWD/kgU in Table I.6.

Further Analyses

In discussions with Westinghouse and the University of Zagreb, it was suggested that the NESTLE model be rerun without the critical boron search, and, additionally, with a geometry that has only one burnable absorber enrichment (1.8 wt% Er_2O_3), with and without a soluble boron search. These calculations were performed to identify modeling errors and assumptions. For these studies, only the integral parameters are reported. For each core the input mass coolant flows are identical, although the heavy metal content and average densities are changed to reflect differences in core makeup.

Integral parameters for the benchmark core with a critical boron search are shown in Table I.7. The EOC occurs slightly above 24 MWD/kgU, since k_{eff} at this point is only 57 pcm from unity. The axial offset is more pronounced than that reported in the above results, and the power peaking as well, suggesting that the axial power distribution is heavily influenced by soluble boron content. The results for the core with a uniform burnable absorber enrichment are shown in Table I.8. The EOC for this core is extrapolated to be 24.83 MWD/kgU, which is 0.15 MWD/kgU less than the core with benchmark specifications. Overall the critical soluble boron ranges from about 50 to 10 ppm less than the benchmark core, as would be expected from the higher erbium content. The power peaking and axial offset parameters are also significantly higher than that of the benchmark core; Fq has a maximum at 3.2 and the percent offset ranges from -52 to 9.5%. The same core without a critical boron search has integral parameters listed in Table I.9. Once again, it is reasonable to assume an EOC at just above 24 MWD/kgU, since k_{eff} is only 31 pcm from unity. The reactivity swing for this core ranges from 754 to 87 pcm less than benchmark core (without soluble boron). The axial offset for this case begins strongly negative at -37.8% and swings up to 5% over the core lifetime, most likely due to moderator density feedback.

Conclusions

This erbium core model begins with a critical soluble boron level near 1100 ppm and has an end of cycle at 24.98 MWD/kgU. Overall the agreement between Westinghouse and UT/ORNL is satisfactory. The soluble boron level is a little higher and the EOC a little longer than the results Westinghouse obtained. This is perhaps due to a difference in assembly level models between UT/ORNL and Westinghouse, but could be due to differences in other assumptions. The cross section conversion utility is probably not the cause of this difference, as, later in burnup, the greatest difference between equivalent assembly models is still on the order of 0.1%.

The maximum nodal power peaking, 2.25, occurs at 0.15 MWD/kgU. The percentage axial offset begins at 17% and ranges to -6% over the core lifetime. This shift is expected due to the lower poison concentration in the top fourth of the core.

Further analyses show that the deviation in axial offset from the Westinghouse core model may be due to soluble boron treatment, although, even without soluble boron, the power peaking in the UT/ORNL model is slightly higher than Westinghouse predictions.

It is also surprising how great an effect soluble boron has on the axial offset for a core with a uniform absorber loading. Since the axial offset is a somewhat sensitive parameter, though, close agreement is difficult to obtain and for the purposes of this work relatively large differences are acceptable.

3.3 Preliminary Conclusions

Two series of benchmarks have been completed among the IRIS neutronics team members to ensure that each member is employing the same assumptions and have models in place that, for the most part, agree with each other. One series examined the use of ZrB_2 as a burnable absorber, and one employed erbium. The core designs that completed each of these benchmarks should be thought of as preliminary and for benchmark purposes only, but already one can see clearly that the IRIS's final core design would benefit from employing an innovative use of burnable absorbers – even a preliminary two-batch core design needs around 1100 ppm of soluble boron at the beginning of its cycle.

Chapter 4

Burnable Poison Design

4.1 Overview of Fixed Burnable Poisons

Burnable poisons currently in use include boron, gadolinium, erbium, and dysprosium. In the original IRIS core design, Westinghouse used boron in the form of a ZrB_2 coating on the fuel pellets (the standard IFBA concept). The remaining burnable absorber materials are rare earth elements that are generally used by uniformly mixing them into the fuel via co-milling the materials in their oxide forms.

Since boron's primary absorption mode is ^{10}B's high thermal neutron capture, it burns away too quickly to control reactivity late in the IRIS long reactor cycle. Large amounts of ZrB_2 also can create undesirable internal fuel pin pressures [14], although this is not a problem in the IRIS since it has plenty of excess plenum volume. Dysprosium has been used in CANDU type reactors, but its burnup chain is long and leads to other absorbers with penalizing residual reactivity at the end of cycle [4]. The choice for IRIS is therefore primarily limited to the gadolinium and erbium burnable absorbers.

Gadolinium has a large thermal cross section of 49,000 barns [4] primarily due to the isotopes ^{155}Gd and ^{157}Gd, which make up 14.8 and 15.7% of the element respectively, by atomic abundance. A graph of the total cross sections for these two isotopes is given in Figure J.1. To make it last in a thermal flux environment for the duration of the core life, it is necessary to lump it among a small number of fuel pins in relatively high concentrations in order to obtain a self-shielding effect. Currently, gadolinium is used in levels up to around eight weight percent enrichment. These studies will assume that ten weight percent is the practical limit on gadolinium loading in the fuel. Gadolinium's high thermal absorption and burnup chain allow for a high consumption of the poison by the end of cycle, a feature that makes the use of this poison very attractive.

Erbium, in comparison to gadolinium, has a low thermal cross section and primarily functions as an epithermal resonance absorber. Its neutronically important isotope is ^{167}Er, giving an elemental resonance integral of 740 barns. Its total cross section is given in Figure J.2. With a significant portion of its absorption lying in the resonance range, the poisoning mode of erbium differs from gadolinium since its presence does not

"disturb the neutron flux" [4] . Erbium may therefore be fabricated to be more dilute among the fuel pins in lower concentrations relative to gadolinium. Like dysprosium, erbium does not completely burn out and therefore usually results in an EOL residual reactivity penalty.

Tantalum was briefly investigated for use as a burnable absorber in an attempt to control reactivity late in the life of an assembly, as natural Ta is almost 100% ^{181}Ta which converts to the poison ^{182}Ta upon the absorption of a neutron. This poison then burns out, so the hope was to have a two-tier poison that suppresses reactivity late in the reactor life. Unfortunately the thermal cross section of ^{182}Ta is 1000 times higher than that of ^{181}Ta, so the effect is to drastically reduce k_∞ at EOL when it is used in appreciable amounts. A graph of the cross sections, available from reference [12], is given as Figure J.3. Thus tantalum was not judged to be of practical use in the IRIS assembly.

4.2 Assembly Studies

Since gadolinium and erbium have such different modes of absorption, it is necessary to concentrate some time on both assembly models. This section explores the effects of varying poison content and geometry on some lattice physics parameters. The models were created using HELIOS, and they are depleted using the critical buckling spectrum. The models are identical with the exception of the libraries used for depletion, choice of material content, and refinement of the burnup calculations.

4.2.1 Gadolinium

The density used for pure Gd_2O_3 is 8.33 g/cc, taken from reference [15]. Gd_2O_3 exists in two phases, cubic and monoclinic, where the monoclinic state has a greater density and is stable over the operating temperature regime of nuclear fuels in a PWR. It is, of course, advantageous to employ Gd_2O_3 in the highest possible density to minimize fuel displacement and maximize self-shielding effects. The mixture density of UO_2 and Gd_2O_3 is calculated using Equation 3.3. Reference [15] also reports that for "0-5 wt% Gd_2O_3 compositions, the increase (in thermal expansion of the mixture) is negligible," although it is known that higher loadings tend to increase the thermal expansion by a slight amount. This research will therefore assume a nominal value of thermal expansion of the UO_2 fuel for all mixtures. Each isotope is handled independently in HELIOS and is set to the natural atomic abundance given in reference [12]. Research is underway to enrich Gd to higher levels of ^{155}Gd and ^{157}Gd in a more economical manner [14], but, these studies will assume only the current technology is available.

To begin in a somewhat academic way, for the moment, assume that there is no limit to the amount of Gd_2O_3 one may mix into the fuel. While this may not lead to a practical solution, it affords the ability to find an optimal design to be used for comparison. Figure J.4 depicts the results from such an assumption. The ideal reactivity

swing for a given assembly design is *no* swing at all from an initial k_∞ just above unity. From visual inspection, Figure J.4 depicts the optimum Gd_2O_3 loading for a given pin geometry. Here, "optimum" (or "ideal") is taken to mean only that k_∞, for the most part, does not exceed 1.05 – other operational and safety parameters are not considered. It may be seen at once that gadolinium must be lumped in a relatively small number of pins; 32 pins at 2.6 wt% seems to be the best solution. Unfortunately, this results in a pin loading of 21.45 wt%, which is too high for practical implementation. Note how, in Figure J.4, none of the curves employing burnable poison completely burn out and rejoin the "No BP" curve – this is the penalty for using Gd_2O_3 in these configurations.

Figure J.5 depicts the same geometries with a hard limit of 10 wt% Gd_2O_3 per pin enforced. It represents a significant loss from the above "ideal" solution, but a core design using 28 pins, the most lumped solution of this study, may still be possible. The use of burnable absorber rods in the place of fuel rods is not examined in this research, as it is felt that the fuel displacement resulting from such a geometry would probably outweigh the benefits of the longer cycle length resulting from the use of burnable poisons. Pin power peaking at BOL for the 28 pin design already ranges over [0.32, 1.24], so decreasing the number of poison pins beyond 28 is also not examined here (as shown in Table J.1).

It is noteworthy that, for these models, a relatively fine depletion step length is used. This is because gadolinium's large thermal cross section results in a fairly rapid, nonlinear burnup that even a predictor/corrector algorithm has difficulty unfolding. Figure J.6 illustrates this fact with the results of three models that are identical with the exception of depletion step length. The model used to generate the above figures uses a combination of a very fine depletion scheme at BOC and a medium one throughout the rest of the cycle. It also uses the 45 neutron group HELIOS library, which differs from the 190 group library results by at most 0.18%.

Before proceeding to the core studies it is wise to check the moderator density coefficient (MDC) and moderator temperature coefficient (MTC). For reactor safety, the MDC should be positive at all times, and the MTC negative. Both of these coefficients are readily modeled in HELIOS by performing branch cases from the main depletion path of the assembly. The assemblies are modeled at hot-full-power conditions with no soluble boron. In the case of the MDC, at burnup points 0, 10, 20, and 30 MWD/kgU, k_∞ is obtained at densities ranging from 0.05 to 1.25 times the nominal moderator density, and the difference to the nominal state is calculated for comparison. For the MTC, the same burnup points are used, but the temperature of the moderator (leaving the fuel temperature and moderator density constant) is permuted at values ranging from 0.5 to 1.5 times the nominal moderator temperature, in increments of 0.05. The true MTC is then calculated by combining the effects of isobaric moderator temperature (and density) changes using water properties obtained from the National Institute of Standards and Technology. The results of these studies are presented in the next chapter of this report.

4.2.2 Erbium

Most of the primary assumptions in the erbium assembly design are addressed in the preceding benchmark section. The density of Er_2O_3 is taken to be about 90% of its theoretical density of 8.6 g/cc [4]. See Table G.1 for the exact isotopic representation. As in the benchmarks, a 190 neutron group library is employed.

Since erbium has a more homogeneous mode of absorption than gadolinium, it is not as necessary to lump erbium among a small number of fuel pins. Therefore it is not as likely an upper limit will be reached, and it is possible that the ideal erbium loading will be a realistic solution. Figure J.7 depicts the optimum Er_2O_3 loading for a given pin geometry. One may immediately notice that the EOL reactivity penalty for using erbium burnable poison is much greater than that for gadolinium. The 80-pin geometry using a 3.1% erbium loading (10.23% by pin) seems to be an ideal solution from a reactivity swing standpoint, but the 104-pin geometry at 2.8% erbium (7.11% by pin) may be a better option since there are less residual effects at EOC. As in the case of gadolinium, keeping the total loading to under 10 wt% means reducing the 80-pin solution to 3.03%, but, for this case, it is a minor concession from the "ideal" solution. Also, Figure J.7 demonstrates that changing the number of pins does not have as large an effect on the reactivity swing as it does for gadolinium – pin numbers here range from 64 to 128, while the number of pins examined for gadolinium only ranges from 28 to 40. Erbium geometries, therefore, allow for more freedom of design. As with the gadolinium assembly, MTC and MDC studies are also performed for an erbium assembly.

4.3 Core Studies

The approach to performing the full core studies is to use the IRIS geometry that has been employed in the previous series of benchmarks, but to use the above optimized assembly designs in the place of the benchmark specifications. A checkerboard pattern of assembly placement has been chosen to emulate a two-batch core. The checkerboard pattern is then surrounded by radial and axial blankets of a lower fuel enrichment. Otherwise, the assemblies are axially uniform with respect to enrichment and burnable absorber loading, and, since there are only two fuel types in the loading pattern, the cores are not radially optimized. The purpose of these studies is to examine the limiting configurations for burnable poison design, in essence to show that the basic methodology of arriving at a final core design is functional. The final design, for submittal to the NRC, will have to address several key design safety margins. Limiting design safety margins include a negative MTC, a positive MDC, maximum critical soluble boron, maximum power peaking among fuel pins and assemblies, maximum average burnups, maximum fuel centerline temperatures, and the maximum critical heat flux. As future work, FORMOSA-P will be employed to shuffle among a wide range of possible configurations to achieve an optimal core design that maximizes discharge burnup within the constraints of maximum soluble boron and power peaking levels.

4.3.1 Gadolinium Core

Even with careful attention to detail with respect to the depletion step length, it was found that suitable homogenized cross sections could not be generated without reducing the steps to values on the order of 0.1 MWD/kgU, especially over a range of burnups spanning from BOL to about 20 MWD/kgU. Figure J.8 depicts the k_∞ pcm difference to HELIOS for k_∞ as calculated by the homogenized cross sections produced by HELIOS. That is, it is k_∞ as calculated using an infinite medium two-group balance condition, shown in Equation 4.1.

$$\begin{aligned} (\Sigma_a^1 + \Sigma_s^{1\to 2})\phi_1 &= \frac{1}{k_\infty}(\nu\Sigma_f^1\phi_1 + \nu\Sigma_f^2\phi_2) \\ \Sigma_a^2\phi_2 &= \Sigma_s^{1\to 2}\phi_1 \end{aligned} \tag{4.1}$$

The "fine" depletion curve is performed at intervals of 0.2 MWD/kgU up to 1 MWD/kgU, and then 1 MWD/kgU intervals until 36 MWD/kgU is reached. The "ultrafine" curve is calculated with 0.1 MWD/kgU intervals up to 6 MWD/kgU, where the new step length becomes 0.5 MWD/kgU up to 26 MWD/kgU. After this point, the two curves have the same depletion steps. There is a sudden increase at 6 MWD/kgU for the "ultrafine" curve, since that is the point at which the depletion steps change from 0.1 to 0.5 MWD/kgU, but the maximum deviation from the HELIOS k_∞ does not exceed 200 pcm.

In addition to further refining the depletion meshpoints, gadolinium may be handled in one of several manners. NESTLE has the capability of controlling some important isotopes (including most of the heavy metals along with xenon, samarium, and a lumped fission product) explicitly through the calculation of microscopic cross sections and initial number densities. Practically, this is done by treating the macroscopic cross section as a "background" cross section after removing the effects of each isotope to be handled explicitly. Although the gadolinium burnup chain is not modeled in the code, NESTLE has the capability of allowing for a "simple" burnable poison model for explicit handling. There are then three approaches to handling gadolinium: leave it in the background, handle either of the primary absorbers independently (^{155}Gd or ^{157}Gd), or weight the two primary absorbers by their number densities and lump the cross sections together. Surprisingly, the best method is to leave the gadolinium in the background cross section, as may be seen in Figure J.9. The "HELXS" data series is k_∞ as calculated by Equation 4.1; it is the name of the cross section conversion utility. The remaining "NESTLE, ..." data series are the k_∞ percent mille differences to HELIOS results obtained from treating gadolinium as a simple burnable poison in various ways (in equivalent infinite lattice models). The "No BP" series means that the simple burnable poison feature of NESTLE is not being employed; i.e. gadolinium is left in the background macroscopic cross section.

Finally, thermal hydraulic feedback is modeled in this core, mostly for determining whether a configuration so heavily loaded with burnable absorbers is feasible. As in

the erbium benchmark case with thermal hydraulic feedback, branch cases from the main depletion path are created at two moderator density states, two soluble boron states, one fuel temperature, and one moderator temperature. The branch case cross sections are processed with the conversion utility to create coefficients based on Taylor expansions; no more than quadratic coefficients are used. The inlet mass flow rate and temperature is set to provide a 1000 MW-thermal reactor, and the core average density and heavy metal makeup are modified to reflect the new loading conditions. The critical soluble boron letdown curve is then calculated up to 28 MWD/kgU.

4.3.2 Erbium Core

Erbium cross section processing is not as difficult as gadolinium. The originally prescribed depletion steps are sufficient, and Figure J.10 shows that there is little difference between treating ^{167}Er explicitly and leaving it in the background macroscopic cross sections. As above, the "HELXS" curve is that calculated by Equation 4.1. Figure J.10 does show that the model worsens as higher burnups are reached; above 40 MWD/kgU the difference amounts to over 300 pcm. The core model only reaches an average burnup of 28 MWD/kgU, however, so this accuracy is sufficient.

Finally, as with the gadolinium core, thermal hydraulic feedback is modeled to allow for the inspection of in-core boiling and accurate power peaking reporting, and the critical soluble boron letdown curve is calculated.

Chapter 5

Results

5.1 Gadolinium vs. Erbium

Figure K.1 shows the final, optimal assembly designs (from the standpoint of reactivity swing minimization) for erbium and gadolinium burnable poisons. The "no BP" case is provided to illustrate the gain in the reactivity control throughout the core life. There are two gadolinium curves; the 32-pin configuration at 2.6 wt% Gd_2O_3 would be the true optimum, but enforcing an upper limit of 10 wt% Gd_2O_3 per pin leads to the choice of the 28-pin configuration at 1.061 wt% Gd_2O_3 per assembly. The optimum erbium design chosen is 104 pins at 1.8 wt% Er_2O_3 by assembly. Unfortunately, this configuration leads to an EOL penalty of about 6 MWD/kgU. Because of the residual penalty resulting from the use of erbium, a final core design may need to employ gadolinium to as great an extent as possible and perhaps use erbium as a supplement if gadolinium alone falls short.

5.1.1 MDC and MTC

It was stated earlier that, ideally, the MDC should be always positive and the MTC negative. Figure K.2 shows that the MDC for the gadolinium configuration is always positive, which means this solution is plausible. This figure was generated using a 28-pin geometry with a 10 wt% Gd_2O_3 loading per burnable aborber pin. The MTC is negative, with values ranging from -10 to -85 pcm/K, as may be seen in Figure K.3. The slight oscillations are an artifact of approximating the derivative of k_∞ with respect to changes in moderator temperature (and density). It is a little surprising that the MTC is not changing uniformly with burnup – at 475 K, the 0 MWD/kgU value has the lowest MTC (-20 pcm/K) and the 20 MWD/kgU value has the highest (-12 pcm/K). The results also intersect at various temperatures. One would expect the effects from burnable absorber doping to uniformly lessen with burnup, as the Gd_2O_3 content must decline over this period. It is perhaps caused by changes in the rate of gadolinium absorption during burnup; at BOL, much of the gadolinium in the 28 pins is shielded

from the normal neutron population. Referring back to Figure J.4, one may see that for very high poison loadings, at BOL k_∞ can *decrease* for a period before rising again. During this early period, the gadolinium that is being removed due to neutron capture is exposing more gadolinium to the thermal flux, thereby decreasing k_∞. In the case of this loading geometry, the decrease is not as significant, but it exists nonetheless.

For an erbium loading, results of permuting the density of the moderator are shown in Figure K.4. Once again, the MDC is positive throughout the core life. This figure was generated using the 80-pin geometry at 2.5 wt% Er_2O_3. The MTC for this case is shown in Figure K.5. It is negative at all four burnup points, rising fairly uniformly with increasing burnup.

5.2 Core Studies

Two core configurations are examined, one employing gadolinium and the other employing erbium. No optimization is performed at the core level. Overall, the results of the core studies are good from the perspective of BOL reactivity suppression, but require further optimization from a safety perspective. Both examined core designs have relatively high peaking factors that will need to be remedied by a more sophisticated burnable poison placement method, specifically, by using different axial and/or radial zones.

5.2.1 Gadolinium Core

Integral parameters for the simple gadolinium core design are shown in Table K.1, and the critical soluble boron letdown curve is depicted in Figure K.6. Note that the maximum soluble boron at BOC is 1460 ppm, less than the 1500 ppm limit discussed earlier. As expected, employing gadolinium as the burnable absorber allows for a relatively longer core life than that of the erbium core given in the benchmark, as there is less residual reactivity and fuel displacement. The estimated EOC for this core (the point at which 10 ppm SB is reached) is 26.32 MWD/kgU. There is also a notable hump in the soluble boron letdown curve at 10 MWD/kgU, where the gadolinium has been fully depleted. Figure K.7 shows the percentage axial offset of the power distribution throughout the core life; it ranges from -14 to 14%. One would expect that, for a uniform axial fuel and absorber enrichment, the axial offset should begin negative and become slightly positive during depletion. For this core model the offset begins positive, swings negative at 2 MWD/kgU, and becomes positive again at 14 MWD/kgU. The minimum value occurs at 10 MWD/kgU. Power peaking parameters (shown in Figure K.8) are too high for a real core design – Fq, the maximum nodal power peaking, ranges from 3.0 to 1.7 over the core life, while FdH, the maximum radial power peaking, ranges from 1.97 to 1.35. An investigation of the coolant density near the top of the core shows values as low as 0.37 g/cc near the core center at BOC (this is confirmed with a hand calculation using FdH and water properties for the channel in question). As future work, this

design should be modified to prevent such power peaking and boiling by using various levels of poison loadings or fuel enrichments axially and radially. Two relative radial power maps are presented in Tables K.2 and K.3, representing the distributions at the beginning and end of cycle. It is obvious from these figures that the central assemblies are causing the most concern, as would be expected from the higher flux levels there. The two assemblies surrounding the center of the core have power peaking levels as high as 1.9 at BOC. The radial power profile along the core symmetry line for several burnup points is also presented in Figure K.9; this line includes the aforementioned assemblies. The zig-zag pattern is due to the checkerboard arrangement of fuel assemblies. By 12 MWD/kgU, the radial peaking begins to favor the outside edge of the core. The axial relative power distribution for several burnups is shown in Figure K.10. This figure better illustrates the underlying cause of the shifts in the axial offset during the depletion cycle. The peaks near the bottom and top of the core are more pronounced at EOC then one usually finds in a standard design – and unfortunate side effect of the need to lump Gd_2O_3 at such high quantities. Finally, the relative assembly-wise burnup is given in Table K.4, where it is seen that the assemblies containing the highest power peaking levels also have the highest burnups, 36.8 MWD/kgU for a core average burnup of 26 MWD/kgU.

5.2.2 Erbium Core

Integral parameters for the simple erbium core design are shown in Table K.5, and the critical soluble boron letdown curve is depicted in Figure K.11. The erbium core, in general, exhibits lower soluble boron levels and lesser power peaking values. The percentage axial offset, for example, ranges from -27 to 7%. The EOC average burnup, however, occurs at just 17.8 MWD/kgU – over 8 MWD/kgU less than the gadolinium core. It also happens to be 7.2 MWD/kgU less than the benchmark erbium core, which reflects the use of more than twice the amount of erbium burnable absorber, by weight. As another comparison, the calculated BOC critical boron is 339 ppm less than the benchmark core. Although the power peaking parameters are, for the most part, less than those for the gadolinium core, they are still too high for a real core design; see Figure K.13. Boiling is again occurring in this model, as the moderator density at the top of the core is as low as 0.30 g/cc in the central node at BOC. The beginning and EOC radial power maps are listed in Tables K.6 and K.7, and the radial power profile along the core symmetry line is given in Figure K.14. This model also has radial power peaking as high as 1.9, but these levels change in a more predictable manner since erbium burns more regularly than gadolinium does. The axial distribution is given in Figure K.15; this figure looks more like what one would expect for an axially uniform loading. The greatest axial peaking (FZ) is 1.52 at 0.15 MWD/kgU, which is slightly more than the 1.45 seen in the gadolinium results. Assembly-wise burnup is depicted in Table K.8. For these results, the highest burnups are 28.5 MWD/kgU at an average burnup of 18 MWD/kgU.

Chapter 6

Conclusions and Future Work

6.1 Conclusions

The original IRIS benchmarks (15×15 assembly design) consisted of several pin cell cases, an assembly case, and a core depletion case [10]. Investigated parameters included fluxes, power peaking, isotopic composition, pin-wise burnups, and reactivity profiles. The results compared well among the neutronics groups of the IRIS consortium, although the core BOL k_{eff} was about 1.2 even with ZrB_2 distributed in varying amounts for ten different assembly types. Thermal hydraulic feedback was intentionally not modeled, making the operational and safety parameters of this core not acceptable, but enabling instead the ability to have a more direct comparison between different computer models. The next set of benchmarks consisted of a series of erbium burnable absorber loadings for a 17×17 assembly design. The results of this benchmark compared well, with some deviations likely due to differences in erbium cross section treatment. A benchmark core was modeled that had a maximum soluble boron of 1360 ppm and an EOC at 24.98 MWD/kgU.

Several assembly configurations that minimize excess reactivity were found using Gd_2O_3 and Er_2O_3 as burnable absorbers. The ideal gadolinium assembly in this respect would be a 32 pin configuration at 2.6 wt% Gd_2O_3 per assembly (21.45 wt% per pin), but this is an unacceptably high poison content. The final gadolinium configuration is the most lumped solution possible: 28 pins at 10 wt% Gd_2O_3 per pin (1.06 wt% by assembly). Both configurations allow for decent reactivity control over the assembly lifetime with little EOL residual penalty. The MDC for such a configuration is positive and the MTC negative. The erbium assembly configuration minimizing excess reactivity includes 104 pins at 2.8 wt% Er_2O_3 (7.11 % by pin). This configuration has a penalty of about 6 MWD/kgU at EOL. The MDC is positive at all points and the MTC negative.

The final gadolinium core design consisted of the above optimal assembly configuration in a checkerboard pattern with fuel at a lower enrichment, emulating a two-batch core. The maximum critical soluble boron for such a design is 1460 ppm at BOC. The EOC average burnup is 26.3 MWD/kgU. The maximum radial power peaking (FdH)

is 1.97, a value that is unacceptably high and indicates in-core boiling. Because of the need for heavy self-shielding, radial and axial power peaking is more pronounced over the life of this core. At 10 MWD/kgU in particular, there is a minimum value in the axial offset, a flattening in the soluble boron profile, and radial peaking begins to dominate at the outside of the core.

The final erbium core design consisted of an identical checkerboard assembly configuration to the gadolinium core, but used the 104-pin configuration at 2.8 wt% Er_2O_3. The maximum critical soluble boron is 1021 ppm, and the EOC average burnup is 17.8 MWD/kgU. The maximum radial power peaking is 2.12; so once again there is in-core boiling in this core model. This core model is better behaved than the gadolinium core, but becomes subcritical much earlier. The Er_2O_3 loading for this core is more than twice that of the Erbium benchmark, and is much more than necessary to meet maximum soluble boron safety margins. The subsequent reduction in cycle length offsets the utility of this design.

Although the final gadolinium and erbium core models are not feasible solutions for the real IRIS core, they are successful in demonstrating the methodology of creating homogenized cross sections using HELIOS for input into a nodal methods code (NESTLE). They are also successful in demonstrating that it is possible to keep soluble boron levels below 1500 ppm, for the IRIS long cycle, without the use of control rods. Additionally, multiple axial and radial burnable poison zones would reduce the axial and overall peaking factors, as well as produce more acceptable axial offset values.

6.2 Future Work

This research has led to the creation of several full core models for the IRIS. Perhaps more importantly, along the way tools have been sharpened and models debugged so that the next full core studies will be faster to implement and produce accurate results. It is simply a matter of getting another cross section conversion utility (the FORMOSA Cross Section Interface Program, or FORCIP) running to enter the homogenized cross sections into FORMOSA-P to perform optimizations that will eventually lead to feasible burnable absorber loadings. It may be that the optimal design should incorporate the use of both Gd_2O_3 and Er_2O_3 to maximize cycle length and minimize power peaking. Future studies will address this issue of arriving at viable and optimized core design alternatives that may ultimately be used in support of the IRIS certifications from the Nuclear Regulatory Commission. In fact, the licensing process has already begun with a pre-application to the NRC.

The IRIS is on schedule to complete a Safety Analysis Report by 2006-2008, attain design certification in 2008-2010, and become deployable in 2010-2015 [2]. To achieve the goal of a long cycle length while minimizing the use of soluble boron, it will almost certainly need to incorporate gadolinium or erbium as a burnable poison. The completion of this research at UT/ORNL, will contribute to further enhancing IRIS marketability.

Bibliography

Bibliography

[1] M. Carelli et al. "IRIS Reactor Conceptual Design". *Int. Conf. On the Back-End of the Fuel Cycle (Global 2001).* Paris, France, Sept. 9-13, 2001.

[2] M. Carelli et al. "IRIS: Proceeding Towards the Preliminary Design". *Proc. 10th International Conference on Nuclear Engineering (ICONE-10).* ASME, April 14-18, 2002, Arlington, VA, USA.

[3] M. D. Carelli, L. E. Conway, G. L. Fiorini, C. V. Lombardi, M. E. Ricotti, L. Oriani, F. Berra, and N. E. Todreas. "Safety by Design: A New Approach to Accident Management in the IRIS Reactor". *Seminar on Status and Prospects of Small and Medium Sized Reactors (Global 2001).* IAEA-SR-218/36, Cairo, Egypt, 27-31 May, 2001, IAEA (2001).

[4] Marielle Asou and Jacques Porta. "Prospects for poisoning reactor cores of the future". *Nuc. Eng. and Des.*, 168:261–270, 1997.

[5] Weston M. Stacey. *Nuclear Reactor Physics.* John Wiley and Sons, Inc., New York, 2001.

[6] Rudi J.J. Stamm'ler and Aldo A. Ferri. "HELIOS: Angularly Dependent Collision Probabilities". *Nuc. Sci. and Eng.*, 122:16–31, 1992.

[7] P.J. Turinsky et al. "Code Abstract - NESTLE: A Few-Group Neutron Diffusion Equation Solver Utilizing the Nodal Expansion Method for Eigenvalue, Adjoint, and Fixed-Source Steady State and Transient Problems". *Nuc. Sci. Eng.*, 120:72, 1995.

[8] D.J. Kropaczek and P.J. Turinsky. "In-Core Nuclear Fuel Management Optimization for PWRs Using Simulated Annealing". *Nucl. Tech.*, 95, 1991.

[9] N. Metropolis, A.W. Rosenbluth, M.N. Rosenbluth, A.H. Teller, and E. Teller. "Equation of State Calculations by Fast Computing Machines". *J. Chem. Phys.*, 21:1087–1092, 1953.

[10] Bojan Petrovic. *Benchmark 44: Core Depletion Analysis, No Feedback*, January 2002. (Internal Report) IRIS-WEC-12, Rev. 2.

[11] Bojan Petrovic. *IRIS 17x17 Fuel with Erbium BA*, January 2003. (Internal Report) IRIS-WEC-24, Rev. 1.

[12] Nuclear Data Evaluation Lab, `http://www2.bnl.gov/ton`. *Table of Nuclides*, January 2003. Copyright 2000-2002.

[13] Bojan Petrovic. Specifications for IRIS Benchmarks 1,2, and 31. (emails between IRIS neutronics team members).

[14] J-P.A. Renier and M.L. Grossbeck. *Development of Improved Burnable Poisons for Commercial Nuclear Power Reactors.* UT-Battelle, LLC. ORNL/TM-2001/238 (2001).

[15] *Gadolinia Fuel Properties for LWR Fuel Safety Evaluation*, December 1982. Exxon Nuclear Company, Inc. XN-NF-79-56(NP)(A) Rev. 1.

Appendixes

Appendix A

IRIS Integral Layout

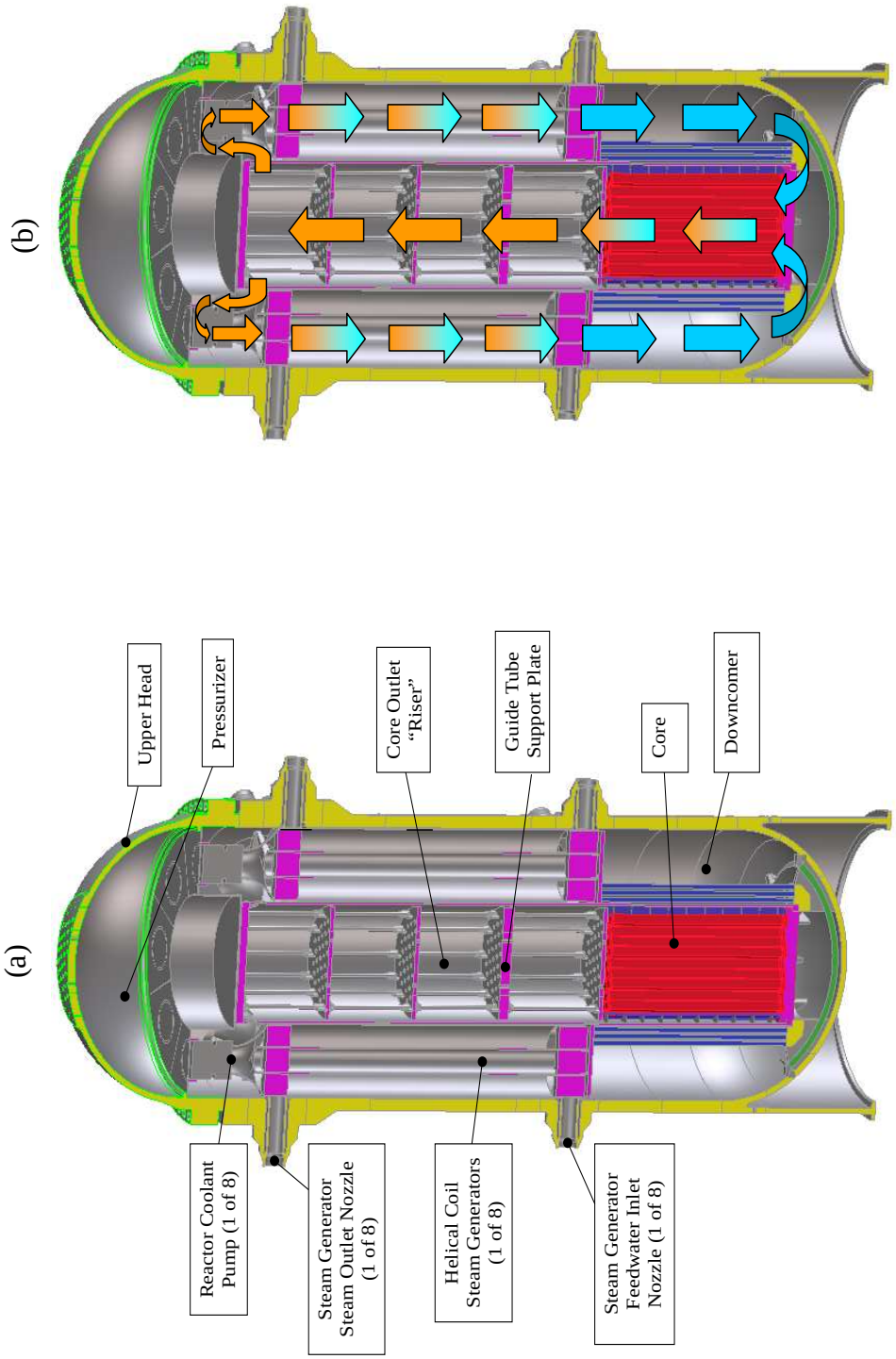

Figure A.1: IRIS integral layout: (a) main components (b) main flow path

Appendix B

Pin Cell Benchmark Results

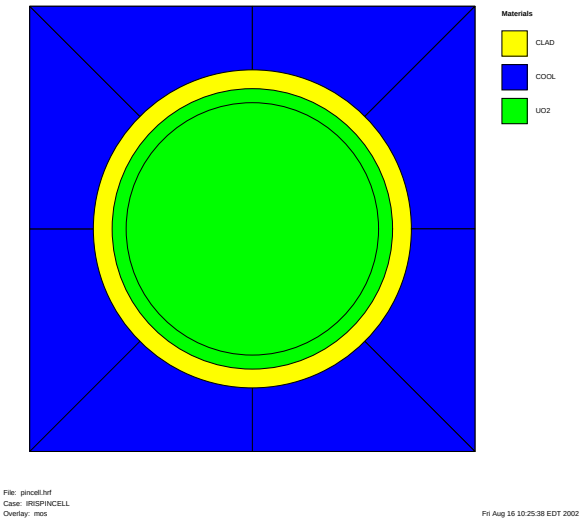

Figure B.1: The Pin Cell Geometry

Table B.1: Pin Cell Benchmark k_∞ Table

Burnup (MWD/kgU)	UT/ORNL	Average Result	% Diff.
0	1.441	1.438	0.23
0.15	1.403	1.400	0.23
1	1.388	1.384	0.24
2	1.377	1.373	0.23
4	1.355	1.351	0.32
8	1.312	1.308	0.35
12	1.272	1.268	0.36
16	1.236	1.232	0.33
20	1.201	1.197	0.33
24	1.169	1.165	0.28
28	1.137	1.135	0.20
32	1.106	1.105	0.13
36	1.076	1.075	0.10
40	1.047	1.047	0.00
44	1.018	1.019	-0.07
48	0.990	0.991	-0.15

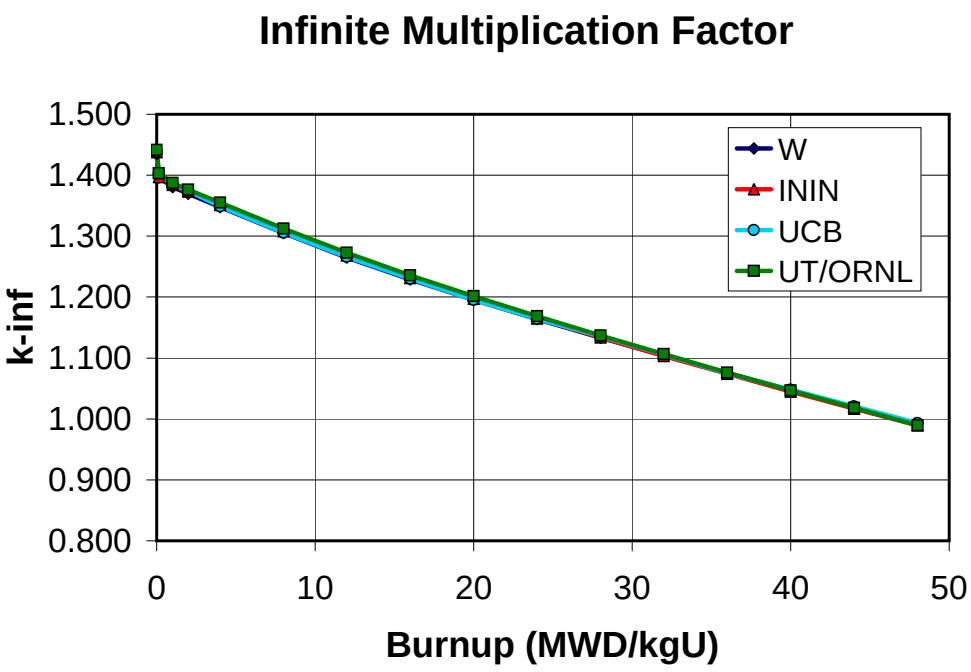

Figure B.2: Pin Cell Benchmark Infinite Multiplication Factor (k_∞) versus Burnup

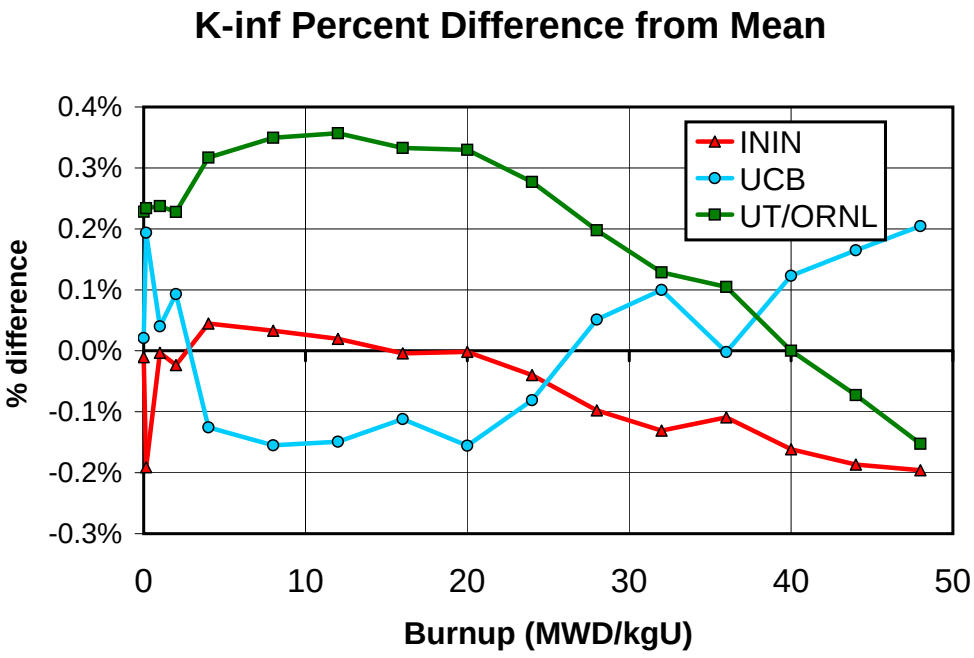

Figure B.3: Pin Cell Benchmark k_∞ Percent Deviation from Mean

Table B.2: EOL Isotopics for Pin Cell Benchmark (atoms/cm^3)

	UT/ORNL	Average Result
U235	2.66E+20	2.68E+20
U236	1.46E+20	1.45E+20
U238	2.06E+22	2.06E+22
NP237	1.47E+19	1.44E+19
Pu238	6.35E+18	5.91E+18
Pu239	1.32E+20	1.32E+20
Pu240	5.70E+19	5.64E+19
Pu241	3.37E+19	3.45E+19
Pu242	1.30E+19	1.34E+19
Am241	2.07E+18	2.07E+18
Am242	3.95E+16	5.78E+16
Am243	2.98E+18	2.90E+18

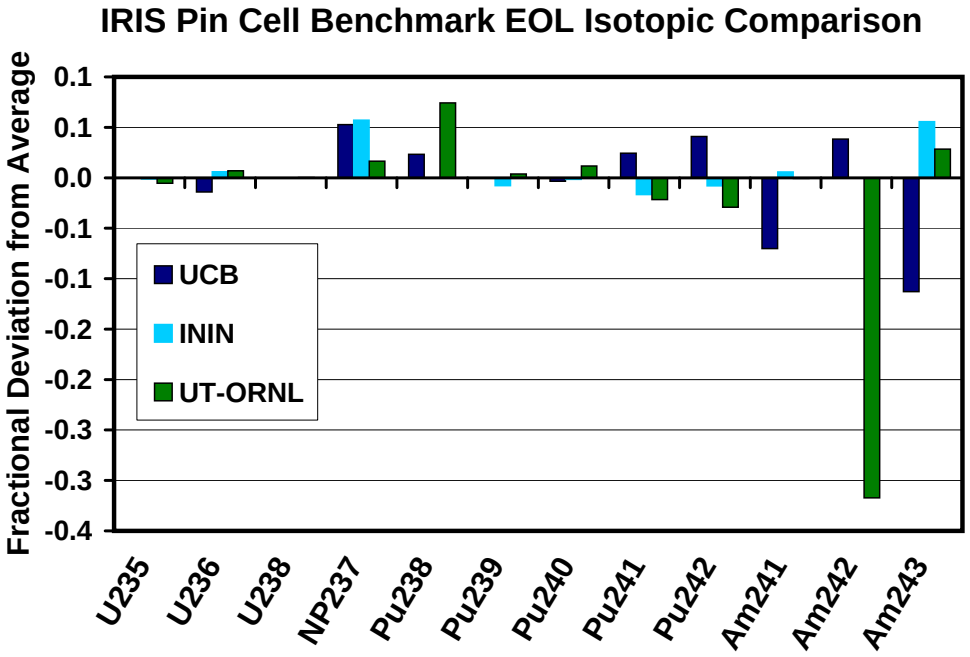

Figure B.4: Pin Cell Benchmark k_∞ EOL Isotopic Comparison

Table B.3: Pin Cell Benchmark Total Cell-Average Flux ($n/cm^2 - s$)

	UT/ORNL	Average Result
0 MWD/kgU	1.414E+14	1.386E+14
Diff. To Average	1.97%	–
48 MWD/kgU	2.033E+14	2.030E+14
Diff. To Average	0.14%	–

Table B.4: Pin Cell Benchmark Spectral Index With 0.625eV Cutoff

	UT/ORNL
0 MWD/kgU	
Fast	1.25E+14
Thermal	1.62E+13
Fast/Thermal	7.72
48 MWD/kgU	
Fast	1.79E+14
Thermal	2.45E+13
Fast/Thermal	7.30

Table B.5: Pin Cell Benchmark Region-wise Flux Ratios, Relative to Cell-average Flux

	UT/ORNL	Average
0 MWD/kgU		
Fuel/Cell	0.9999	1.0004
Clad/Cell	1.0003	0.9999
Moderator/Cell	1.0000	0.9997
Percent Difference To Average at 0 MWD/kgU		
Fuel/Cell	-0.05%	–
Clad/Cell	0.04%	–
Moderator/Cell	0.03%	–
48 MWD/kgU		
Fuel/Cell	0.9968	0.9977
Clad/Cell	0.9996	0.9998
Moderator/Cell	1.0017	1.0006
Percent Difference To Average at 48 MWD/kgU		
Fuel/Cell	-0.09%	–
Clad/Cell	-0.03%	–
Moderator/Cell	0.11%	–

Appendix C

Assembly Benchmark Results

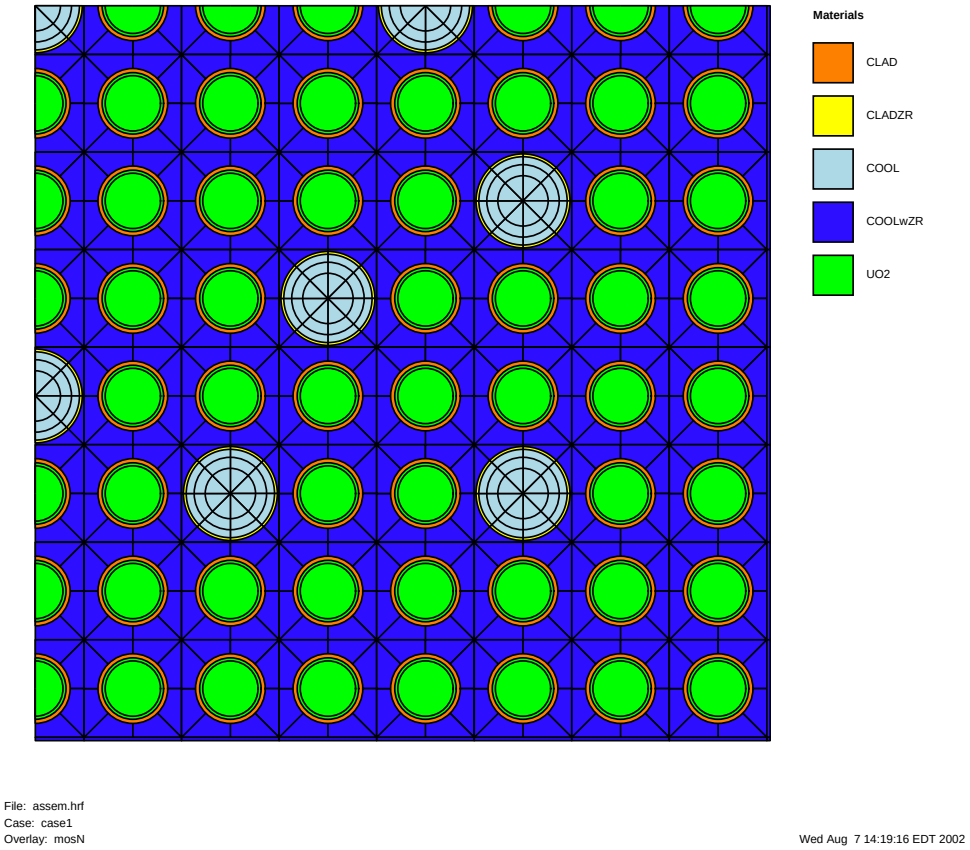

Figure C.1: The Quarter-Assembly Nodalization Geometry.

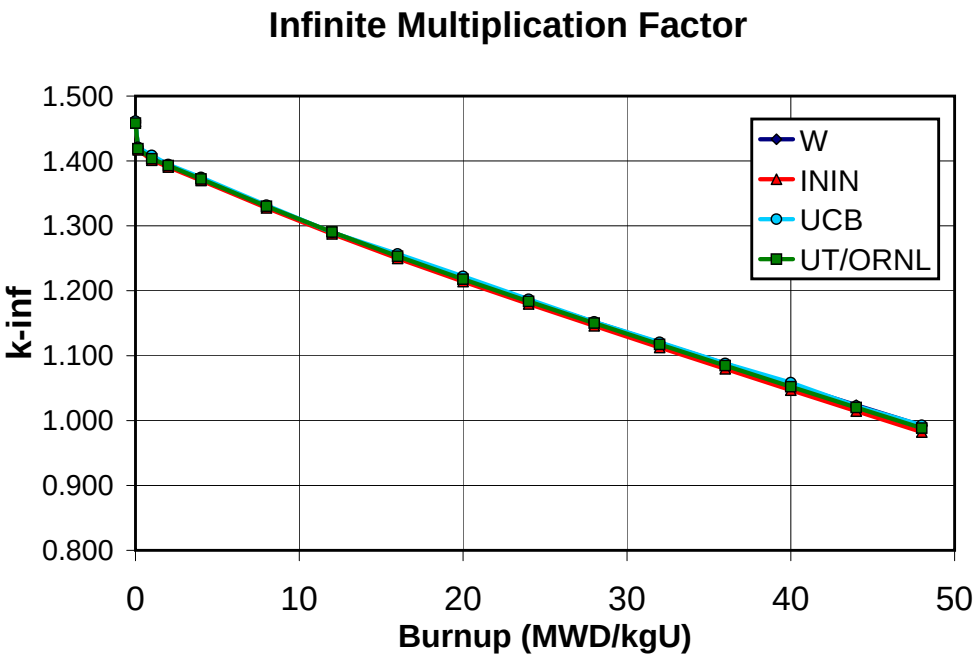

Figure C.2: Assembly Benchmark k_∞ Versus Burnup

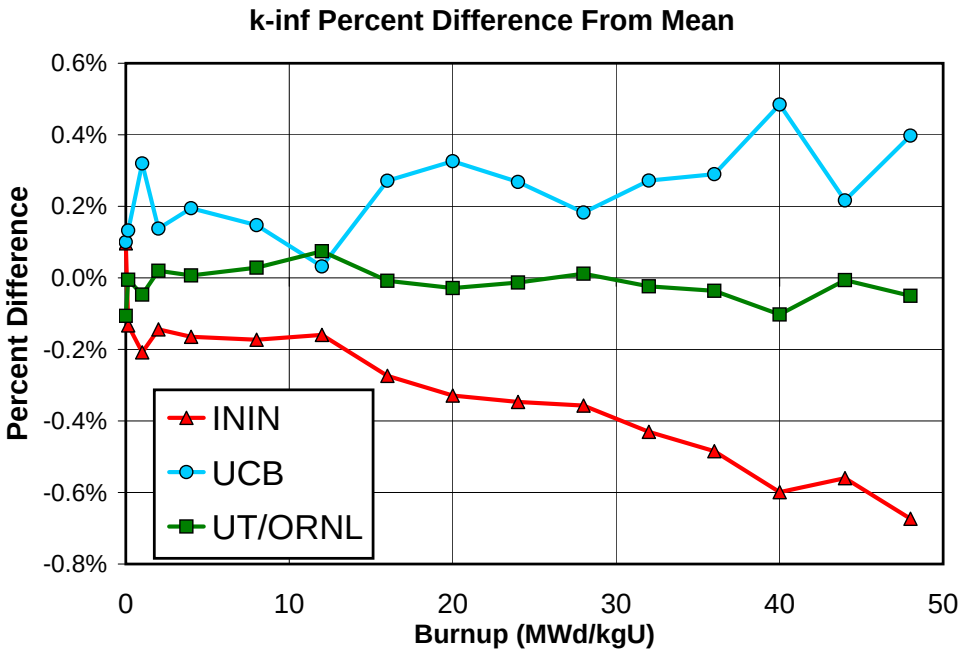

Figure C.3: Assembly Benchmark Percent Deviation from Mean

Table C.1: Assembly Benchmark k_∞ Table

Burnup (MWD/kgU)	UT/ORNL	Average Result	% Diff.
0	1.458	1.460	-0.11
0.15	1.419	1.419	-0.01
1	1.403	1.404	-0.05
2	1.393	1.393	0.02
4	1.372	1.372	0.01
8	1.330	1.330	0.03
12	1.291	1.290	0.07
16	1.253	1.253	-0.01
20	1.218	1.218	-0.03
24	1.184	1.184	-0.01
28	1.150	1.150	0.01
32	1.117	1.117	-0.02
36	1.085	1.085	-0.04
40	1.052	1.053	-0.10
44	1.020	1.020	-0.01
48	0.988	0.989	-0.05

Table C.2: Pin Burnup Distribution at 48 MWD/kgU (1/8 Assembly Shown)

46.3	UT/ORNL (MWD/kgU)						
46.2	46.8						
46.4	47.9						
46.5	47.4	49.1	49.4				
46.6	47.6	49.4	50.3				
46.7	48.4		50.3	49.5	47.9		
46.6	47.6	49.8	50.1	48.3	47.1	47.2	
46.5	47.1	49.4		48.9	47.0	48.0	

Table C.3: Relative Pin Power Distribution at 0.0 MWD/kgU

0.951							
0.947	0.965						
0.953	1.001						
0.954	0.981	1.034	1.040				
0.956	0.986	1.044	1.073				
0.959	1.014		1.073	1.045	0.994		
0.955	0.986	1.057	1.066	1.006	0.967	0.974	
0.953	0.971	1.043		1.026	0.967	1.002	

Table C.4: Relative Pin Power Distribution at 48.0 MWD/kgU

0.983							
0.983	0.988						
0.986	0.997						
0.988	0.996	1.008	1.013				
0.989	0.998	1.009	1.017				
0.990	1.002		1.017	1.012	1.003		
0.989	0.998	1.013	1.016	1.006	0.996	0.997	
0.989	0.994	1.009		1.007	0.995	1.000	

Table C.5: Calculation Method Comparison for Relative Pin Power Distribution at 48 MWD/kgU

0.983	$\kappa\Sigma_f$-based power peaking						
0.984	Σ_f-based power peaking						
0.1%	Percent Difference						
0.983	0.988						
0.983	0.989						
0.1%	0.0%						
0.986	0.997						
0.986	0.997						
0.1%	-0.0%						
0.988	0.996	1.008	1.013				
0.988	0.996	1.007	1.013				
0.1%	0.0%	-0.0%	-0.0%				
0.989	0.998	1.009	1.017				
0.990	0.998	1.009	1.016				
0.1%	0.0%	-0.0%	-0.1%				
0.990	1.002		1.017	1.012	1.003		
0.990	1.002		1.016	1.011	1.003		
0.1%	-0.0%		-0.1%	-0.1%	0.0%		
0.989	0.998	1.013	1.016	1.006	0.996	0.997	
0.990	0.999	1.012	1.015	1.006	0.996	0.997	
0.1%	0.0%	-0.1%	-0.1%	0.0%	0.0%	0.0%	
0.989	0.994	1.009		1.007	0.995	1.000	
0.989	0.995	1.009		1.007	0.995	1.000	
0.1%	0.0%	-0.0%		-0.0%	0.0%	0.0%	

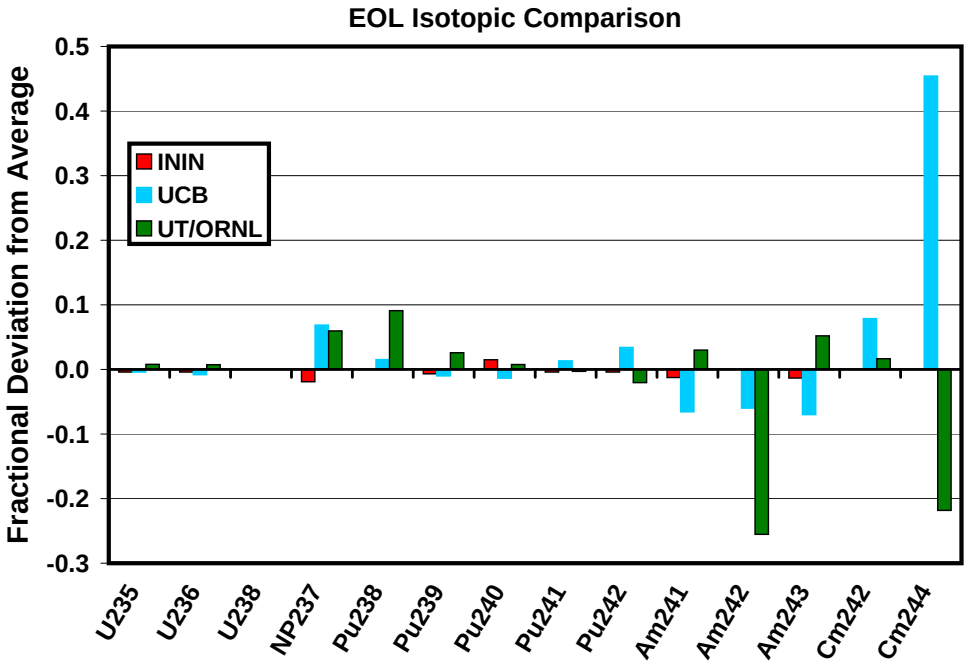

Figure C.4: EOL Isotopic Comparison for Assembly Benchmark

Table C.6: EOL Isotopics Table for Assembly Benchmark (atoms/cm^3)

Isotope	UT/ORNL	Average Result
U235	2.49E+20	2.47E+20
U236	1.45E+20	1.44E+20
U238	2.06E+22	2.06E+22
NP237	1.37E+19	1.29E+19
Pu238	5.66E+18	5.19E+18
Pu239	1.16E+20	1.13E+20
Pu240	5.49E+19	5.45E+19
Pu241	3.05E+19	3.06E+19
Pu242	1.32E+19	1.34E+19
Am241	1.84E+18	1.79E+18
Am242	3.27E+16	4.40E+16
Am243	2.79E+18	2.65E+18
Cm242	4.38E+17	4.30E+17
Cm244	9.15E+17	1.17E+18

Table C.7: BOL and EOL Flux Parameters for Assembly Benchmark

Burnup	Total Flux	Thermal Flux	Fast Flux	Ratio (Fast/Thermal)
0 MWD/kgU	1.26E+14	1.68E+13	1.10E+14	6.533
48 MWD/kgU	1.86E+14	2.81E+13	1.58E+14	5.616

Appendix D

Zirconium Diboride Coating Thickness Parameterizations

In the specifications for the original IRIS pin-cell benchmark using a zirconium diboride (ZrB_2) Integral Fuel Burnable Absorber (IFBA), the method in modeling the ZrB_2 coating was left to the modeler. A parametric study was performed to examine the effects of varying the thickness of the ZrB_2 coating while holding the boron loading constant. That is to say, for a given IFBA loading, the coating thickness was increased while the density was decreased to maintain a constant optical density. The exterior diameter was held constant, so similar changes also had to be made in the cladding density due to the infringement of the coating.

Calculations were performed using both HELIOS and MCNP due to a suspicion that HELIOS may lose accuracy at chord lengths reaching the minimum allowed value. The data are all for the beginning-of-life depletion point and the range of coating thicknesses examined is 0.001 cm to 0.01 cm. A visual comparison was then made between the two code outputs to determine if any numerical problems emerged. For the MCNP results, 25 cycles were skipped and 525 cycles are calculated. The maximum standard deviation is 0.0005.

The results are presented in the below figures. To summarize, there is a fairly significant effect in varying the ZrB_2 coating thickness due to self-shielding. For instance, at a concentration of 3 mg/cm, according to the MCNP results there exists a 0.5% difference in using a 0.005 cm thickness with respect to using a 0.001 cm thickness.

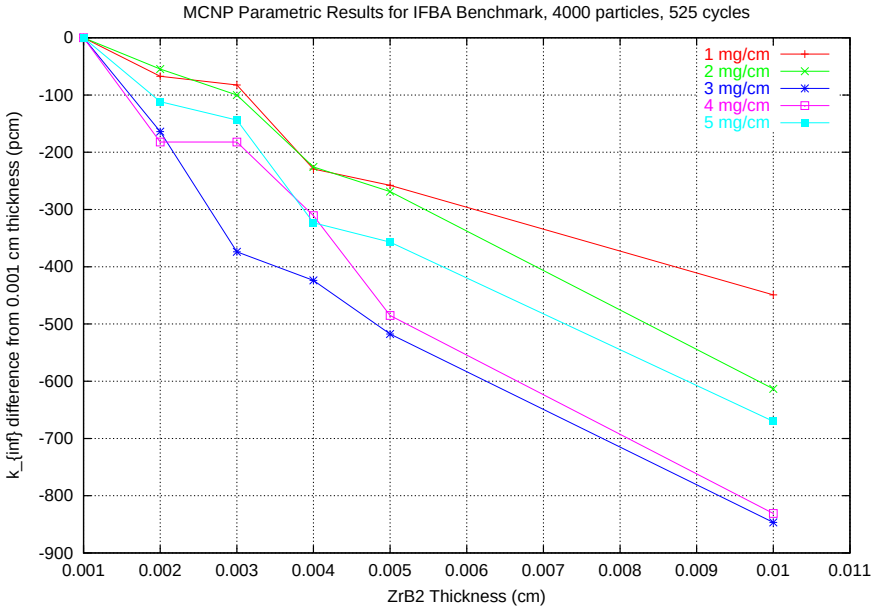

Figure D.1: MCNP results

A similar trend is found by refining the HELIOS collision parameters.[1] The effect is not quite as pronounced, however.

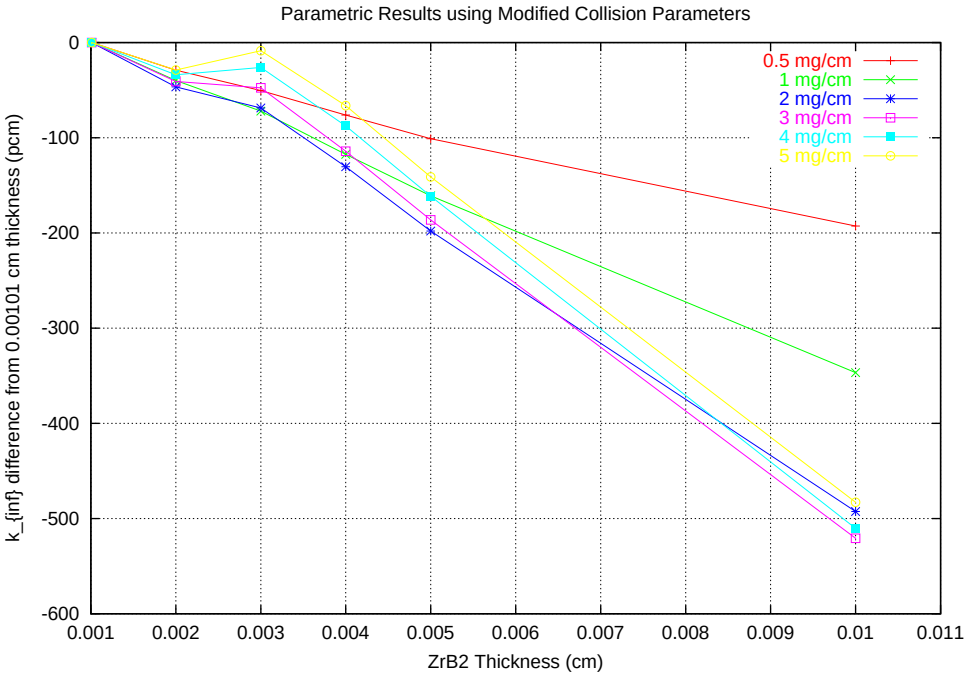

Figure D.2: HELIOS results, refined collision parameters

[1]Note that in the HELIOS case, the reference coating thickness is 0.00101 cm, which is slightly greater than the minimum value of 0.001.

Finally, leaving the collision parameters at their default values produces a numerical problem at the smallest allowable thickness:

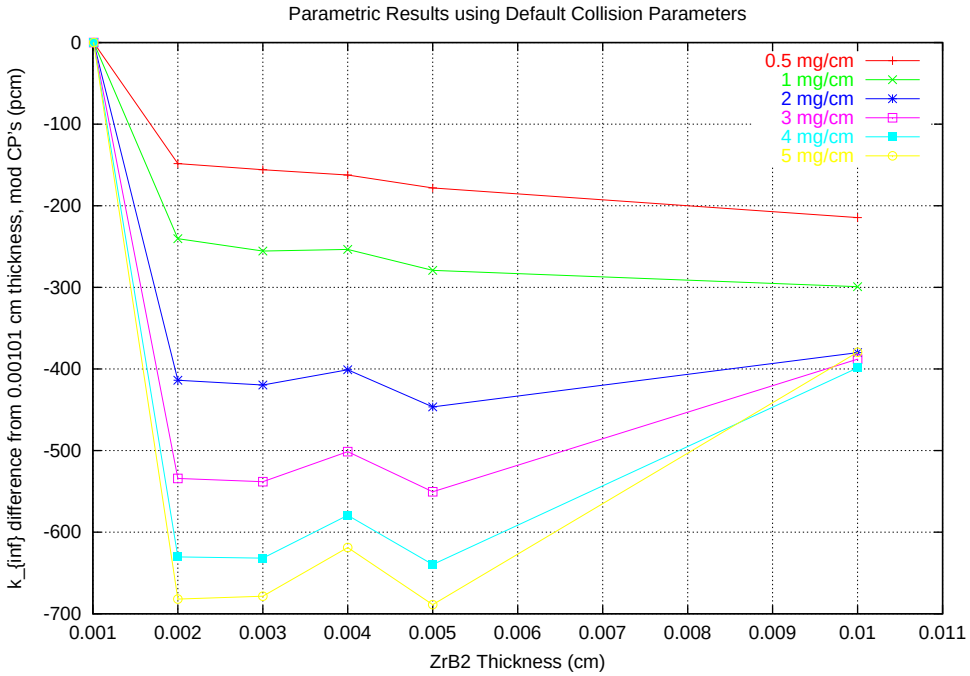

Figure D.3: HELIOS results, default collision parameters

The conclusion is to proceed with the IFBA pin-cell benchmark using the refined HELIOS collision parameters at a thickness of 0.00101 cm. For the "refined results," the maximum distance between two chords is halved, the minimum allowed width of macrobands is halved, the tolerance in cross section differences for variational collision probablity calculations is halved, and the minimum number of integration directions is doubled. All of these modifications are easily configurable in the "CP" section of the RUN command in HELIOS.

Appendix E

IFBA Benchmark Results

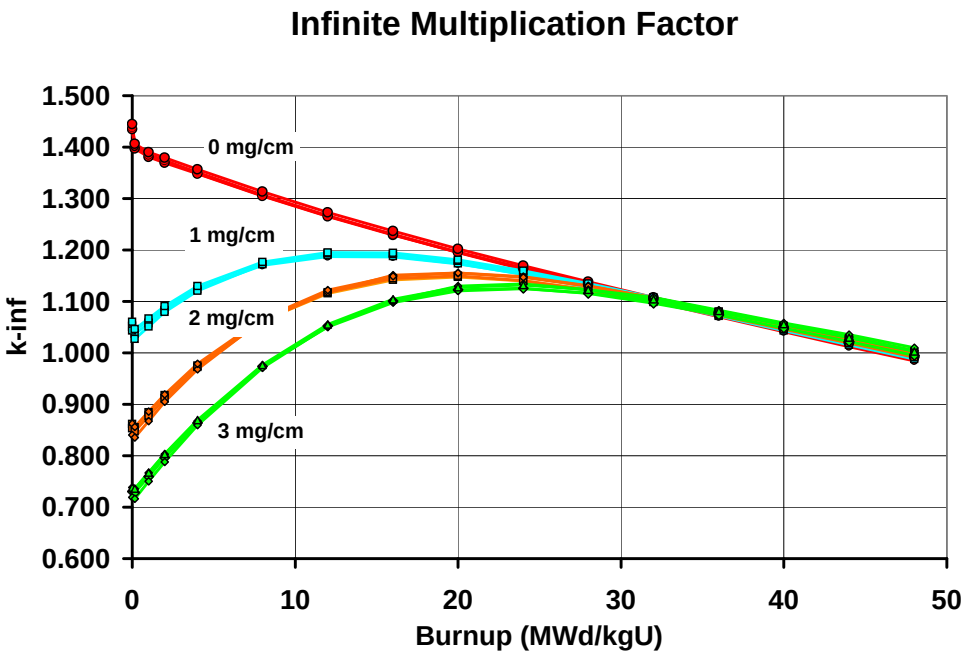

Figure E.1: IFBA Benchmark k_∞ Versus Burnup

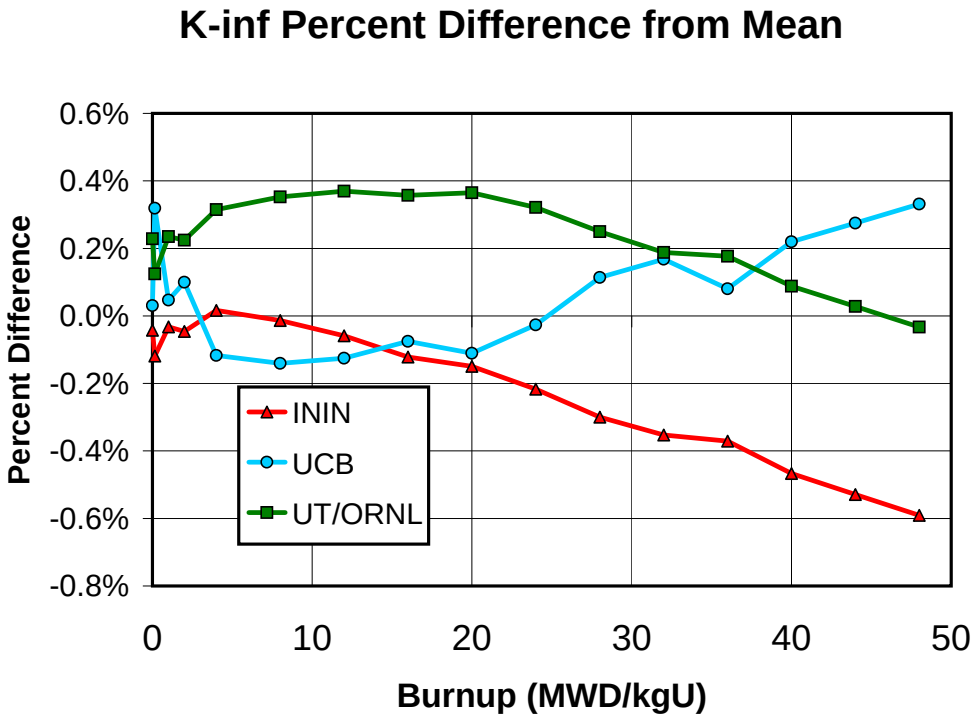

Figure E.2: IFBA Benchmark k_∞ Percent Deviation from Mean, 0 mg/cm

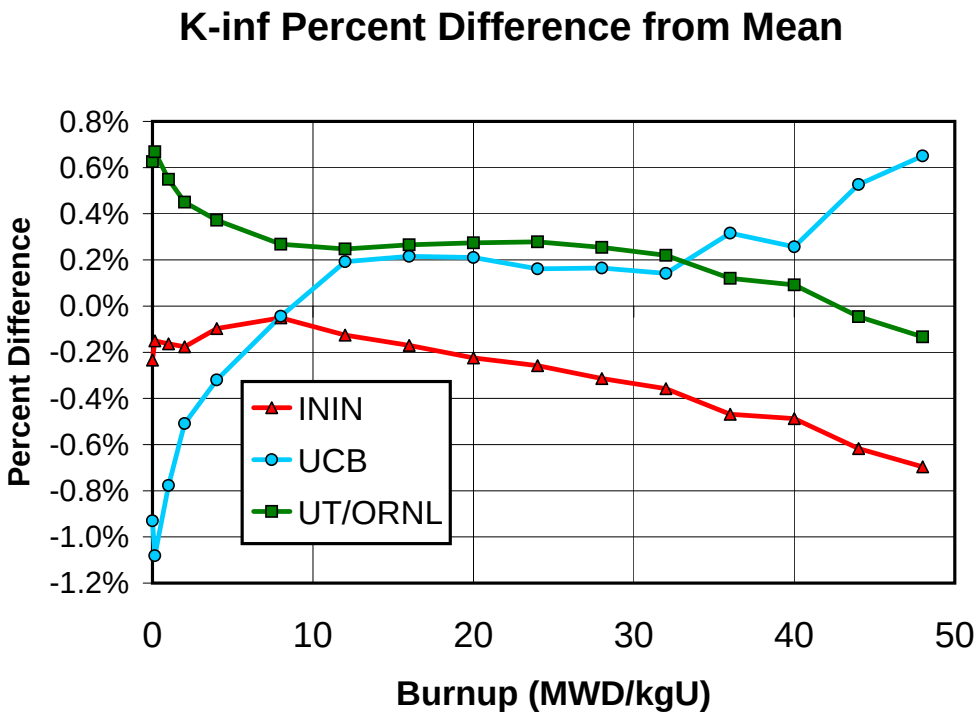

Figure E.3: IFBA Benchmark k_∞ Percent Deviation from Mean, 1 mg/cm

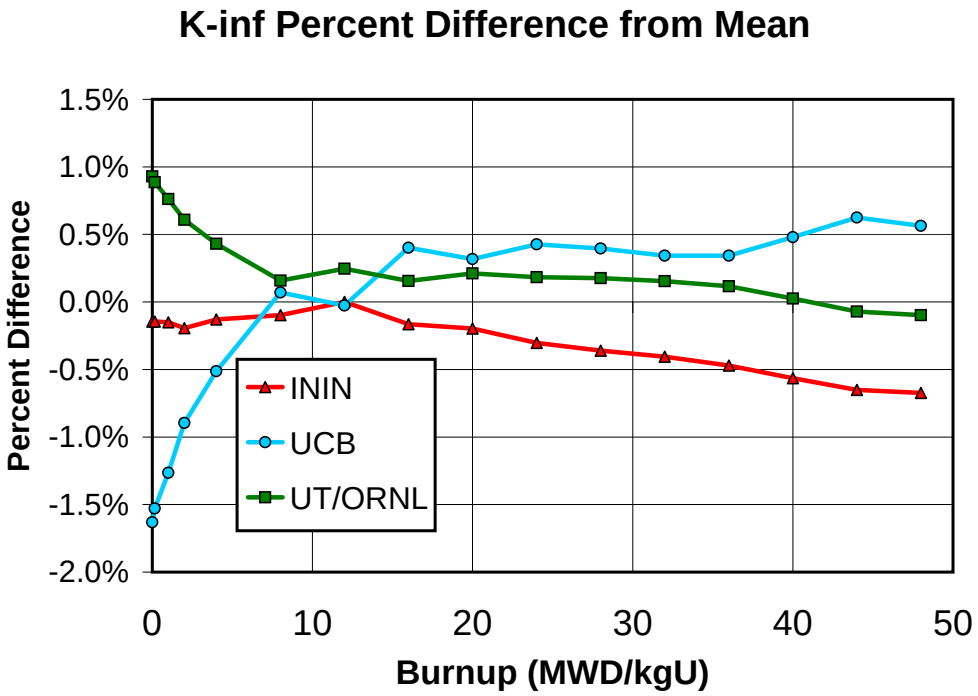

Figure E.4: IFBA Benchmark k_∞ Percent Deviation from Mean, 2 mg/cm

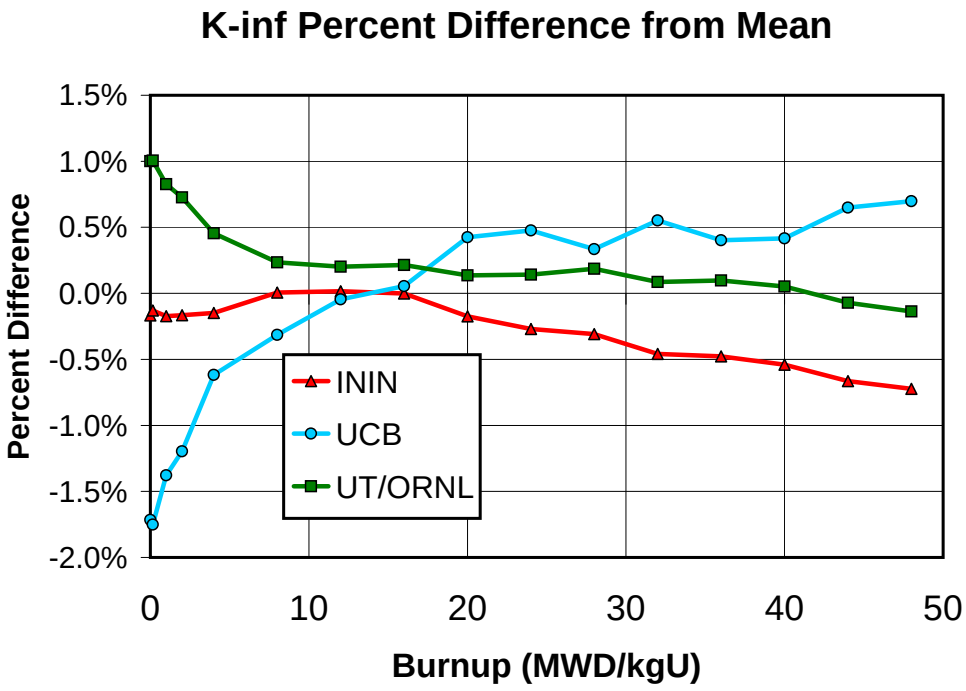

Figure E.5: IFBA Benchmark k_∞ Percent Deviation from Mean, 3 mg/cm

Appendix F

Core Benchmark Specifications and Results

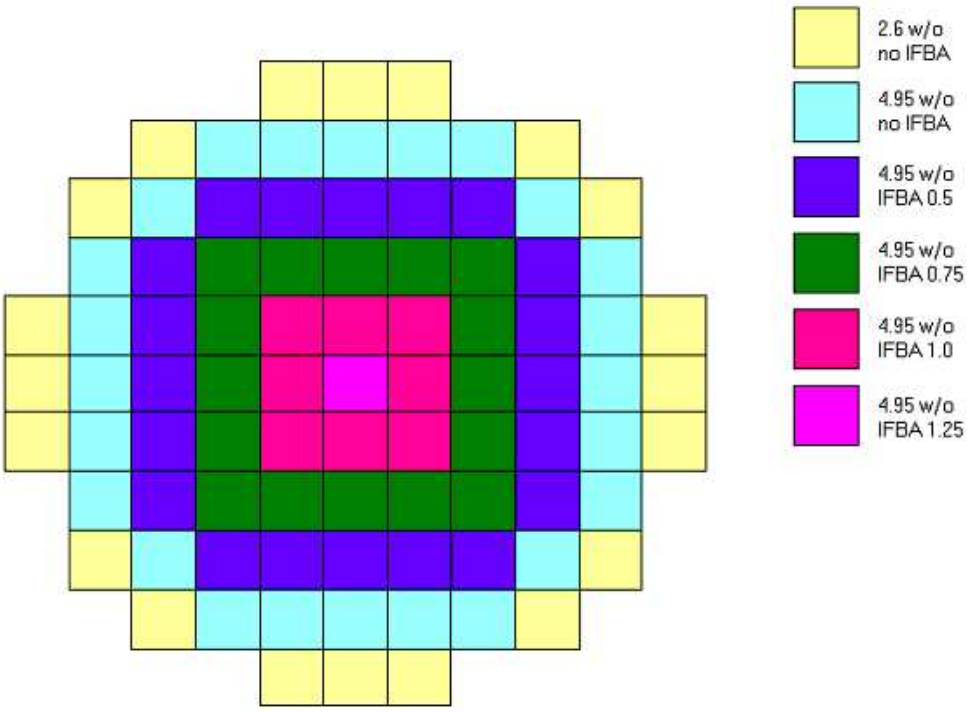

Figure F.1: IRIS core layout by fuel enrichment and IFBA concentration. (upper-half loading shown)

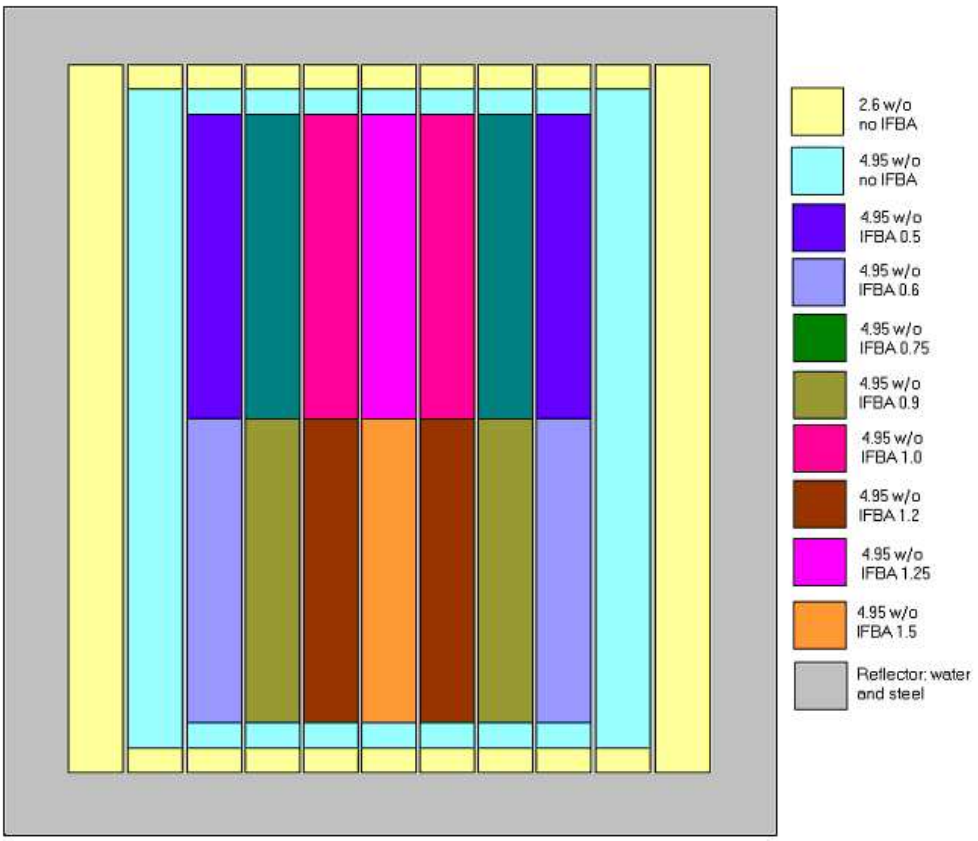

Figure F.2: IRIS core layout by fuel enrichment and IFBA concentration. Axial profile.

Table F.1: NESTLE geometry input for lower half of IRIS core

1	3	5	7	9	10	11	11
3	3	5	7	9	10	11	11
5	5	5	7	9	11	11	11
7	7	7	9	10	11	11	11
9	9	9	10	11	11	11	
10	10	11	11	11	11		
11	11	11	11	11			
11	11	11	11				

Table F.2: HELIOS, NESTLE, and the percent difference of NESTLE to HELIOS k_∞ for a single assembly with infinite reflection.

Burnup (MWD/kgU)	HELIOS	NESTLE	% difference
0	1.458	1.404	-3.74%
0.15	1.419	1.405	-0.99%
1	1.403	1.397	-0.42%
2	1.393	1.388	-0.34%
4	1.372	1.368	-0.29%
8	1.330	1.327	-0.21%
12	1.291	1.288	-0.18%
16	1.253	1.251	-0.16%
20	1.218	1.216	-0.15%
24	1.184	1.182	-0.13%
28	1.150	1.149	-0.12%
32	1.117	1.116	-0.10%
36	1.085	1.084	-0.10%
40	1.052	1.051	-0.10%
44	1.020	1.019	-0.11%
48	0.988	0.987	-0.14%

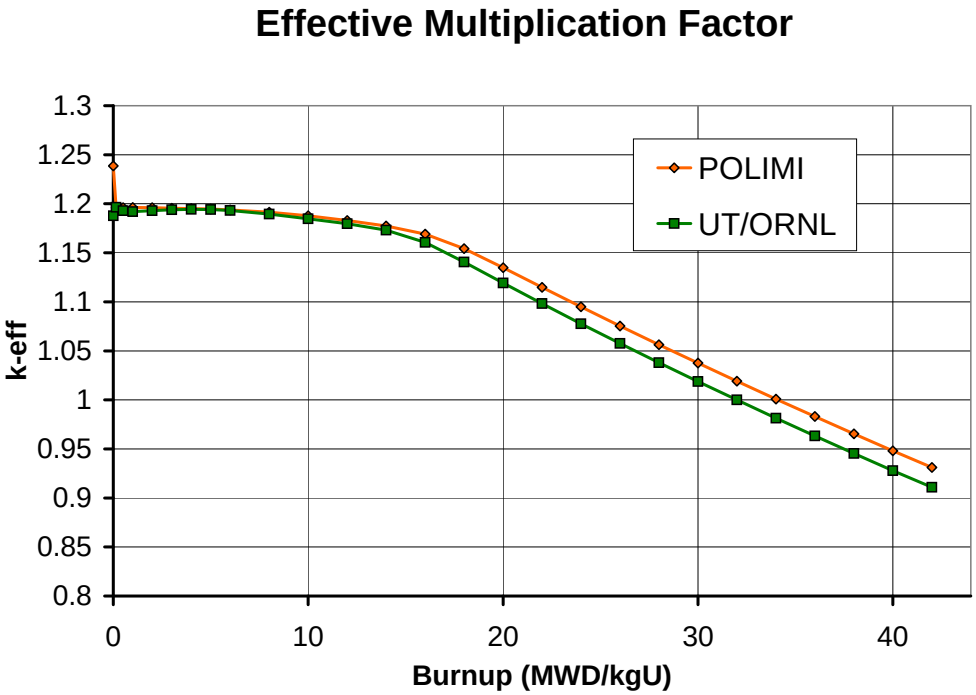

Figure F.3: Core Benchmark k_{eff} versus Burnup

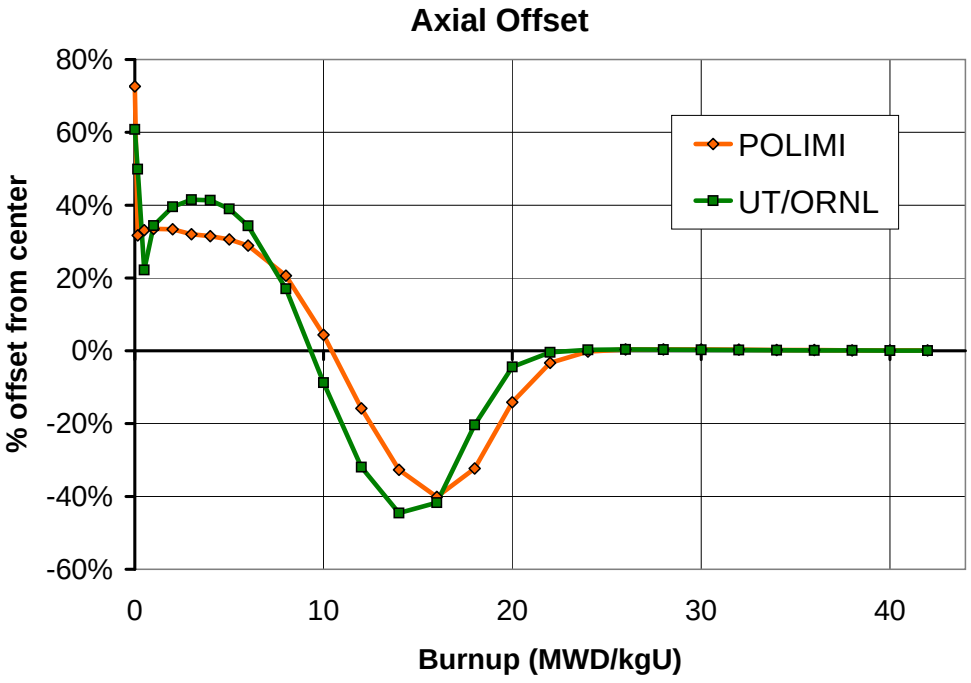

Figure F.4: Core Benchmark Axial Offset

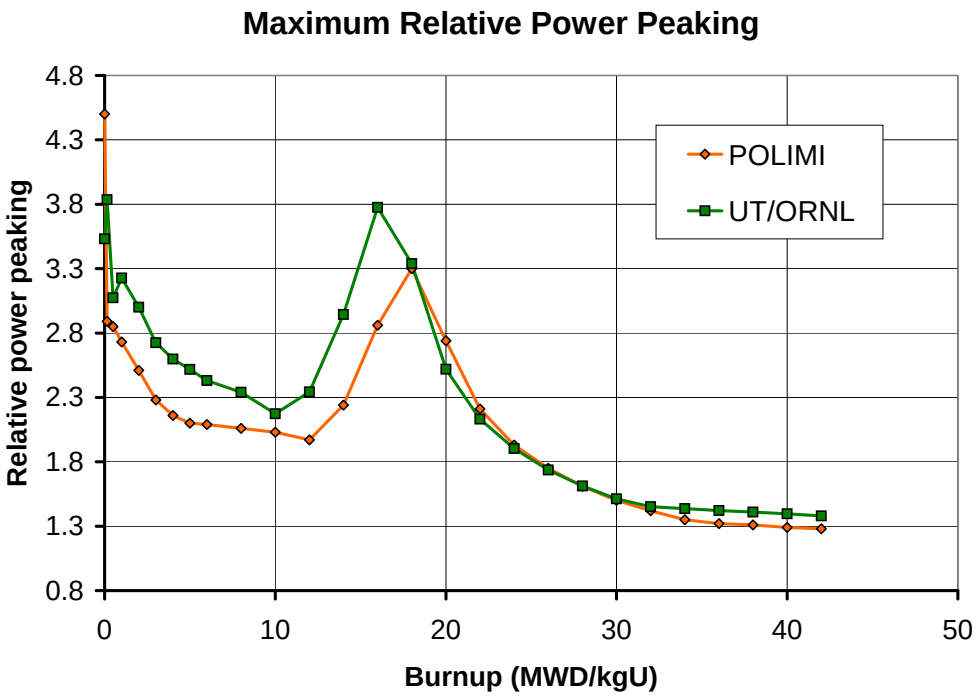

Figure F.5: Core Benchmark Maximum Relative Nodal Power Peaking

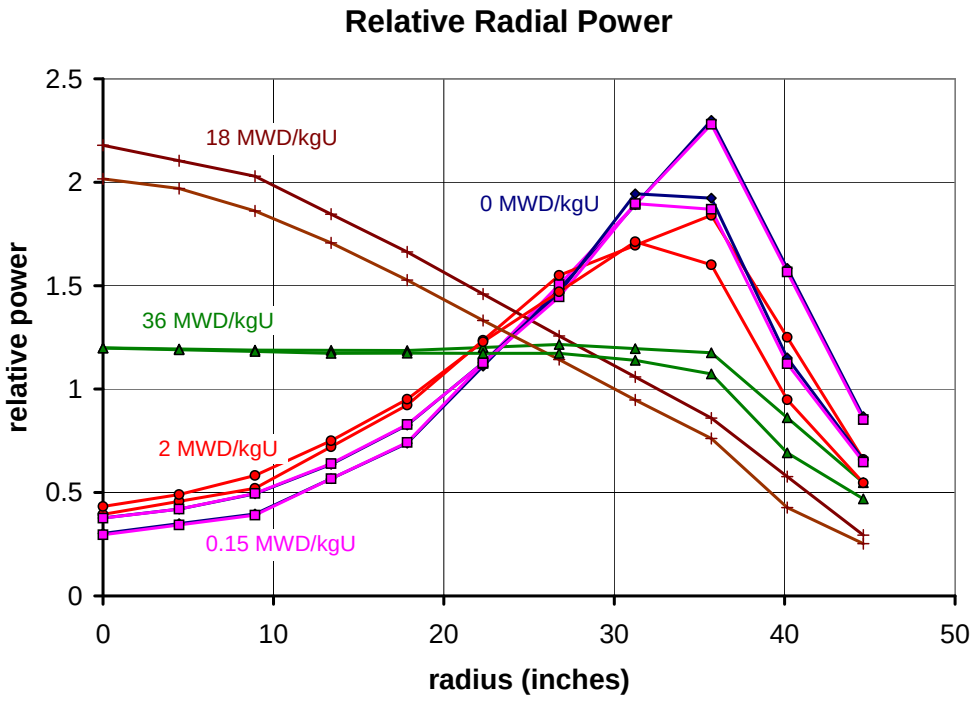

Figure F.6: Relative Radial Power Comparison (POLIMI and UT/ORNL)

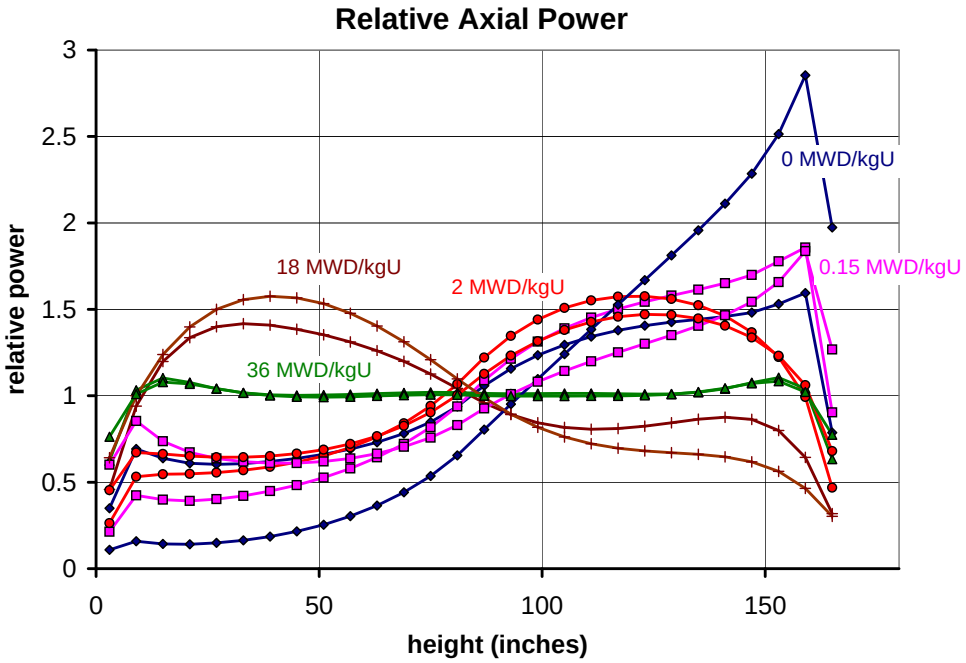

Figure F.7: Relative Axial Power Comparison (POLIMI and UT/ORNL)

Table F.3: Core Burnup at 32 MWD/kgU (average) by Fuel Bundle, $k_{eff} = 0.999948$

43.827	44.313	44.652	43.394	36.681	13.273
44.313	44.320	44.327	42.337	32.809	9.312
44.652	44.327	43.053	38.897	22.599	
43.394	42.337	38.897	30.964	9.9057	
36.681	32.809	22.599	9.9057		
13.273	9.3124				

Appendix G

Erbium Pin Cell Benchmark

Table G.1: The Composition of Natural Erbium

Isotope	Complete	Simplified
^{162}Er	0.14 a/o	–
^{164}Er	1.61 a/o	–
^{166}Er	33.60 a/o	35.35 a/o
^{167}Er	22.95 a/o	22.95 a/o
^{168}Er	26.80 a/o	26.80 a/o
^{170}Er	14.90 a/o	14.90 a/o

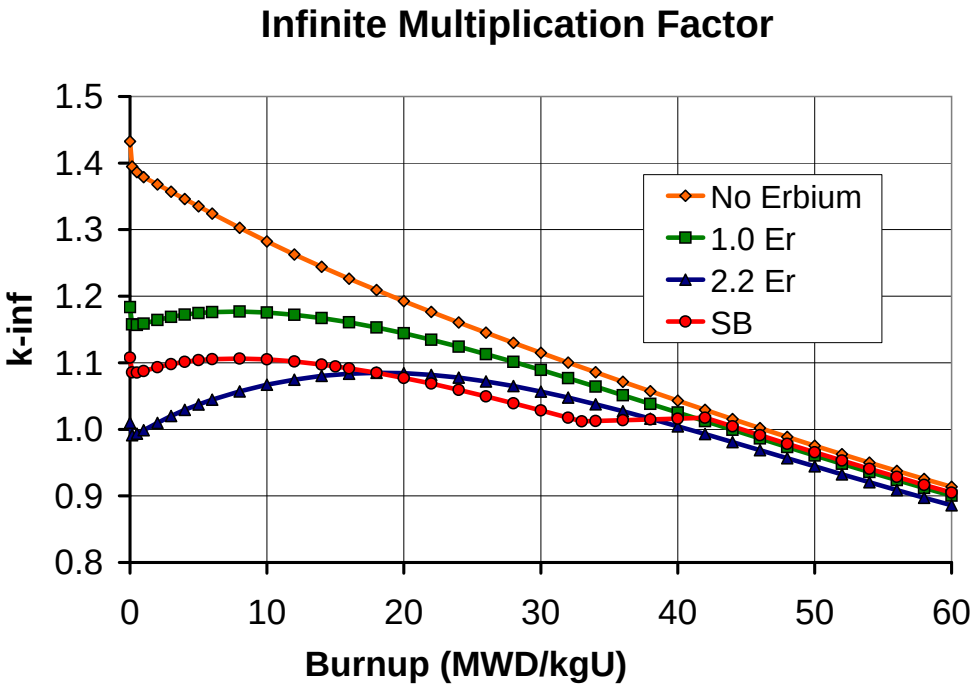

Figure G.1: Erbium Pin Cell Benchmark k_∞

Table G.2: Erbium Pin Cell Benchmark k_∞Table

Burnup (MWD/kg)	No Er	1.0 Er	2.2 Er	SB
0	1.43252	1.18358	1.00996	1.10784
0.15	1.39466	1.15775	0.99133	1.08564
0.5	1.38628	1.15688	0.99352	1.08536
1	1.37892	1.15876	0.99859	1.08756
2	1.36788	1.16427	1.00979	1.09329
3	1.35707	1.16888	1.02007	1.09801
4	1.34607	1.17225	1.02921	1.10149
5	1.33499	1.17460	1.03734	1.10393
6	1.32402	1.17607	1.04465	1.10550
8	1.30264	1.17688	1.05690	1.10644
10	1.28219	1.17547	1.06698	1.10521
12	1.26273	1.17218	1.07469	1.10209
14	1.24414	1.16722	1.08024	1.09733
15	–	–	–	1.09437
16	1.22633	1.16083	1.08365	1.09149
18	1.20917	1.15316	1.08497	1.08488
20	1.19257	1.14440	1.08438	1.07724
22	1.17640	1.13469	1.08187	1.06869
24	1.16062	1.12419	1.07769	1.05940
26	1.14517	1.11306	1.07198	1.04955
28	1.12997	1.10137	1.06497	1.03923
30	1.11502	1.08926	1.05680	1.02853
32	1.10028	1.07684	1.04766	1.01756
33	–	–	–	1.01197
34	1.08574	1.06416	1.03774	1.01252
36	1.07135	1.05129	1.02718	1.01361
38	1.05717	1.03833	1.01609	1.01476
40	1.04314	1.02532	1.00460	1.01606
42	1.02925	1.01227	0.99282	1.01761
44	1.01551	0.99925	0.98086	1.00443
46	1.00199	0.98631	0.96877	0.99134
48	0.98864	0.97344	0.95665	0.97838
50	0.97550	0.96073	0.94448	0.96562
52	0.96262	0.94819	0.93245	0.95305
54	0.94993	0.93585	0.92052	0.94066
56	0.93753	0.92373	0.90875	0.92853
58	0.92541	0.91185	0.89719	0.91664
60	0.91358	0.90027	0.88586	0.90499

Table G.3: Erbium Pin Cell Isotopics (atoms/barn $\cdot$ cm) at 60 MWD/kgU

Nuclide	No Er	1.0 wt% Er	2.2 wt % Er	SB
92235	1.7558E-04	1.7956E-04	1.8406E-04	1.8791E-04
92238	2.1148E-02	2.0856E-02	2.0508E-02	2.0841E-02
94238	1.0990E-05	1.0994E-05	1.1000E-05	1.1354E-05
94239	1.3853E-04	1.3949E-04	1.4061E-04	1.4282E-04
94240	7.0256E-05	7.0006E-05	6.9730E-05	7.1257E-05
94241	4.1564E-05	4.1856E-05	4.2204E-05	4.2962E-05
94242	2.2073E-05	2.1925E-05	2.1731E-05	2.2099E-05
95241	2.7786E-06	2.8559E-06	2.9504E-06	3.0114E-06
95342	5.2817E-08	5.4545E-08	5.6660E-08	5.8060E-08
95243	6.2752E-06	6.2393E-06	6.1881E-06	6.3114E-06
96242	7.2778E-07	7.3301E-07	7.3936E-07	7.5631E-07
96244	3.0304E-06	3.0104E-06	2.9827E-06	3.0660E-06
54635	6.9098E-09	6.9423E-09	6.9751E-09	7.1016E-09
62649	9.0348E-08	9.1256E-08	9.2263E-08	9.3987E-08
68166	0	9.8007E-05	2.1645E-04	9.7850E-05
68167	0	2.2367E-06	4.8084E-06	2.2442E-06
68168	0	1.6880E-04	3.6842E-04	1.6876E-04
68170	0	4.5428E-05	9.9511E-05	4.5379E-05

Table G.4: Erbium Pin Cell Fluxes at 0 and 60 MWD/kgU (n/cm$^2 \cdot$ s)

Burnup	Flux	No Er	1.0 wt% Er	2.2 wt% Er	SB
0 MWD/kgU	Fast	1.242E+14	1.397E+14	1.545E+14	1.465E+14
	Thermal	1.594E+13	1.537E+13	1.491E+13	1.521E+13
	Ratio	7.80	9.09	10.36	9.63
60 MWD/kgU	Fast	1.904E+14	1.899E+14	1.890E+14	1.889E+14
	Thermal	2.670E+13	2.603E+13	2.527E+13	2.527E+13
	Ratio	7.13	7.29	7.48	7.48

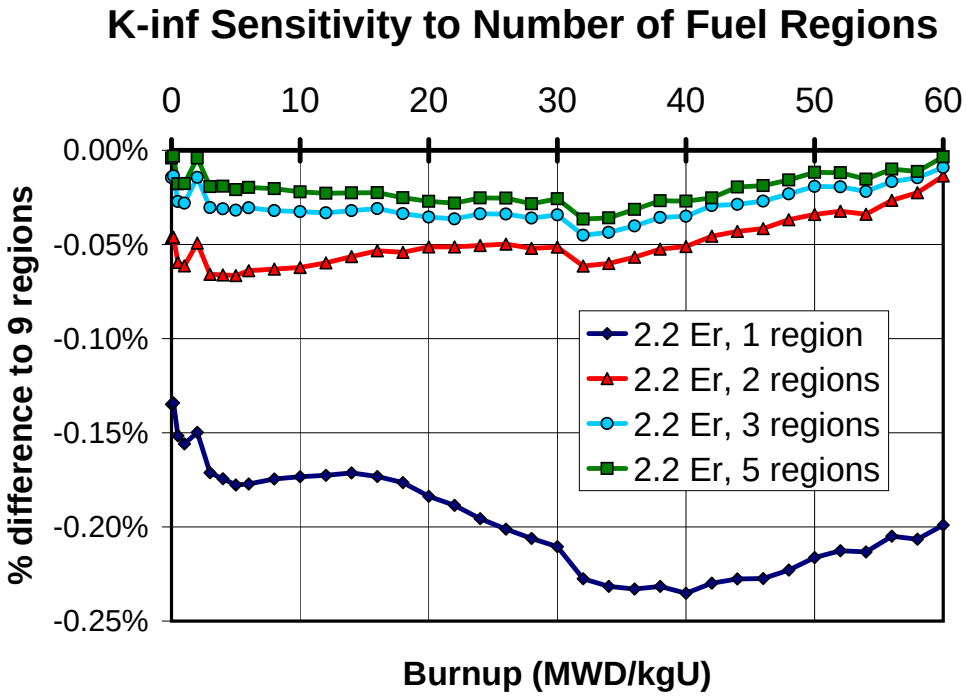

Figure G.2: Erbium Pin Cell Sensitivity Study, k_∞ Percent Difference to Base Case for Varying the Number of Fuel Regions

Appendix H

Erbium Assembly Benchmark

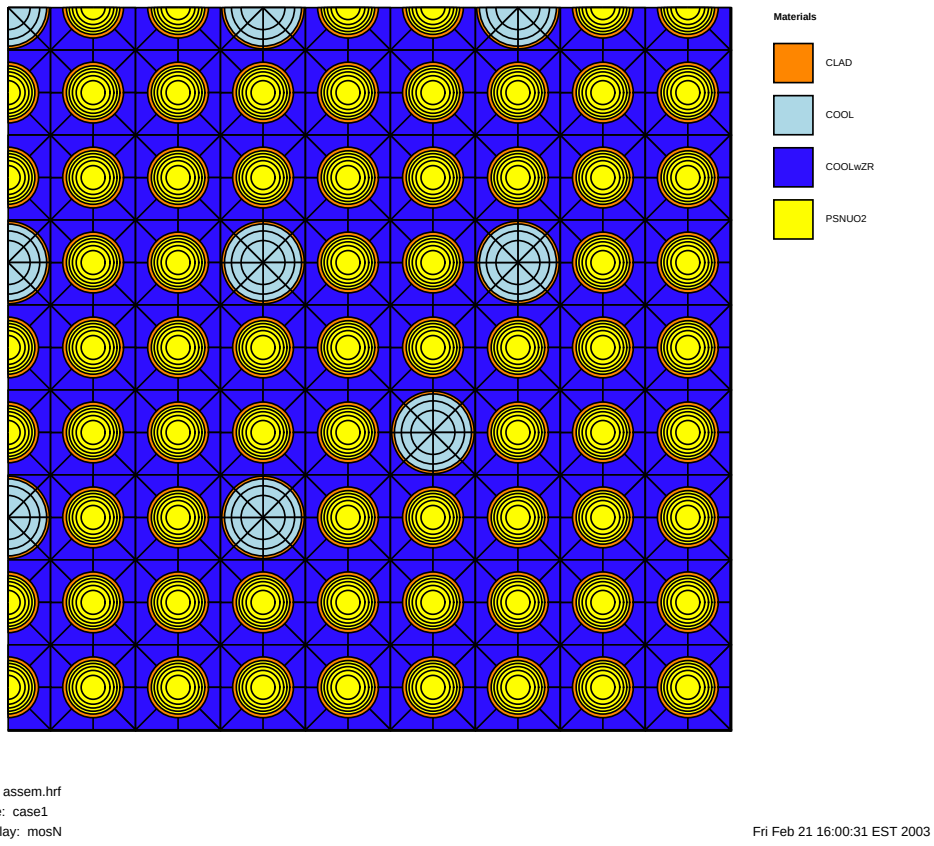

Figure H.1: The Erbium Benchmark Quarter-Assembly Geometry

Table H.1: Thermal Expansion Parameters

Material	$\frac{\delta l}{l}, \mathrm{K}^{-1}$
Fuel	9.70E-06
Clad	5.85E-06
Steel	1.65E-05
Grids	5.85E-06
AgInCd	2.31E-05

Table H.2: Erbium Assembly Benchmark k_∞Table

Burnup (MWD/kg)	No Er	1.0 Er	2.2 Er	SB, 1.0 Er
0	1.44645	1.20182	1.02554	1.11152
0.15	1.40761	1.17489	1.00602	1.08886
0.5	1.3992	1.17375	1.00784	1.08838
1	1.39206	1.17550	1.01293	1.09046
2	1.38147	1.18085	1.02430	1.09599
3	1.37106	1.18532	1.03477	1.10054
4	1.36046	1.18859	1.04409	1.10386
5	1.34977	1.19084	1.05242	1.10615
6	1.3391	1.19223	1.05987	1.10755
8	1.31808	1.19278	1.07235	1.10818
10	1.29778	1.19109	1.08242	1.10654
12	1.27827	1.18746	1.09005	1.10299
14	1.25949	1.18214	1.09537	1.09780
15	–	–	–	1.09463
16	1.24136	1.17536	1.09845	1.09160
18	1.22378	1.16728	1.09938	1.08468
20	1.20666	1.15806	1.09829	1.07666
22	1.18991	1.14787	1.09532	1.06776
24	1.17348	1.13685	1.09061	1.05810
26	1.15729	1.12511	1.08434	1.04780
28	1.14129	1.11275	1.07667	1.03697
30	1.12546	1.09990	1.06779	1.02573
32	1.10978	1.08663	1.05788	1.01416
33	–	–	–	1.00824
34	1.0942	1.07304	1.04708	1.00975
36	1.07874	1.05919	1.03555	1.01278
38	1.06335	1.04512	1.02342	1.01598
40	1.04807	1.03093	1.01082	1.01952
42	1.03289	1.01665	0.99786	1.02347
44	1.01781	1.00233	0.98461	1.00890
46	1.00285	0.98798	0.97118	0.99443
48	0.98805	0.97372	0.95766	0.98007
50	0.97341	0.95954	0.94410	0.96581
52	0.95894	0.94545	0.93056	0.95172
54	0.94472	0.93157	0.91712	0.93781
56	0.93074	0.91789	0.90382	0.92409
58	0.91703	0.90444	0.89069	0.91064
60	0.90369	0.89133	0.87783	0.89748

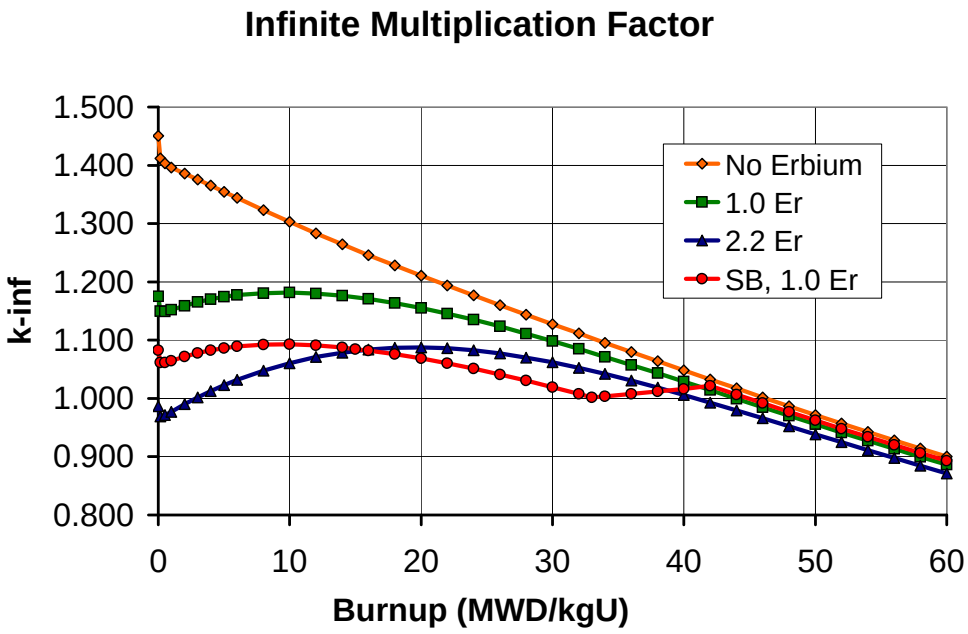

Figure H.2: Erbium Assembly Benchmark k_∞

Table H.3: Erbium Assembly Relative Pin Power Distribution at 0.0 MWD/kgU, No Erbium

0.938								
0.933	0.930							
0.937	0.941	0.973						
0.947	0.959	1.019						
0.958	0.985	1.045	1.063	1.046				
0.967	1.012		1.048	1.049				
0.966	0.990	1.028	1.014	1.017	1.040	1.015		
0.966	0.989	1.026	1.010	1.013	1.038	1.014	1.014	
0.974	1.014		1.035	1.039		1.040	1.040	

Table H.4: Erbium Assembly Relative Pin Power Distribution at 0.0 MWD/kgU, 1.0 wt% Erbium

0.932								
0.927	0.924							
0.931	0.935	0.970						
0.941	0.955	1.021						
0.953	0.984	1.050	1.071	1.051				
0.963	1.013		1.053	1.054				
0.962	0.989	1.031	1.015	1.018	1.044	1.017		
0.962	0.988	1.028	1.011	1.014	1.041	1.015	1.015	
0.970	1.015		1.038	1.042		1.043	1.043	

Table H.5: Erbium Assembly Relative Pin Power Distribution at 0.0 MWD/kgU, 2.2 wt% Erbium

0.928								
0.923	0.919							
0.926	0.931	0.969						
0.937	0.952	1.023						
0.950	0.983	1.055	1.076	1.055				
0.960	1.015		1.056	1.057				
0.960	0.989	1.034	1.016	1.019	1.046	1.017		
0.959	0.987	1.030	1.011	1.015	1.043	1.016	1.015	
0.968	1.016		1.040	1.044		1.045	1.045	

Table H.6: Erbium Assembly Relative Pin Power Distribution at 0.0 MWD/kgU, SB

0.938								
0.933	0.930							
0.936	0.940	0.973						
0.946	0.958	1.020						
0.957	0.985	1.048	1.066	1.048				
0.966	1.013		1.049	1.050				
0.965	0.990	1.029	1.013	1.016	1.040	1.014		
0.964	0.989	1.027	1.009	1.012	1.038	1.013	1.012	
0.973	1.014		1.035	1.039		1.040	1.039	

Table H.7: Erbium Assembly Relative Pin Burnup Distribution at 60.0 MWD/kgU, No Erbium

57.4								
57.3	57.3							
57.5	57.7	59.0						
57.9	58.4	60.5						
58.4	59.5	61.6	62.2	61.8				
58.7	60.3		61.7	61.8				
58.8	59.7	61.0	60.7	60.8	61.5	60.8		
58.8	59.7	60.9	60.6	60.7	61.4	60.8	60.7	
59.1	60.4		61.3	61.4		61.5	61.5	

Table H.8: Erbium Assembly Relative Pin Burnup Distribution at 60.0 MWD/kgU, 1.0 wt% Erbium

57.3								
57.2	57.1							
57.4	57.6	58.9						
57.8	58.4	60.6						
58.3	59.5	61.6	62.3	61.9				
58.7	60.4		61.7	61.8				
58.7	59.7	61.0	60.7	60.9	61.5	60.8		
58.7	59.7	60.9	60.6	60.7	61.5	60.8	60.8	
59.1	60.5		61.3	61.5		61.5	61.5	

Table H.9: Erbium Assembly Relative Pin Burnup Distribution at 60.0 MWD/kgU, 2.2 wt% Erbium

57.1								
57.0	57.0							
57.2	57.5	58.9						
57.7	58.3	60.6						
58.3	59.5	61.7	62.4	62.0				
58.6	60.4		61.8	61.9				
58.7	59.7	61.1	60.8	60.9	61.6	60.8		
58.6	59.7	61.0	60.6	60.8	61.5	60.9	60.8	
59.0	60.5		61.4	61.5		61.6	61.6	

Table H.10: Erbium Assembly Relative Pin Burnup Distribution at 60.0 MWD/kgU, SB

57.4								
57.3	57.2							
57.5	57.7	59.0						
57.9	58.4	60.6						
58.4	59.5	61.6	62.3	61.9				
58.7	60.4		61.7	61.8				
58.7	59.7	61.0	60.7	60.8	61.5	60.8		
58.7	59.7	60.9	60.5	60.7	61.4	60.7	60.7	
59.0	60.5		61.3	61.4		61.5	61.5	

Table H.11: Erbium Assembly Isotopics (atoms/barn $\cdot$ cm) at 60 MWD/kgU

Nuclide	No Er	1.0 wt% Er	2.2 wt% Er	SB
92235	1.55159E-04	1.58792E-04	1.62971E-04	1.68066E-04
92238	2.08791E-02	2.05919E-02	2.02502E-02	2.05756E-02
94238	9.76790E-06	9.76548E-06	9.76383E-06	1.01421E-05
94239	1.20160E-04	1.20739E-04	1.21405E-04	1.23848E-04
94240	6.61935E-05	6.58725E-05	6.55095E-05	6.71479E-05
94241	3.69935E-05	3.72101E-05	3.74714E-05	3.83405E-05
94242	2.24926E-05	2.23448E-05	2.21544E-05	2.25726E-05
95241	2.40032E-06	2.46370E-06	2.54125E-06	2.62409E-06
95342	4.25429E-08	4.38575E-08	4.54670E-08	4.71959E-08
95243	6.00746E-06	5.97702E-06	5.93339E-06	6.06886E-06
96242	6.78400E-07	6.82989E-07	6.88476E-07	7.09023E-07
96244	2.71784E-06	2.70277E-06	2.68093E-06	2.76815E-06
54635	6.05256E-09	6.07963E-09	6.10776E-09	6.24778E-09
62649	7.53446E-08	7.59701E-08	7.66668E-08	7.85366E-08
68166	0	9.72834E-05	2.14623E-04	9.71434E-05
68167	0	2.13984E-06	4.61287E-06	2.14575E-06
68168	0	1.66454E-04	3.63472E-04	1.66400E-04
68170	0	4.49842E-05	9.85474E-05	4.49371E-05

Table H.12: Erbium Assembly Fluxes at 0 and 60 MWD/kgU ($n/cm^2 \cdot s$)

Burnup	Flux	No Er	1.0 wt% Er	2.2 wt% Er	SB
0 MWD/kgU	Fast	1.097E+14	1.228E+14	1.357E+14	1.299E+14
	Thermal	1.632E+13	1.589E+13	1.553E+13	1.573E+13
	Ratio	6.72	7.73	8.74	8.26
60 MWD/kgU	Fast	1.707E+14	1.701E+14	1.692E+14	1.690E+14
	Thermal	3.092E+13	3.020E+13	2.938E+13	2.918E+13
	Ratio	5.52	5.63	5.76	5.79

Table H.13: Erbium Assembly k_∞ for Control Rods at BOL

Case	Uncontrolled	Rodded	$\frac{\delta k}{k}$
No Er%	1.44645	1.01573	29.32%
No Er, 1000 ppm	1.32642	0.95738	29.06%
Er 1.0%	1.20182	0.86935	31.82%
Er 1.0%, 1000 ppm	1.11134	0.82457	31.29%
Er 2.2%	1.02554	0.76218	33.69%
Er 2.2% 1000 ppm	0.9554	0.72682	32.92%

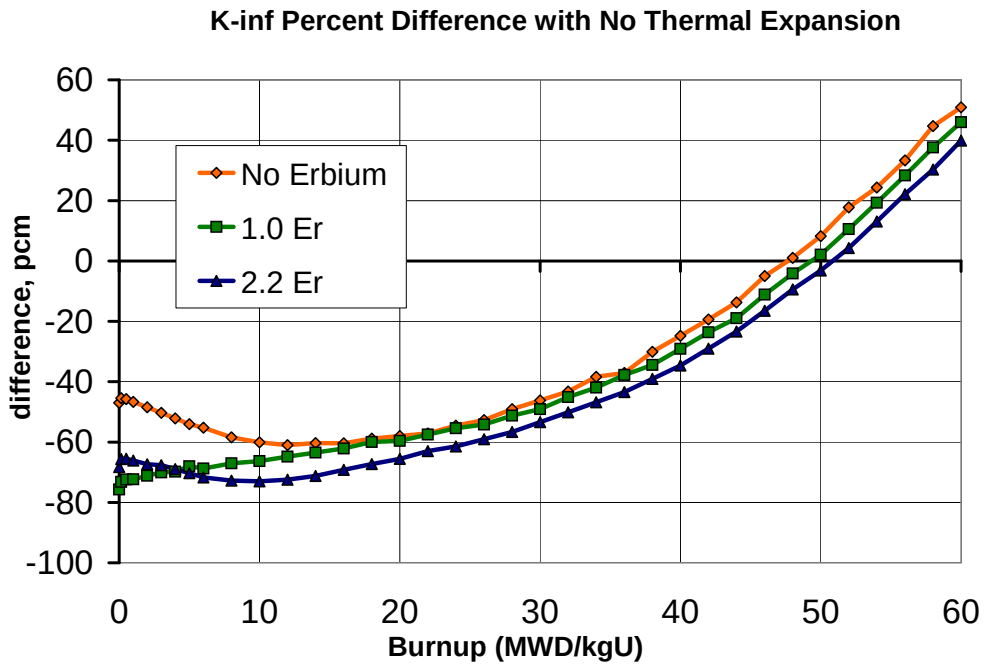

Figure H.3: Erbium Assembly Sensitivity Study, k_∞ Percent Difference with No Thermal Expansion

Appendix I

Erbium Core Benchmark

Table I.1: NESTLE Geometry Input for Lower Right Quarter of Erbium Benchmark Core

3	1	3	1	1	3	5	5
1	3	1	3	1	3	5	5
3	1	3	1	4	5	5	5
1	3	1	3	3	5	5	5
1	1	4	3	5	5	5	
3	3	5	5	5	5		
5	5	5	5	5			
5	5	5	5				

Table I.2: Erbium Model Cross Section Conversion Utility Results

Burnup (MWD/kgU)	HELIOS k_∞	NESTLE k_∞	Diff., pcm
0	1.0683	1.0425	-2419
0.15	1.0473	1.0424	-468
0.5	1.0481	1.0459	-201
1	1.0517	1.0510	-70
2	1.0603	1.0601	-20
3	1.0680	1.0678	-18
4	1.0743	1.0742	-17
5	1.0797	1.0795	-17
6	1.0841	1.0839	-14
8	1.0905	1.0905	2
10	1.0944	1.0944	-2
12	1.0960	1.0960	-1
14	1.0955	1.0955	2
16	1.0931	1.0932	6
18	1.0889	1.0891	17
20	1.0832	1.0835	30
22	1.0762	1.0766	44
24	1.0679	1.0685	61
26	1.0585	1.0593	71
28	1.0483	1.0492	83
30	1.0374	1.0383	89
32	1.0259	1.0269	98
34	1.0138	1.0149	107
36	1.0014	1.0026	118
38	0.9887	0.9900	125
40	0.9759	0.9771	131
42	0.9628	0.9642	142
44	0.9497	0.9511	146
46	0.9366	0.9379	148
48	0.9235	0.9248	144
50	0.9105	0.9116	124
52	0.8976	0.8986	109
54	0.8849	0.8856	89
56	0.8724	0.8728	55
58	0.8601	0.8603	19
60	0.8481	0.8480	-14

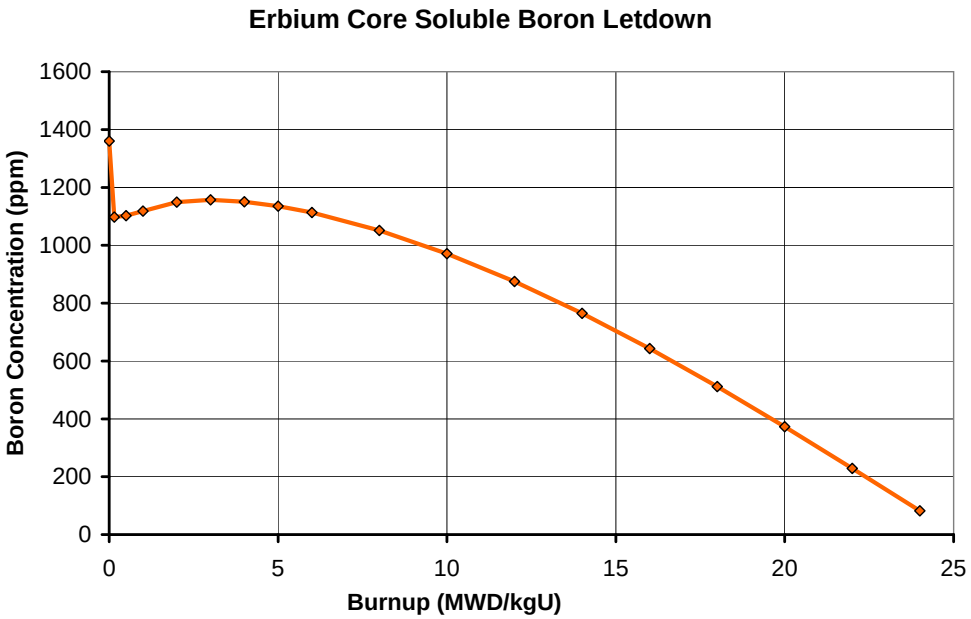

Figure I.1: Erbium Benchmark Core Soluble Boron Letdown Curve

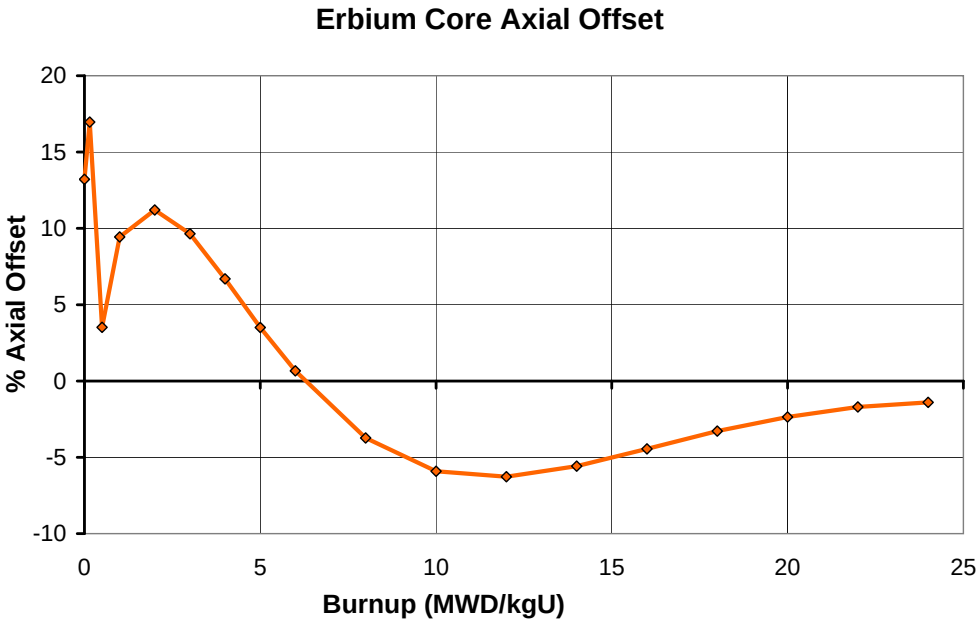

Figure I.2: Erbium Benchmark Core Percentage Axial Offset

Table I.3: Erbium Benchmark Core Parameters versus Burnup

Burnup (MWD/kgU)	k_{eff}	SB (ppm)	FQ*	FdH*	FZ*	Axial Offset (%)
0	1.000	1360.2	2.1075	1.4630	1.4273	13.210
0.15	1.000	1097.4	2.2492	1.4120	1.5020	16.961
0.5	1.000	1102.3	1.8643	1.3752	1.2785	3.519
1	1.000	1118.1	2.0106	1.3427	1.3588	9.436
2	1.000	1149.0	2.0627	1.3931	1.3727	11.204
3	1.000	1156.9	2.0049	1.4203	1.3325	9.641
4	1.000	1150.7	1.9018	1.4375	1.2702	6.691
5	1.000	1135.4	1.7991	1.4460	1.2102	3.510
6	1.000	1113.3	1.7255	1.4481	1.1630	0.661
8	1.000	1051.1	1.7363	1.4373	1.1830	-3.729
10	1.000	970.7	1.7176	1.4129	1.1920	-5.911
12	1.000	874.5	1.6776	1.3800	1.1938	-6.277
14	1.000	764.5	1.6730	1.3674	1.1925	-5.584
16	1.000	643.0	1.6752	1.3706	1.1852	-4.450
18	1.000	511.6	1.6740	1.3676	1.1772	-3.284
20	1.000	372.7	1.6583	1.3595	1.1633	-2.358
22	1.000	229.0	1.6413	1.3475	1.1543	-1.700
24	1.000	81.9	1.6314	1.3328	1.1519	-1.402

* FQ, FdH, and FZ are unitless parameters describing the maximum nodal power peaking, maximum radial peaking by bundle, and maximum axial power peaking, respectively.

Table I.4: Erbium Benchmark Core Relative Radial Power Map, 0 MWD/kgU

1.0730	1.2677	1.0457	1.1239	0.8380	0.4127
1.2677	1.0672	1.2568	1.0329	0.9911	0.3756
1.0457	1.2568	1.0813	1.3088	1.4630	
1.1239	1.0329	1.3088	0.9910	0.6486	
0.8380	0.9911	1.4630	0.6486		
0.4127	0.3756				

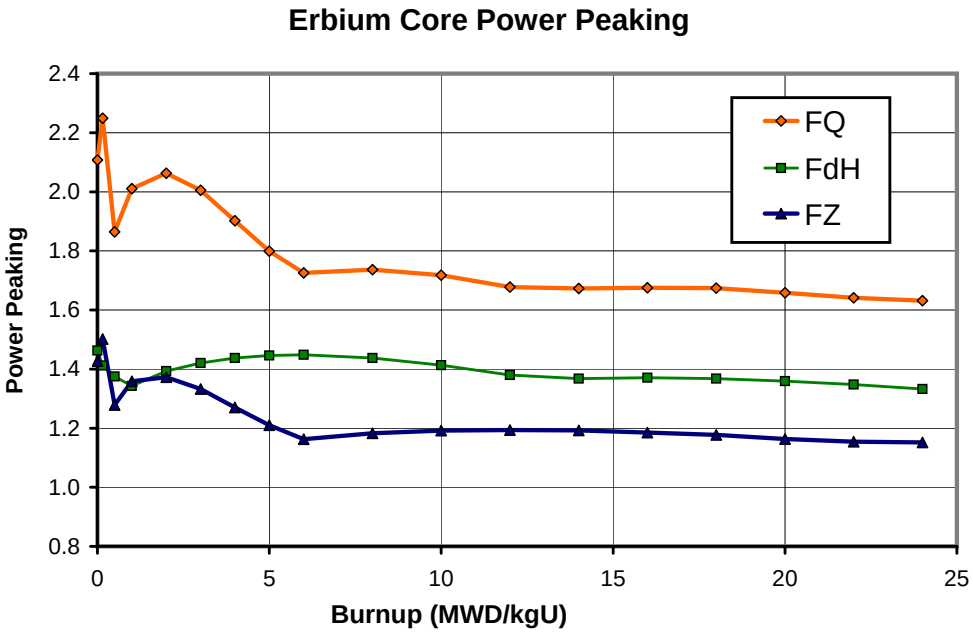

Figure I.3: Erbium Benchmark Core Power Peaking

Table I.5: Erbium Benchmark Core Relative Radial Power Map, 24 MWD/kgU

0.9433	1.2191	0.9797	1.3328	1.3171	0.6899
1.2191	0.9573	1.2526	1.0139	1.2347	0.5741
0.9797	1.2526	0.9719	1.2285	1.0461	
1.3328	1.0139	1.2285	0.8067	0.5196	
1.3171	1.2347	1.0461	0.5196		
0.6899	0.5741				

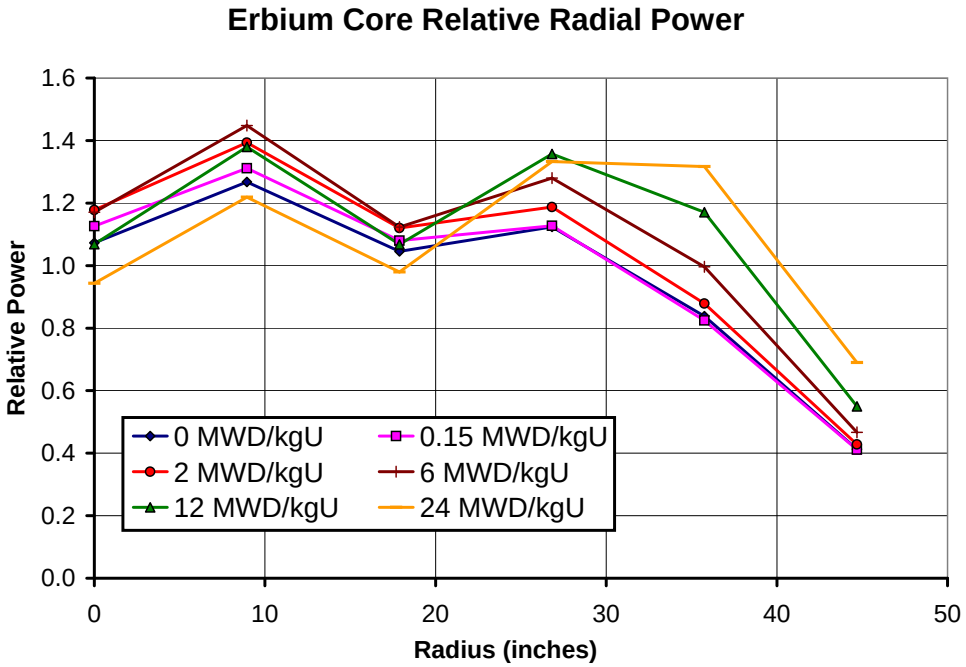

Figure I.4: Erbium Benchmark Core Relative Radial Power

Table I.6: Erbium Benchmark Core Burnup Map, 24 MWD/kgU, SB = 82 ppm

25.627	32.384	25.475	31.514	27.223	13.207
32.384	25.544	32.047	24.870	26.904	11.126
25.475	32.047	24.780	30.053	26.767	
31.514	24.870	30.053	19.602	12.157	
27.223	26.904	26.767	12.157		
13.207	11.126				

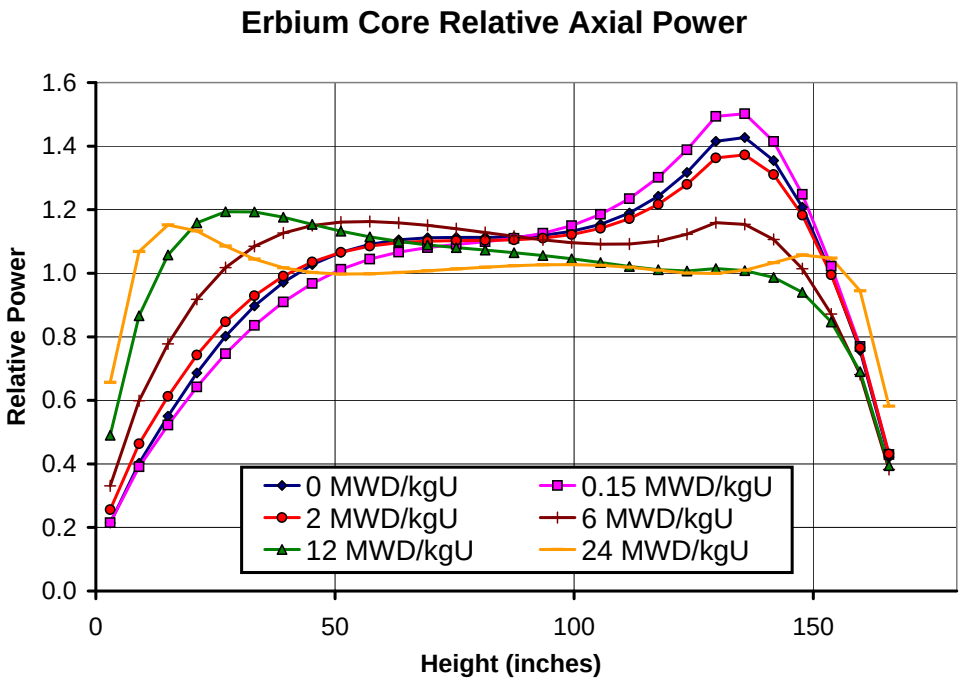

Figure I.5: Erbium Benchmark Core Relative Axial Power

Table I.7: Erbium Benchmark Core Benchmark, No Critical Boron Search

Burnup (MWD/kgU)	k_{eff}	SB (ppm)	FQ*	FdH*	FZ*	Axial Offset (%)
0	1.1428	–	2.205	1.349	1.943	-48.316
0.15	1.1121	–	2.511	1.374	2.230	-60.138
0.5	1.1186	–	1.818	1.348	1.282	7.686
1	1.1121	–	1.916	1.373	1.381	-17.367
2	1.1119	–	1.922	1.414	1.350	-15.706
3	1.1108	–	1.867	1.433	1.281	-11.563
4	1.1088	–	1.796	1.443	1.223	-7.948
5	1.1061	–	1.733	1.447	1.186	-5.485
6	1.1030	–	1.728	1.447	1.158	-3.665
8	1.0957	–	1.709	1.434	1.121	-0.754
10	1.0872	–	1.654	1.408	1.130	1.414
12	1.0776	–	1.595	1.374	1.131	2.503
14	1.0668	–	1.586	1.348	1.126	3.173
16	1.0550	–	1.600	1.360	1.114	3.202
18	1.0424	–	1.609	1.365	1.106	3.204
20	1.0291	–	1.622	1.366	1.110	3.379
22	1.0151	–	1.648	1.362	1.122	3.614
24	1.0006	–	1.654	1.362	1.136	3.847

* FQ, FdH, and FZ are unitless parameters describing the maximum nodal power peaking, maximum radial peaking by bundle, and maximum axial power peaking, respectively.

Table I.8: Erbium Core Benchmark, Uniform Poison Distribution, Critical Soluble Boron Search

Burnup (MWD/kgU)	k_{eff}	SB (ppm)	FQ*	FdH*	FZ*	Axial Offset (%)
0	1.000	1308.1	3.164	1.486	1.779	-43.323
0.15	1.000	1059.8	3.188	1.415	1.946	-51.785
0.5	1.000	1069.1	2.251	1.392	1.386	-17.331
1	1.000	1072.8	2.386	1.352	1.539	-27.585
2	1.000	1100.0	2.238	1.383	1.521	-26.439
3	1.000	1107.9	2.136	1.414	1.450	-21.571
4	1.000	1103.3	2.036	1.432	1.372	-15.969
5	1.000	1090.2	1.930	1.441	1.301	-10.328
6	1.000	1070.9	1.858	1.443	1.254	-5.090
8	1.000	1014.8	1.830	1.434	1.241	3.470
10	1.000	940.4	1.847	1.413	1.264	8.289
12	1.000	848.8	1.845	1.383	1.275	9.468
14	1.000	742.4	1.803	1.361	1.269	8.144
16	1.000	623.4	1.729	1.366	1.252	5.921
18	1.000	494.3	1.665	1.365	1.222	3.855
20	1.000	357.5	1.630	1.359	1.204	2.315
22	1.000	215.6	1.614	1.348	1.182	1.280
24	1.000	70.1	1.615	1.334	1.160	0.541

* FQ, FdH, and FZ are unitless parameters describing the maximum nodal power peaking, maximum radial peaking by bundle, and maximum axial power peaking, respectively.

Table I.9: Erbium Core Benchmark, Uniform Poison Distribution, No Critical Soluble Boron Search

Burnup (MWD/kgU)	k_{eff}	SB (ppm)	FQ*	FdH*	FZ*	Axial Offset (%)
0	1.1395	–	3.762	1.336	2.363	-72.086
0.15	1.1101	–	3.560	1.357	2.354	-71.500
0.5	1.1102	–	2.324	1.339	1.547	-32.291
1	1.1084	–	2.445	1.367	1.666	-37.471
2	1.1071	–	2.479	1.403	1.646	-38.341
3	1.1056	–	2.296	1.421	1.518	-31.213
4	1.1036	–	2.110	1.430	1.398	-23.303
5	1.1012	–	1.961	1.435	1.307	-16.150
6	1.0985	–	1.864	1.436	1.249	-9.931
8	1.0920	–	1.806	1.427	1.218	0.441
10	1.0842	–	1.830	1.408	1.241	7.620
12	1.0752	–	1.855	1.379	1.271	11.479
14	1.0649	–	1.858	1.343	1.294	12.672
16	1.0535	–	1.820	1.354	1.294	11.634
18	1.0411	–	1.752	1.362	1.284	9.809
20	1.0279	–	1.720	1.365	1.266	8.105
22	1.0141	–	1.703	1.362	1.255	6.790
24	0.9997	–	1.702	1.361	1.245	5.982

* FQ, FdH, and FZ are unitless parameters describing the maximum nodal power peaking, maximum radial peaking by bundle, and maximum axial power peaking, respectively.

Appendix J

Burnable Poison Design Appendix

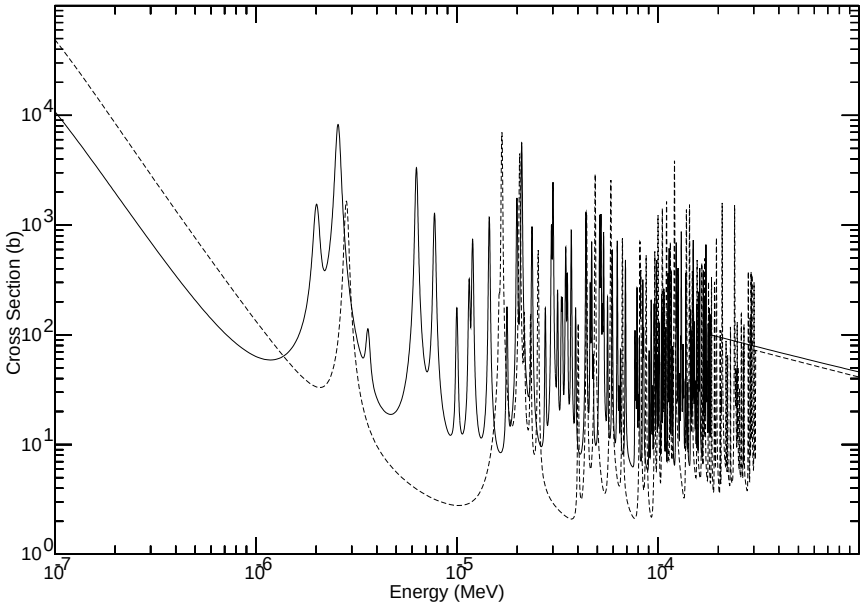

Figure J.1: Gadolinium Neutron Cross Sections

The hashed line is ^{157}Gd; the solid is ^{155}Gd.

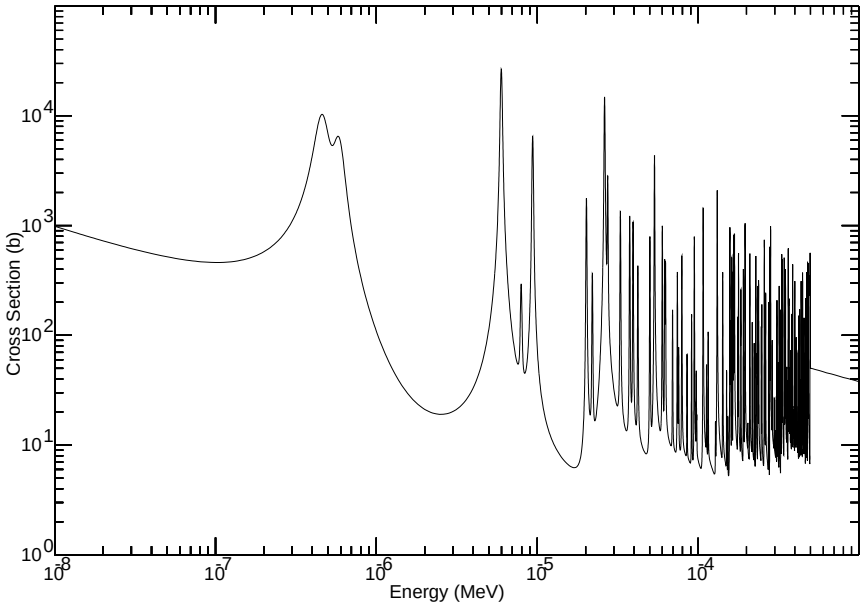

Figure J.2: ^{167}Er Neutron Cross Sections

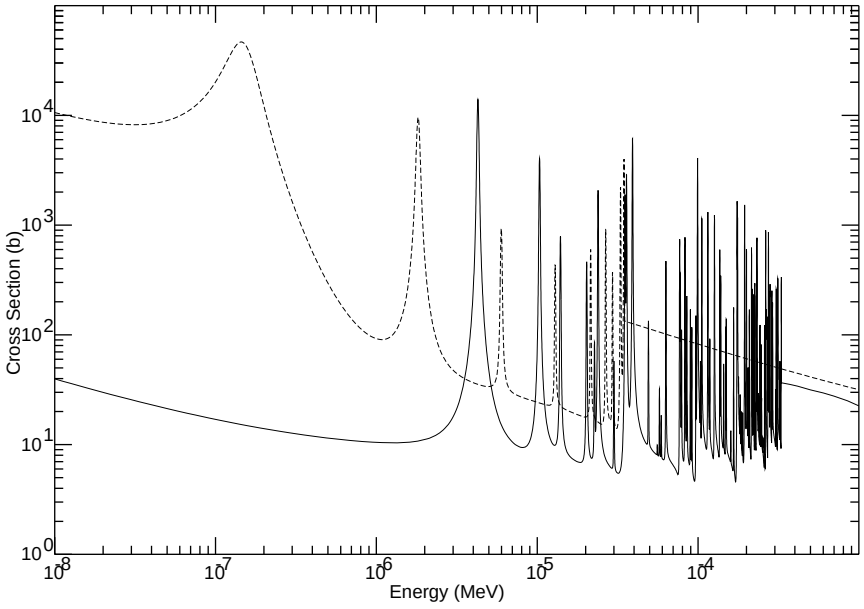

Figure J.3: Tantalum Neutron Cross Sections

The hashed line is ^{182}Ta; the solid is ^{181}Ta.

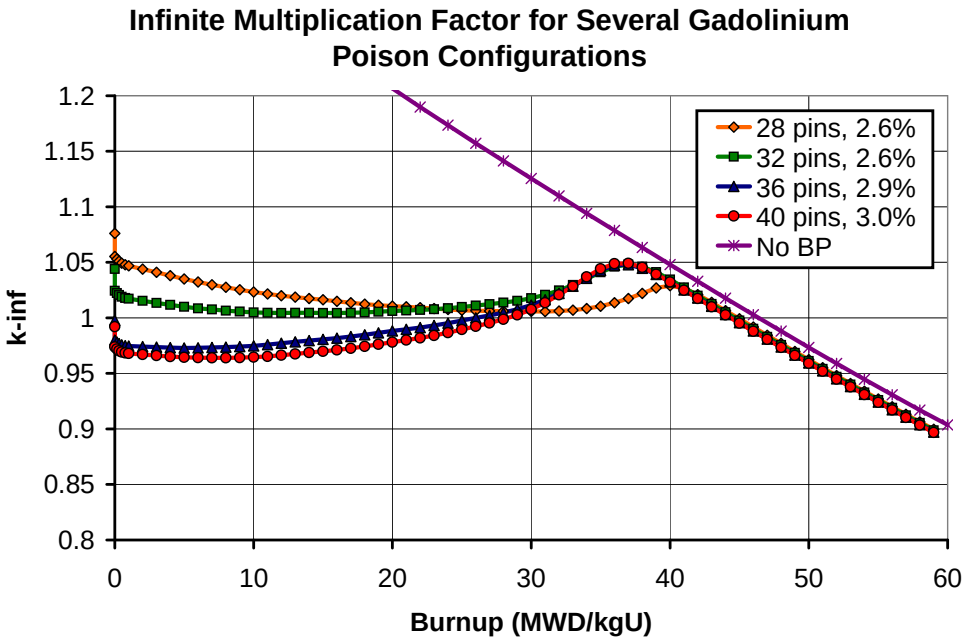

Figure J.4: k_∞ for Several Gadolinium Poison Configurations

Table J.1: Gadolinium Assembly Relative Pin Power Distribution at 0.0 MWd/kgU, 10.0 wt% Gadolinium in 28 Pins

1.124								
1.084	1.047							
1.063	0.323	0.320						
0.993	1.018	1.006						
1.107	1.047	0.323	0.993	0.318				
1.103	1.065		1.018	1.040				
1.099	1.037	0.320	1.006	1.065	1.064	0.321		
1.109	1.075	1.023	0.998	1.063	1.111	1.072	1.119	
1.119	1.120		0.320	1.062		1.151	1.174	

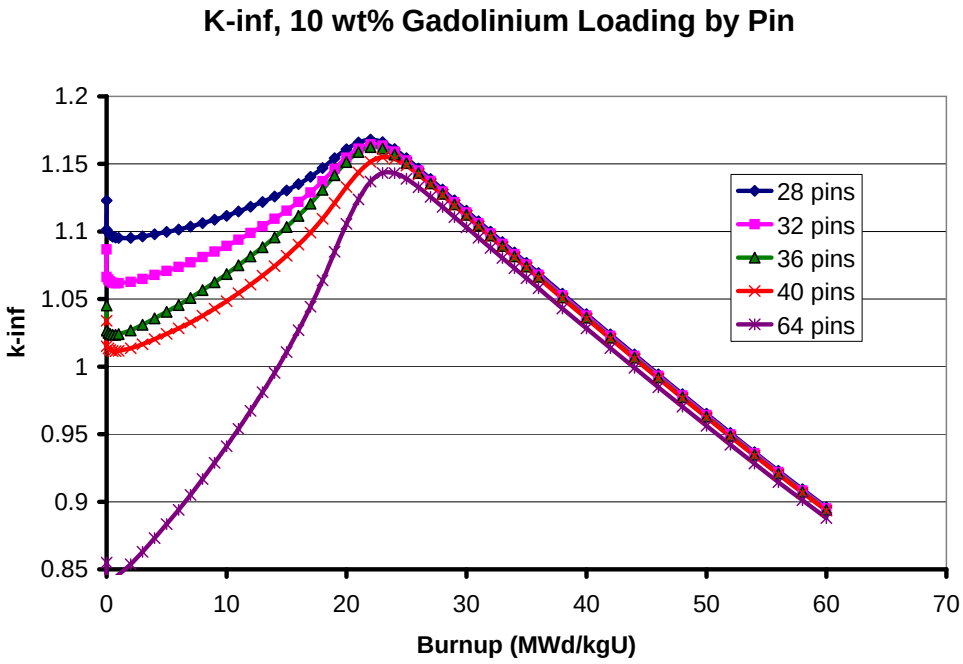

Figure J.5: k_∞, 10 wt% Gadolinium Loading by Pin

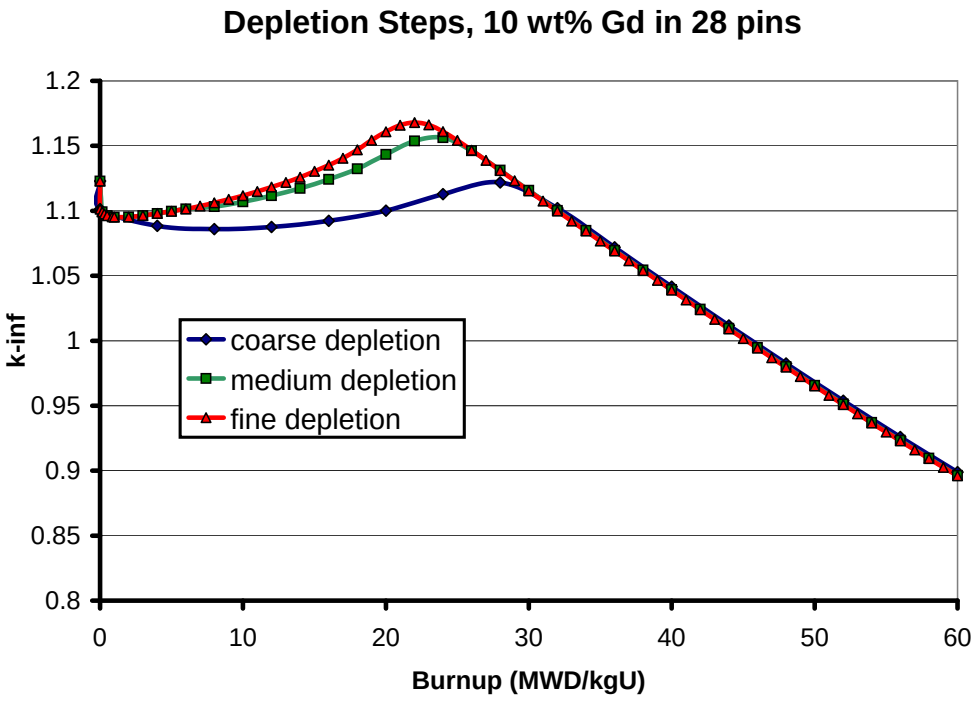

Figure J.6: The Effect of Varying Depletion Step Length on a Gadolinium Assembly

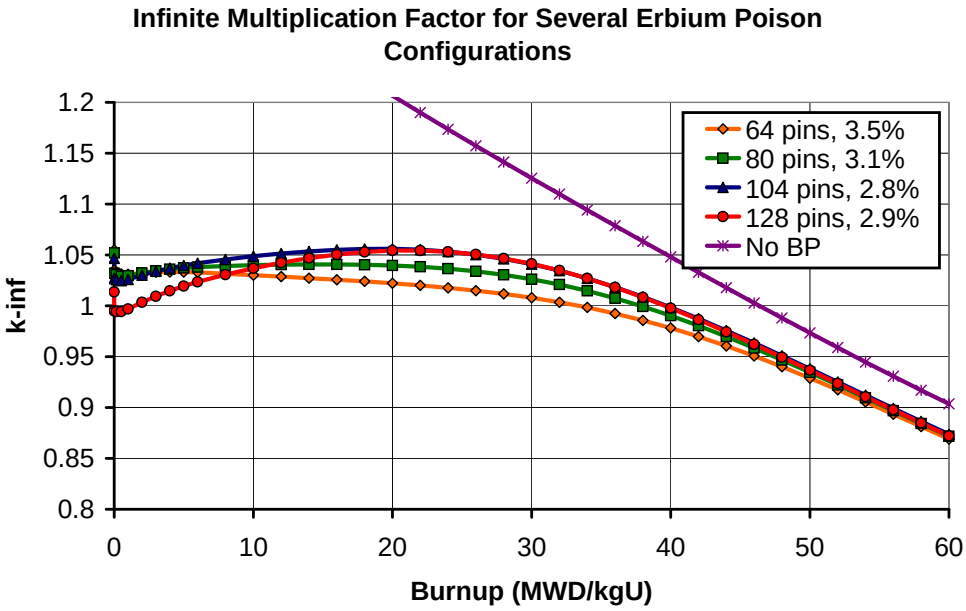

Figure J.7: $k_\infty$for Several Erbium Poison Configurations

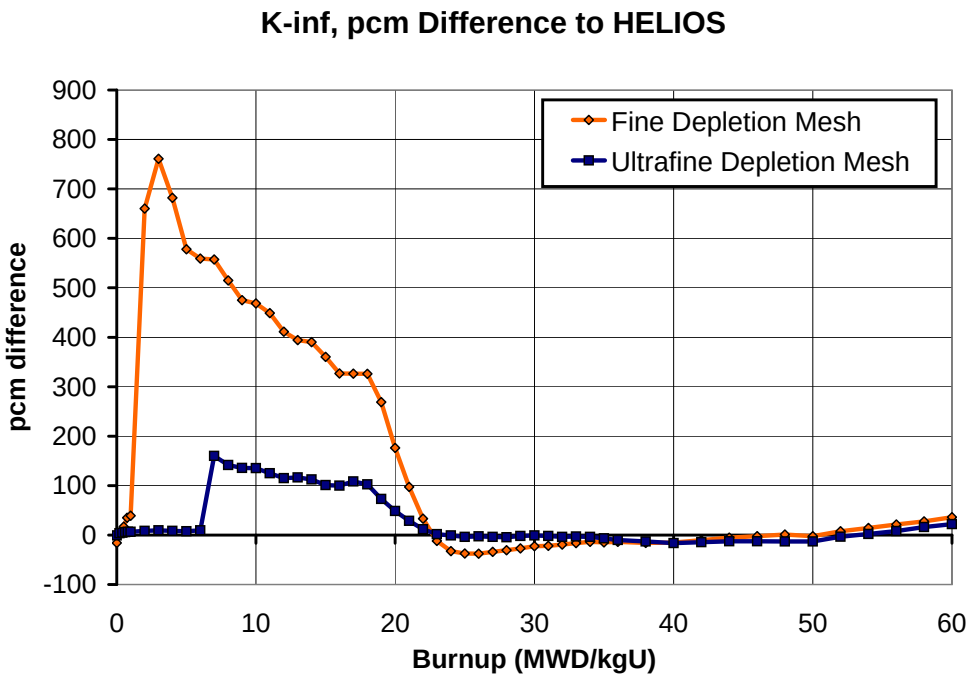

Figure J.8: Gadolinium Macroscopic Cross Section Calculation of k_∞

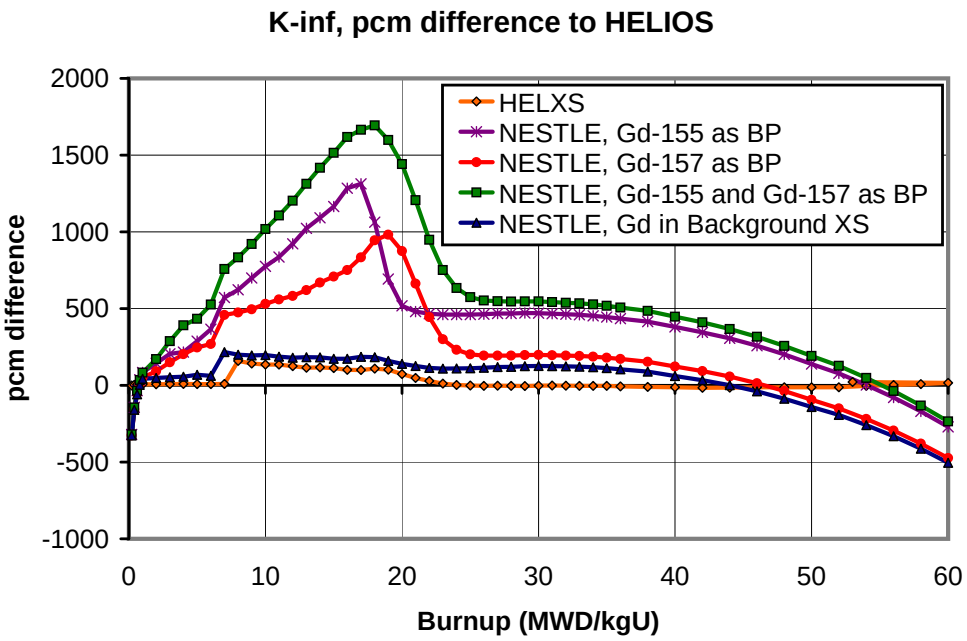

Figure J.9: Gadolinium Cross Section Approaches for NESTLE

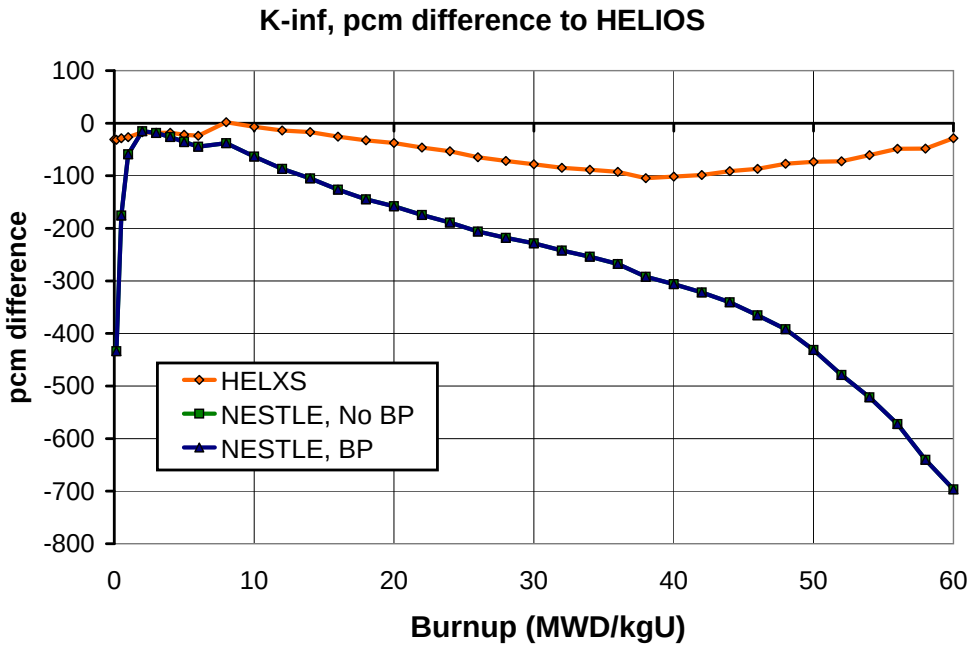

Figure J.10: Erbium Cross Section Approaches for NESTLE

Appendix K

Results Appendix

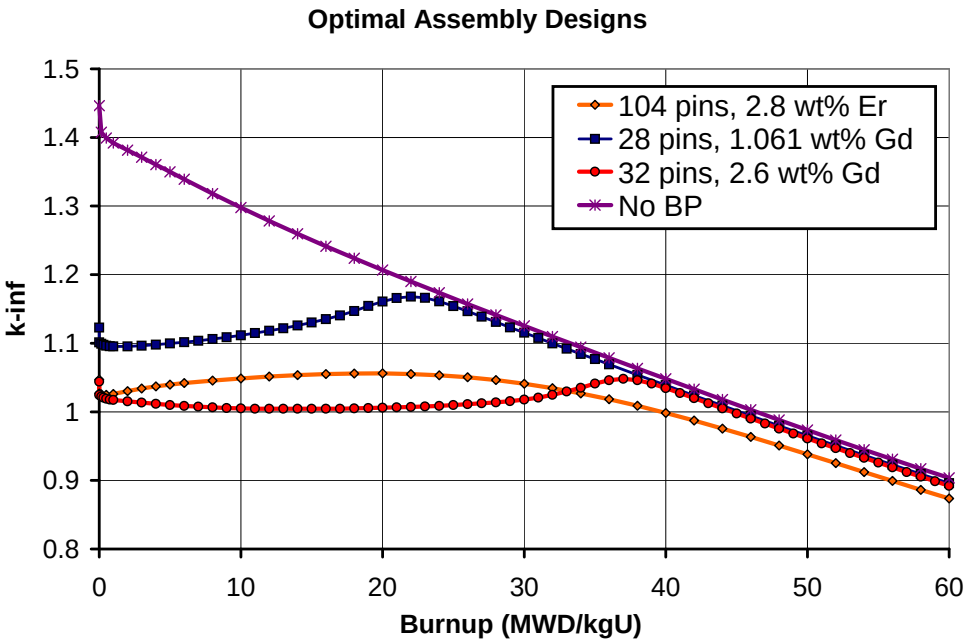

Figure K.1: Optimal Assembly Designs

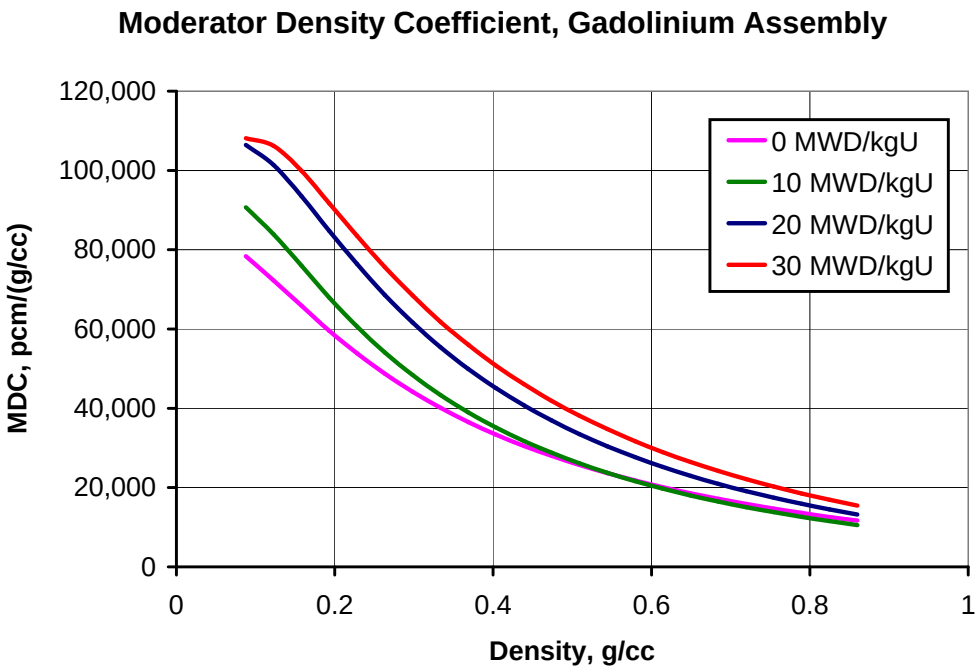

Figure K.2: Moderator Density Coefficient Study for a 28-pin Geometry at 10 wt% Gd_2O_3 per Pin

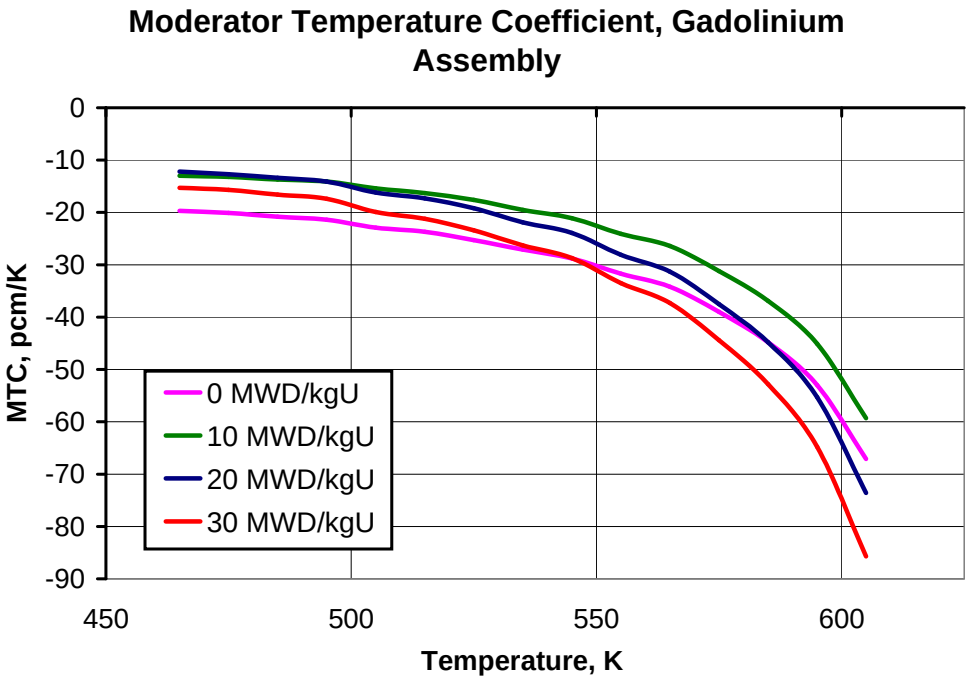

Figure K.3: Moderator Temperature Coefficient Study for a 28-pin Geometry at 10 wt% Gd_2O_3 per Pin

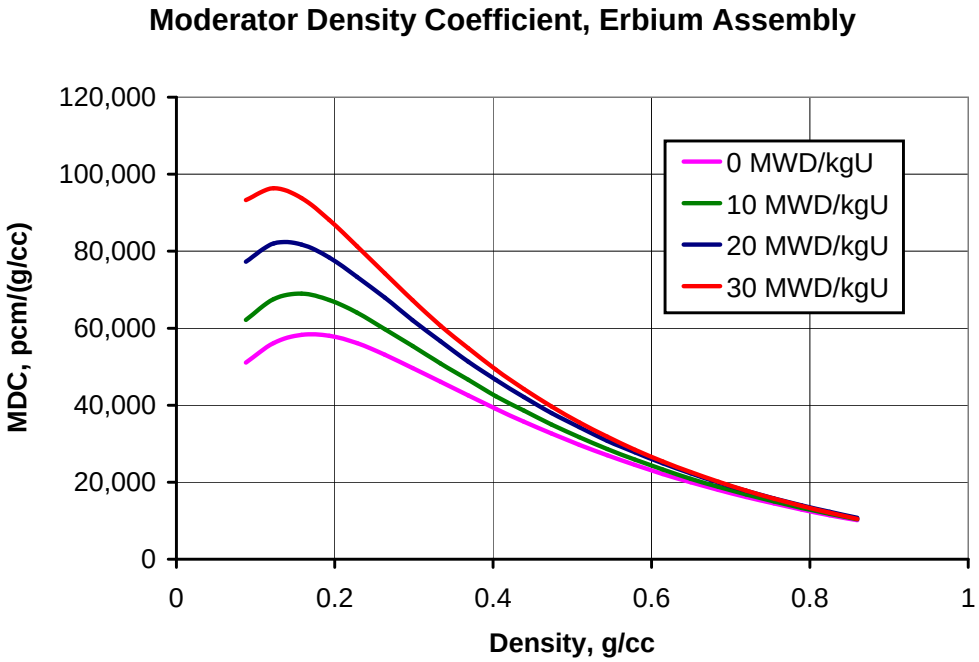

Figure K.4: Moderator Density Coefficient Study for an 80-pin Geometry at 2.5 wt% Er_2O_3 per Pin

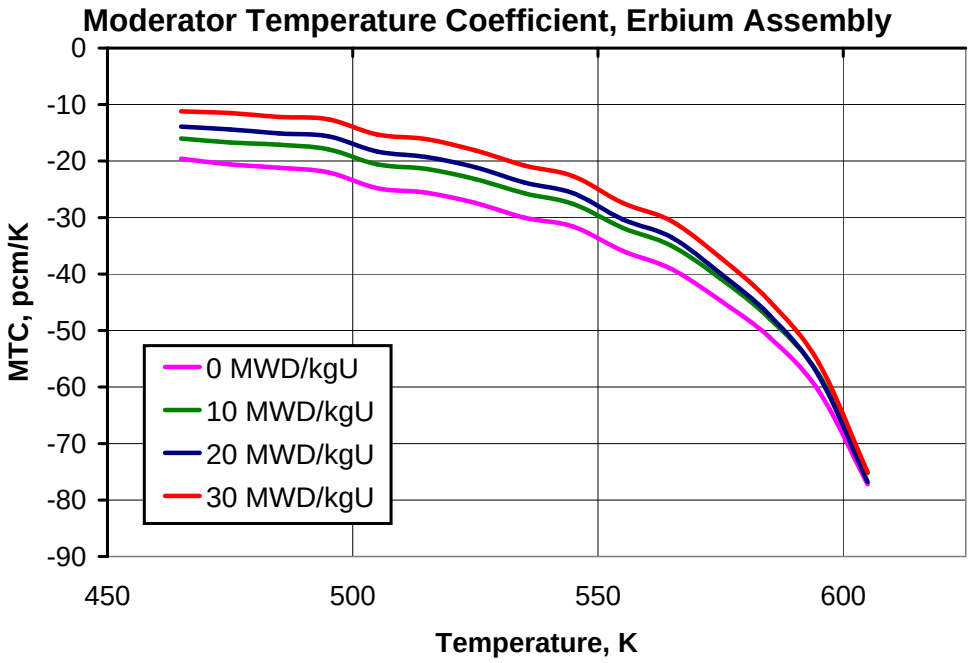

Figure K.5: Moderator Temperature Coefficient Study for a 80-pin Geometry at 2.5 wt% Er_2O_3 per Pin

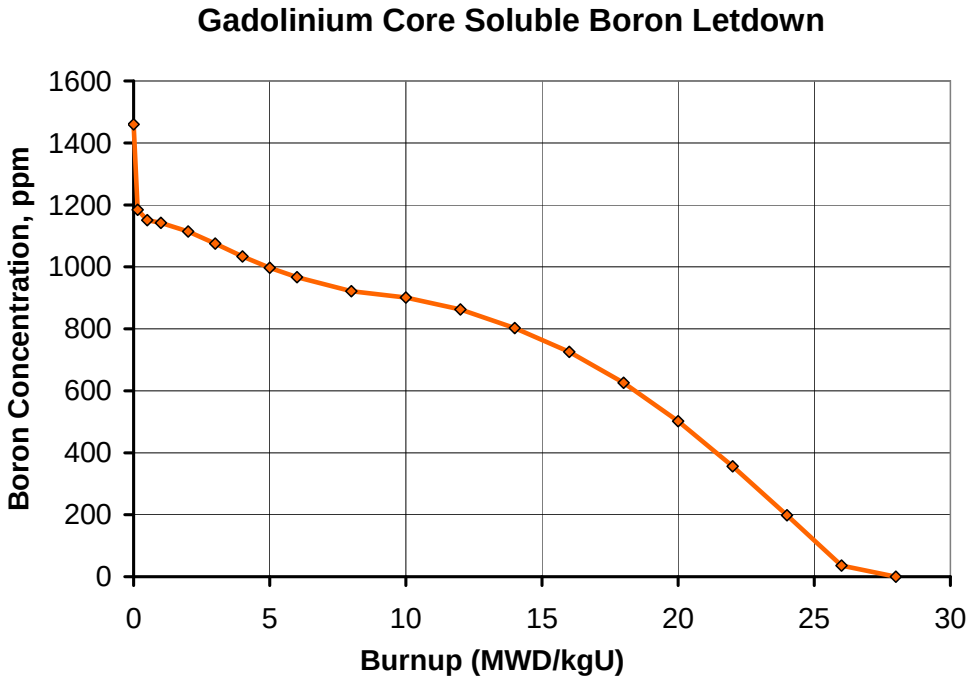

Figure K.6: Gadolinium Core Soluble Boron Letdown

Table K.1: Gadolinium Core Integral Parameters

Burnup (MWD/kgU)	k_{eff}	SB (ppm)	FQ*	FdH*	FZ*	Axial Offset (%)
0	1.000	1459.8	2.978	1.963	1.432	13.498
0.15	1.000	1184.1	3.017	1.967	1.446	10.933
0.5	1.000	1151.0	2.501	1.857	1.273	1.276
1	1.000	1142.0	2.522	1.853	1.286	1.726
2	1.000	1114.3	2.401	1.824	1.255	0.245
3	1.000	1075.4	2.246	1.770	1.215	-1.622
4	1.000	1033.4	2.224	1.731	1.223	-4.464
5	1.000	997.3	2.228	1.707	1.239	-6.471
6	1.000	966.9	2.237	1.692	1.253	-7.828
8	1.000	921.7	2.355	1.688	1.306	-11.064
10	1.000	900.8	2.369	1.686	1.358	-14.185
12	1.000	862.5	1.935	1.539	1.204	-5.623
14	1.000	802.4	1.906	1.502	1.169	0.046
16	1.000	725.7	1.923	1.467	1.215	3.638
18	1.000	626.1	1.935	1.449	1.301	6.706
20	1.000	501.7	2.026	1.453	1.368	7.441
22	1.000	356.5	2.042	1.437	1.387	5.653
24	1.000	198.2	1.928	1.409	1.325	2.804
26	1.000	35.7	1.808	1.374	1.259	0.745
28	0.9879	0.0	1.747	1.349	1.236	2.268

* FQ, FdH, and FZ are unitless parameters describing the maximum nodal power peaking, maximum radial peaking by bundle, and maximum axial power peaking, respectively.

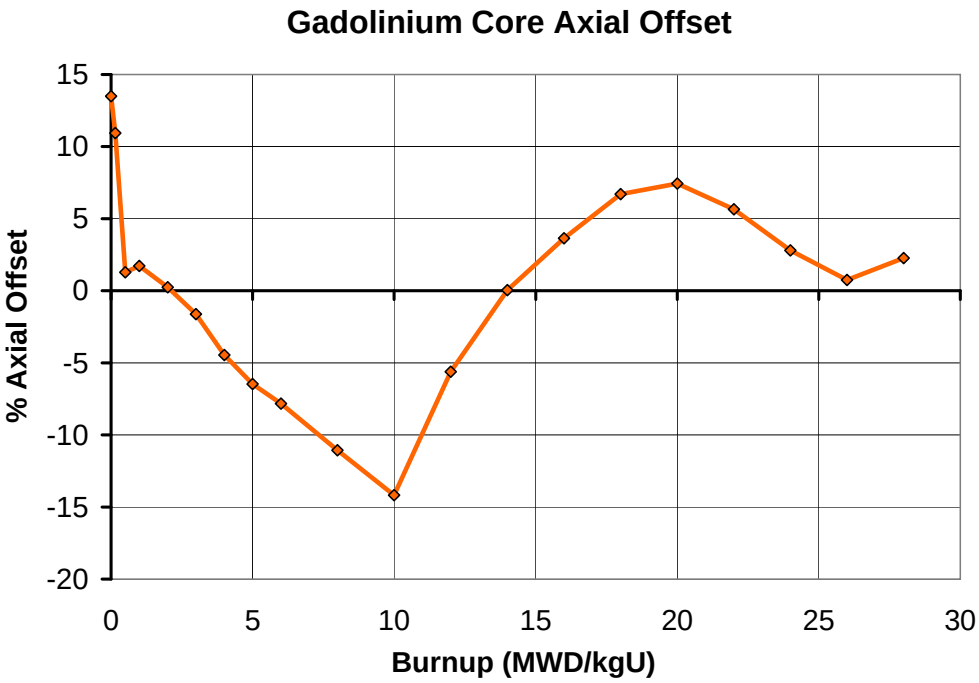

Figure K.7: Gadolinium Core Percentage Axial Offset

Table K.2: Gadolinium Core Relative Radial Power Map, 0 MWD/kgU

1.8892	1.9628	1.5699	1.3957	0.9001	0.3665
1.9628	1.7201	1.6856	1.1469	0.8311	0.2881
1.5699	1.6856	1.2753	1.0978	0.6086	
1.3957	1.1469	1.0978	0.6550	0.3078	
0.9001	0.8311	0.6086	0.3078		
0.3665	0.2881				

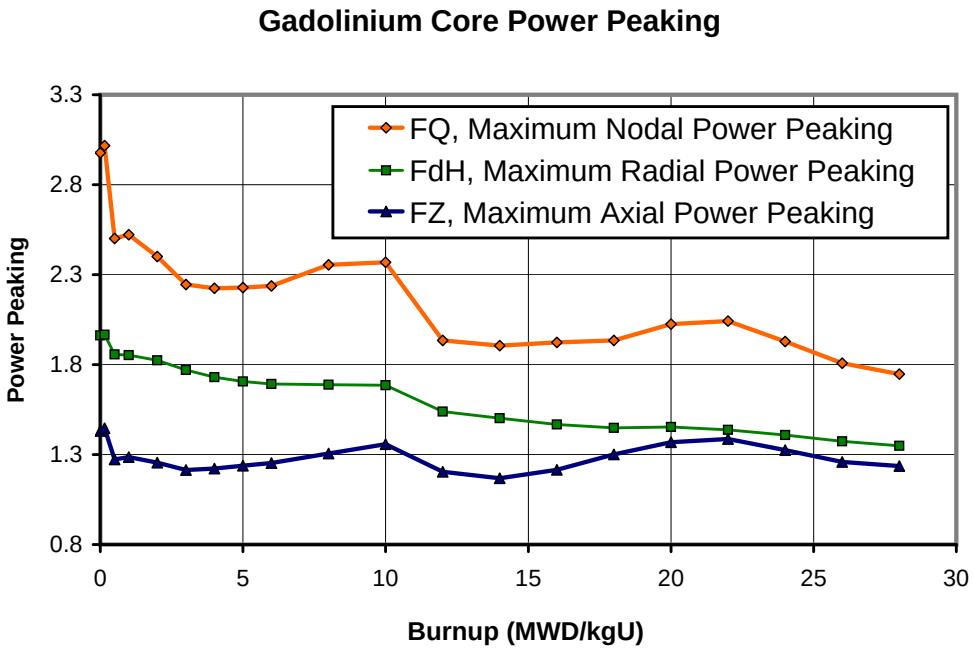

Figure K.8: Gadolinium Core Power Peaking

Table K.3: Gadolinium Core Relative Radial Power Map, 26 MWD/kgU

0.7540	1.0243	0.8393	1.2701	1.3736	0.7086
1.0243	0.7936	1.1305	0.9797	1.3434	0.6032
0.8393	1.1305	0.9171	1.3145	1.1773	
1.2701	0.9797	1.3145	0.8790	0.5790	
1.3736	1.3434	1.1773	0.5790		
0.7086	0.6032				

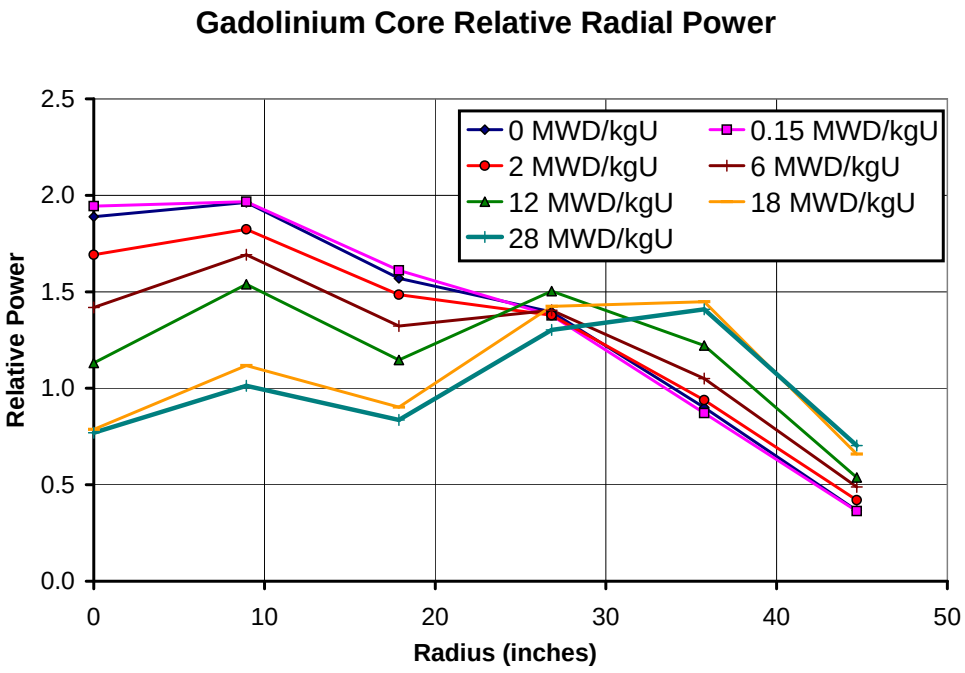

Figure K.9: Gadolinium Core Relative Radial Power

Table K.4: Gadolinium Core Burnup Map, 26 MWD/kgU, SB = 36 ppm

29.06	36.80	28.99	36.60	32.12	14.83
36.80	28.98	36.56	27.79	29.65	12.04
28.99	36.56	27.66	32.29	22.89	
36.60	27.79	32.29	20.12	11.35	
32.12	29.65	22.89	11.35		
14.83	12.04				

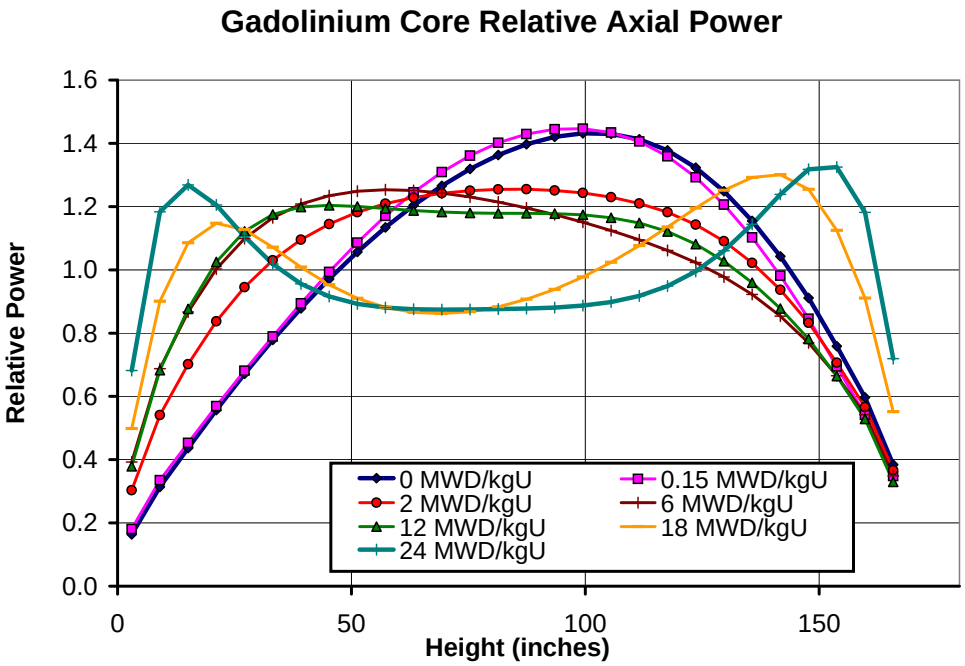

Figure K.10: Gadolinium Core Relative Axial Power

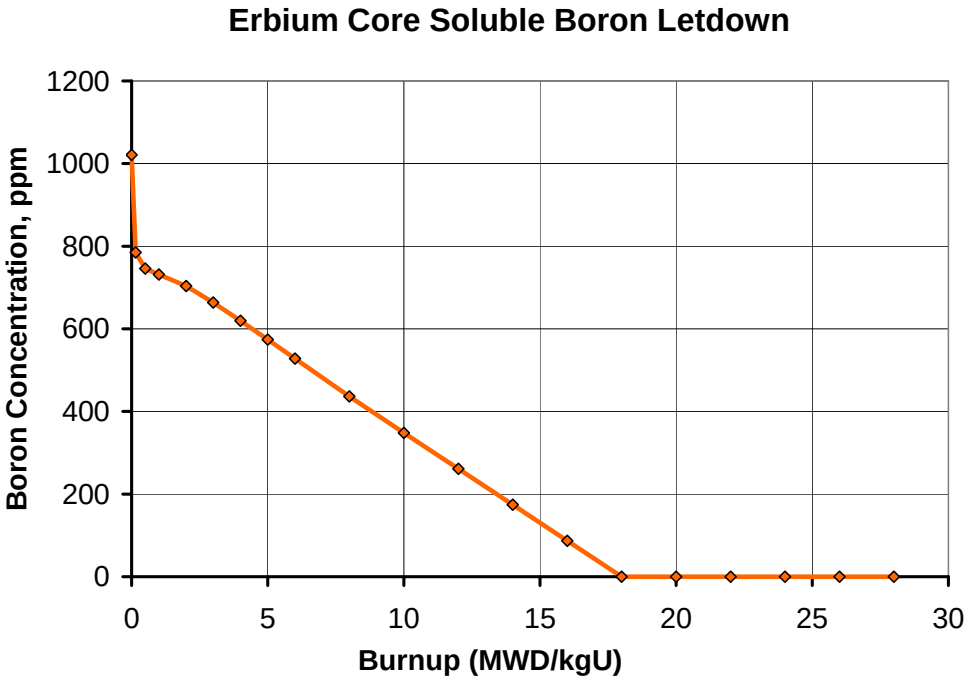

Figure K.11: Erbium Core Soluble Boron Letdown

Table K.5: Erbium Core Integral Parameters

Burnup (MWD/kgU)	k_{eff}	SB (ppm)	FQ*	FdH*	FZ*	Axial Offset (%)
0	1.000	1021.2	3.079	2.093	1.373	-12.613
0.15	1.000	784.8	3.390	2.116	1.522	-26.523
0.5	1.000	746.0	2.590	1.902	1.257	-10.268
1	1.000	731.6	2.681	1.900	1.319	-14.847
2	1.000	703.5	2.476	1.809	1.266	-11.798
3	1.000	663.8	2.272	1.753	1.211	-8.550
4	1.000	619.6	2.132	1.708	1.178	-6.527
5	1.000	573.9	2.034	1.668	1.160	-5.550
6	1.000	528.2	1.962	1.632	1.153	-5.172
8	1.000	436.6	1.844	1.566	1.147	-5.013
10	1.000	347.9	1.734	1.507	1.142	-4.868
12	1.000	261.0	1.634	1.450	1.133	-4.350
14	1.000	174.4	1.585	1.394	1.118	-3.484
16	1.000	87.0	1.548	1.356	1.102	-2.390
18	0.9998	0.0	1.535	1.348	1.087	-1.173
20	0.9901	0.0	1.506	1.349	1.105	2.291
22	0.9809	0.0	1.542	1.346	1.139	4.509
24	0.9708	0.0	1.580	1.337	1.167	5.826
26	0.9602	0.0	1.616	1.360	1.187	6.725
28	0.9491	0.0	1.641	1.374	1.206	7.147

* FQ, FdH, and FZ are unitless parameters describing the maximum nodal power peaking, maximum radial peaking by bundle, and maximum axial power peaking, respectively.

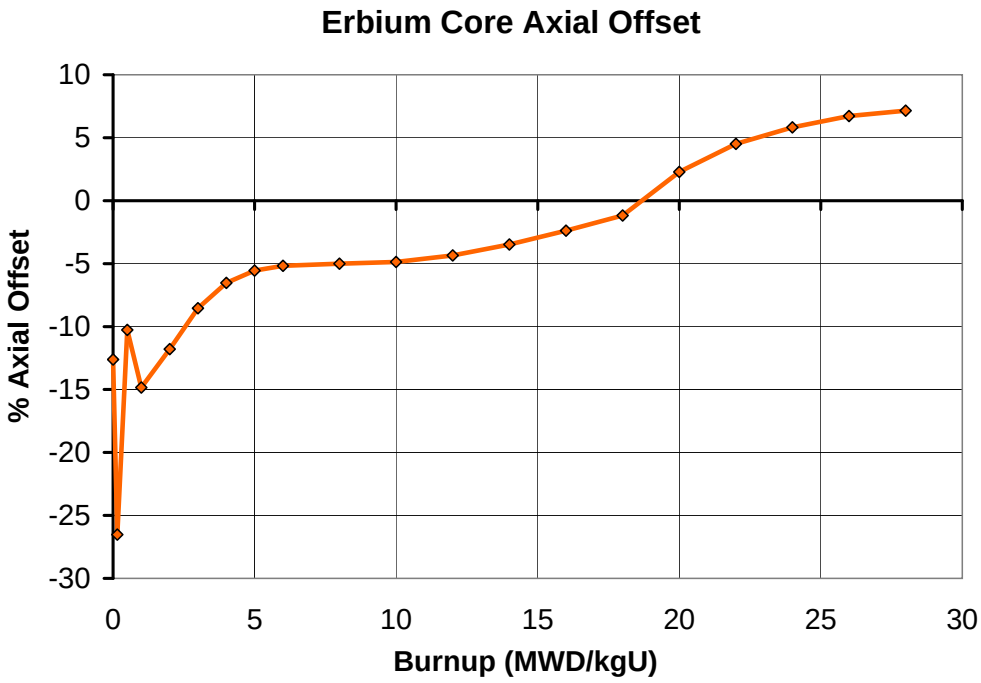

Figure K.12: Erbium Core Percentage Axial Offset

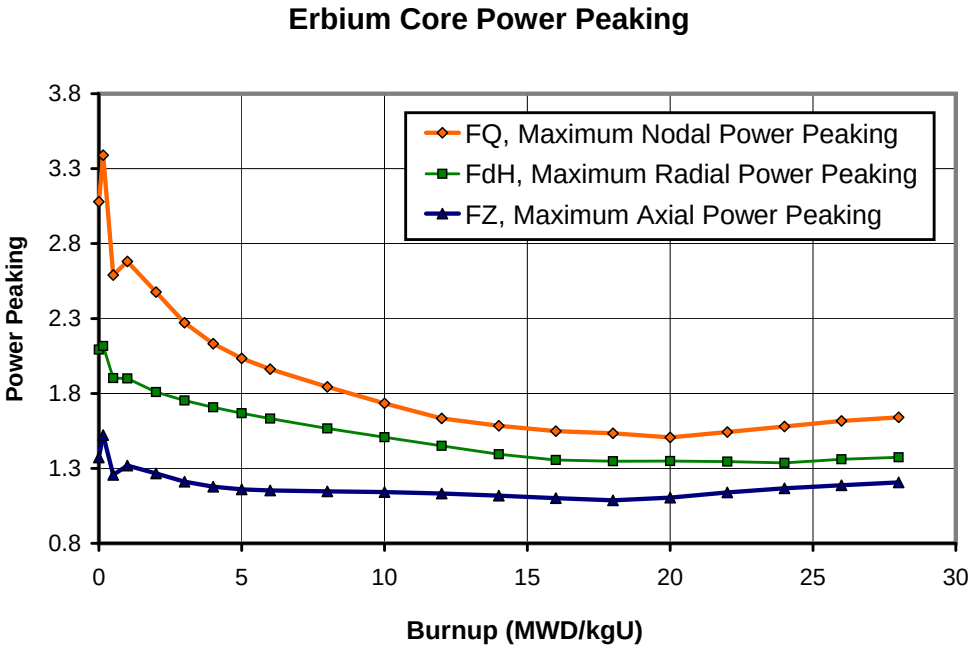

Figure K.13: Erbium Core Power Peaking

Table K.6: Erbium Core Relative Radial Power Map, 0 MWD/kgU

2.0928	1.9541	1.7117	1.2956	0.7520	0.3738
1.9541	1.8982	1.6609	1.1919	0.7147	0.2901
1.7117	1.6609	1.3906	1.0500	0.5361	
1.2956	1.1919	1.0500	0.7439	0.3594	
0.7520	0.7147	0.5361	0.3594		
0.3738	0.2901				

Table K.7: Erbium Core Relative Radial Power Map, 18 MWD/kgU

1.0029	1.2842	1.0562	1.3475	1.2173	0.7026
1.2842	1.0298	1.3232	1.0723	1.1231	0.5691
1.0562	1.3232	1.0543	1.2236	0.8732	
1.3475	1.0723	1.2236	0.8703	0.5338	
1.2173	1.1231	0.8732	0.5338		
0.7026	0.5691				

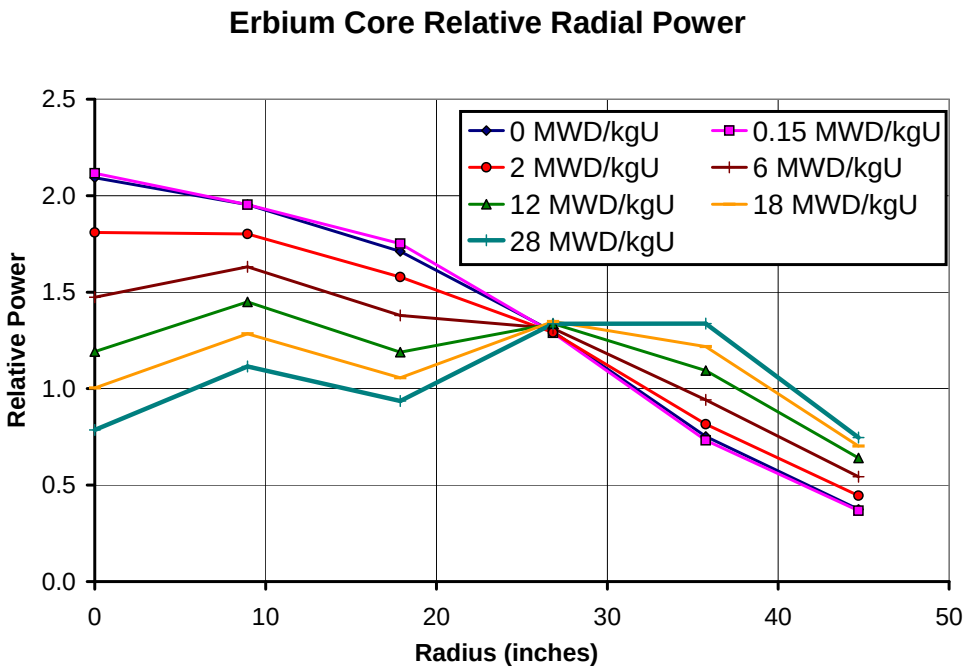

Figure K.14: Erbium Core Relative Radial Power

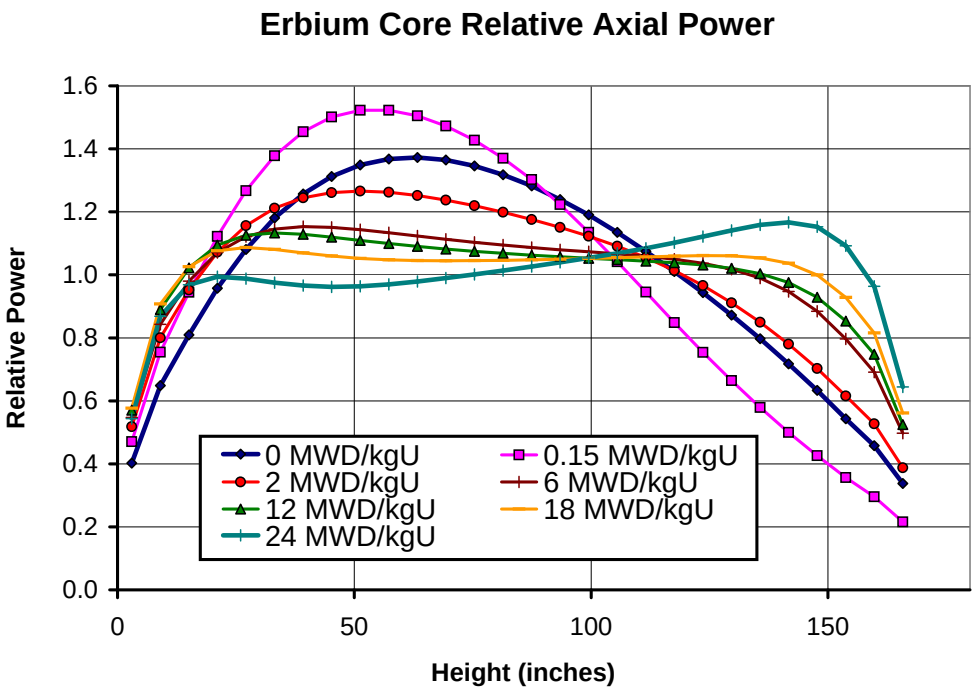

Figure K.15: Erbium Core Relative Axial Power

Table K.8: Erbium Core Burnup Map, 18 MWD/kgU, SB = 0 ppm

24.82	27.96	23.54	23.79	18.17	10.46
27.96	24.26	26.41	20.49	16.90	8.27
23.54	26.41	21.74	20.83	13.02	
23.79	20.49	20.83	15.37	8.60	
18.17	16.90	13.02	8.60		
10.46	8.27				

Vita

Allan Benton Wollaber was born in Albany, New York on April 25, 1979. In 1986 he moved to Gray, TN, and in 1987 to Nolensville, TN. He graduated valedictorian at Page High School in 1997. From there he attended the University of Tennessee at Knoxville. In the 1999 academic year he participated in the student exchange program at the University of Wales in Swansea. In May of 2002 he graduated Summa Cum Laude, receiving a BS in Nuclear Engineering with a minor in Mathematics. In August of 2003 he received an MS in Nuclear Engineering. He has worked for the Tennessee Valley Authority in the summer of 1998, Westinghouse Electric Corporation during the summer of 2001, and part time at the Oak Ridge National Laboratory from November of 2001 through August 2003.

Allan is currently pursuing his doctorate in Nuclear Engineering at the University of Michigan in Ann Arbor.